Investigations of Novel High Dielectric Materials and New Mechanisms

by

Meng Guo

A dissertation submitted in partial fulfillment
of the requirements for the degree of
Doctor of Philosophy
(Chemistry)
in The University of Michigan
2009

Doctoral Committee:

Professor Theodore G. Goodson III, Chair
Professor Peter F. Green
Professor Raoul Kopelman
Assistant Professor Kristina I. Hakansson
Assistant Professor Kevin J. Kubarych

Dedication

I dedicate this dissertation to my family, especially to my grandparents.

Acknowledgements

First, I would like to give my sincere thanks to my advisor, Professor Theodore Goodson III for all kinds of support he has provided during my graduate study at the Department of Chemistry, University of Michigan. It is a really great opportunity to work with him and I have learned a lot in both the scientific and social aspects. I sincerely appreciate the freedom Professor Goodson allowed me to pursue the pioneering research into the field of polymeric energy storage materials, to explore other research areas I am interested in, to develop the business knowledge and connections necessary for the entrepreneurship. I am also thankful for the opportunities to present in various conferences, participate in the proposal writing et al.

At the same time, I am grateful to Professor Peter F. Green, Professor Raoul Kopelman, Professor Kristina I. Hakansson and Professor Kevin J. Kubarych for their service on my committee as well as all knowledgeable suggestions and help on my research, dissertation and job hunting.

Next, I want to share the credit with my collaborators, Professor Asa-Maki Kakimoto and his group members from Tokyo Institute of Technology for the synthesis of hyperbranched copper phthalocyanine materials; And Professor Mireille Blanchard-Desce with her group members from Université de Rennes for the synthesis of dendrimer

G1 to G4 nanodots. The wonderful collaboration with them has led to at least five good publications.

Definitely, I want to thank all my group colleagues for their company during my stay in Professor Goodson's group, we have a lot of pleasant memories to share with. Special thanks to the following colleagues: Dr. Xingzhong Yan, Dr. Oleg P.Varnavski, Dr. Guda Rama Krishna, Dr. Michael Harpham, Mr. Ozgun Suzer for their valuable advices and great help in my research and career aspects.

Most importantly, I would like to express my deepest appreciation to my family. No matter success or failure, they are always there and showing their full support and unconditional love. They watched every step I walked to grow up and shared all the great moments in my life. I will love them forever.

Prologue

Chapter 3 is adapted from work published by the American Chemical Society (*Journal of the American Chemical Society* **2006**, *128*, 14820-14821) and WILEY-VCH Verlag GmbH & Co. (*Advanced Materials* **2008**, *20*, 4167) who hold the copyright thereto. Chapter 6 is adapted from work published by the American Chemical Society (*Journal of Physical Chemistry A* **2009**, *113*, 4763-4771) who holds the copyright thereto.

Table of Contents

List of Figures

List of Schemes

List of Tables

Chapter 1

Introduction and Background

1.1. Introduction

A high dielectric constant material is defined as a material with a dielectric constant comparable to that of the silicon oxide (k>7). The impetus of designing a high dielectric material is located in extending Moore's Law, which states the number of transistors on an integrated circuit doubles approximately every two years. The development of high dielectric constant, low loss dielectric materials will enable the miniaturization of the next generation electronics. A high dielectric constant is critical to a variety of other applications as well: [1-12] (1) High energy and high power capacitors for defrillators, hybrid cars, pulsed plasma thrusters and electric ships; (2) Complementary metal oxide semiconductor (CMOS) field effect transistors for printed circuit boards, electronic switches and converters applications; (3) Memory storage applications; (4) Photonic band gap materials for use as microlasers, optical switches, optical quantum computing and biological probes for tumor detection; (5) Smart skin applications including radar-absorbing materials and microelectromechanical systems (MEMS).

An extensive effort has been made to create a high dielectric constant material with high dielectric constant, low dielectric loss and high breakdown voltage. Typical high dielectric constant materials are ceramics, such as silicon oxide, silicon nitride and barium titanate. They can exhibit high dielectric constant; however, the dielectric loss is

large (>> 0.01) and the processing of materials is very expensive and complicated, in addition to the high leakage current and low breakdown voltage. Hence, conjugated polymers have been an attractive alternative for high dielectric constant applications.

Conjugated polymers are π-bonded macromolecules with many repeating units of fundamental monomers. The delocalization of π electrons along the polymer backbone offers unique electronic and optical properties to conjugated polymers in comparison to saturated polymers, metal and ceramic semiconductors. Since the first report of π-conjugated conductive polyaniline dated back to mid 1800s, a remarkable progress has been achieved towards the understanding of unique properties of such π-conjugated polymers. In 1976, Alan J. Heeger, Alan MacDiarmid and Hideki Shirakawa discovered metallic conductivity in iodine-doped polyacetylene and which led them to win the Nobel Prize in 2000. [13]This breakthrough boosted a more extensive research in the photophysics of a large family of π-conjugated polymers during last three decades. Examples of widely investigated π-conjugated polymers are polythiophenes, [14-22]polyaniline and [23-28]polyfluorene [29-36]. Their molecular structures are shown in Figure 1.1. One of the most important characteristics of conjugated polymers is their ability to undergo a transition between the metal and the insulator state. Generally speaking, the undoped, pristine conjugated polymers are semiconductors or insulators with a large energy gap between the highest occupied molecular orbital (HOMO) and the lowest occupied molecular orbital (LUMO); Whereas, through n-type or p-type doping, conjugated polymers may show metallic conductivities, typically in the order of 10^3-10^5 S/cm. The resulted conductivity by doping is due to the movement of generated mobile charge carriers along the polymer backbone and limited by the disorder in the conjugated polymers. Several

reviews have been conducted on the charge transport properties in conjugated polymers. [37,38]To our particular interest, the conjugated polymers have the ability to show low dielectric loss and high breakdown voltage, while maintaining good processibility and excellent thermal stability. The major concern about the conjugated polymers for high dielectric constant applications is their low dielectric constant (~3 in general).

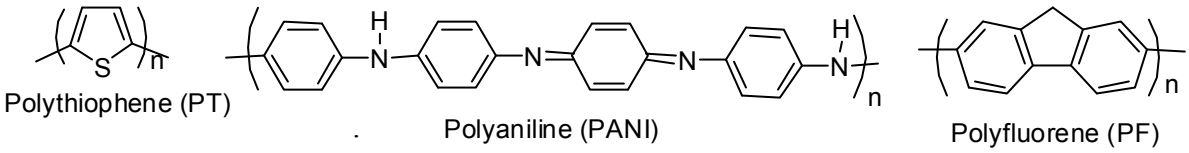

Figure 1.1 Molecular structures of several conjugated polymer examples. [14,27,32]

In order to be competitive with inorganic or metal high dielectric constant materials, several strategies have been projected towards enhancing the dielectric constant in conjugated polymers, mainly focused on poly(vinylidene fluoride) (PVDF) based ferroelectric polymers. A more detailed discussion on different strategies and selection of materials will be given in the later part of this chapter. There is no doubt that the dielectric constant can be greatly enhanced in such ferroelectric polymer systems; whereas, the dielectric loss and dielectric dispersion are still relatively high especially at higher frequency range. Our group has performed an extensive research on the electronic and optical properties of a series of dendrimers. [39-43]Examples of some investigated dendrimer structures are illustrated in Figure 1.2. And we found an ultrafast delocalization process in some of these dendritic structures, which may suggest a novel strategy to create all organic high dielectric constant materials for high frequency applications. In addition, the properties of the dendritic structures can be easily tailored by a precise control on the parameters such as molecule weight and size, the morphology, the branching pattern and the functional group. With the development of synthesis

methods, the scope of the application potential in dendritic structures could be extended. In this dissertation, we will pay particular interests in utilizing the long-range delocalization in dendritic or hyper-branched structures for high dielectric applications. And our goal is to design and develop an all-organic high dielectric constant material with high dielectric constant, low dielectric loss at high frequencies (MHz range).

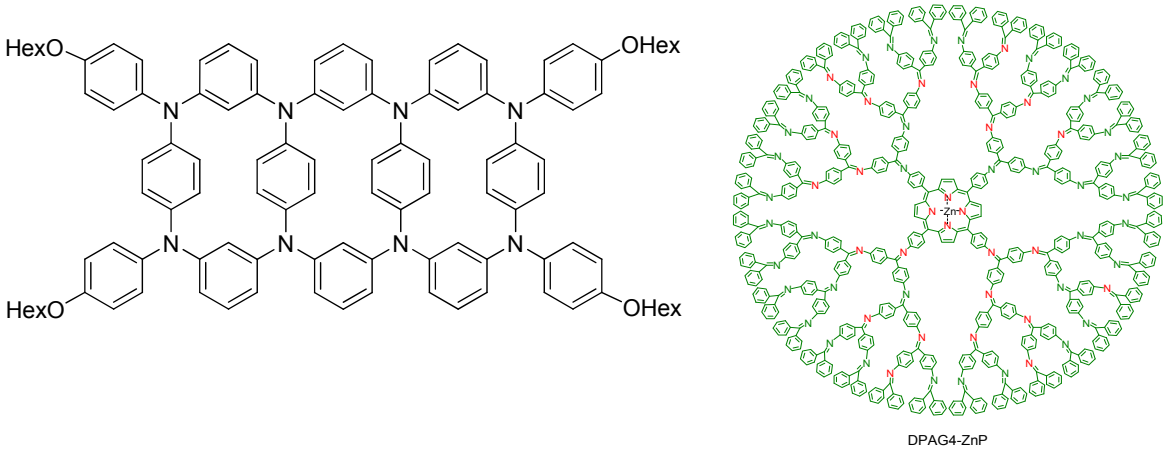

Figure 1.2 Molecular structures of several conjugated polymer examples. [39,44]

1.2 Properties of High Dielectric Constant Materials

There are three important electrical properties of the high dielectric constant materials which are crucial in the realization of above applications.

(1) *Dielectric Constant (relative permittivity)*

The dielectric constant (k) is the relative permittivity of a dielectric material, refers to the ability to store the charge under the applied electromagnetic field and then transmit the energy. It is a function of the temperature, the frequency and the structure of a material. It is expressed in terms of the ratio between the real permittivity of the dielectric material to that of the vacuum:

$$k = \frac{\varepsilon_r}{\varepsilon_0} \tag{1.1}$$

Where, ε_r is the real permittivity of the dielectric material, F/m and ε_0 is the permittivity of vacuum, 8.85×10^{-12} F/m.

A high dielectric constant is required as it will control the size of the devices. For example, the size of a dielectric resonator is proportional to $\sqrt{k}$. [45] In regards to energy storage applications, the energy density is proportional to k. Therefore, high dielectric constant material will be able to achieve high energy density.

(2) *Dielectric Loss (loss tangent, dissipation factor)*

The dielectric loss (tanδ) is the energy consumed to overcome the inertia resistance in an alternating electric field. It is described in terms of the ratio between the real (ε_r) and the imaginary (ε_i) part of the complex dielectric permittivity as:

$$\tan\delta = \frac{\varepsilon_i}{\varepsilon_r} \tag{1.2}$$

A low dielectric loss is necessary for high performance devices as it may result in higher efficiency and lower noise, [45] which is especially important for high frequency applications (e.g. MHz). It also alleviates the thermal failure problem. Moreover, the frequency and temperature dependence of the dielectric loss provide important information on the charge transfer mechanisms operative in the materials.

(3) *Breakdown Voltage*

The breakdown voltage (E) is the field value at which the device fails and becomes conducting. In generally, it is determined by the average of multiple tests conducted in contact mode in ramp test (Figure 1.3). [46] A high breakdown voltage is essential as it increases the energy density of the energy storage device, because the energy density is proportional to E^2. It also improves the device lifetime.

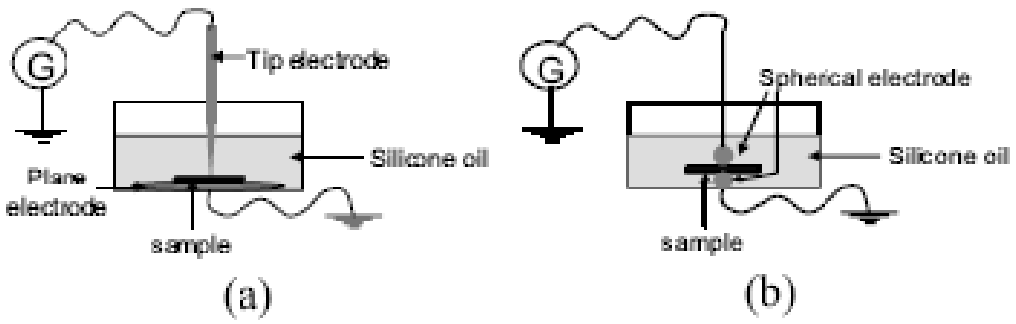

$$E = \frac{2 \times V}{r \times \ln(1 + \frac{4d}{r})} \qquad E = \beta \times E_m$$

Figure 1.3 the experimental apparatus to measure the dielectric breakdown. [46]

1.3 Important Issues Relate to High Dielectric Constant

1.3.1 Polarization Mechanisms

When a dielectric material is exposed to an electromagnetic field, the electric field will influence the distribution of existing dipoles and induce the formation of new dipoles. This effect is called the polarization (P, C/cm^2). In principle, there are five types of polarization mechanisms which prevail at different time domains: electronic polarization (atomic polarization), orientation polarization (dipole polarization), ionic polarization, interface or surface polarization (Maxwell-Wagner) and hyperelectronic polarization. In a dielectric material, at least one of these five types of polarization mechanisms functions under static fields. Here, only a brief and simple discussion on different polarization mechanisms will be given and a more detailed description on this topic will be referred to in later chapters.

1.3.1.1 Electronic Polarization

The displacement of the charge center of electrons from the neutral nucleus will induce a dipole moment and produce an electronic polarization. This polarization is present in all materials, along with a wide frequency range. In nonpolar solids where there is no existence of permanent dipoles or ions in the solid, such as silicon (Si), only electronic polarization exists For other solids, electronic polarization may act simultaneously with other polarization mechanisms including orientation polarization and ionic polarization.

To calculate the electronic polarizability, one generally assumes that the atom is in a perfect spherical symmetry. This assumption is only valid for inert gases consisting of only one atom, such as Argon (Ar). In this ideal situation, the electronic polarizability of one atom is expressed as: [47]

$$\alpha_e = 4\pi \cdot \varepsilon_0 \cdot R^3 \tag{1.3}$$

Where ε_0 is the vacuum permittivity and R is the sphere radius. For ideal solids, the electronic polarizability is $N\alpha_e$, where N is the concentration of atoms in the solid and α_e is the electronic polarizability of one atom. Moreover, the electronic polarization in such a spherical solid is very weak. For molecular solids bounded by weak van der waals forces, such as sodium chloride (NaCl), each particle (atom or ion) can be treated as a quasi-isolated particle, therefore, the electronic polarizability becomes $\sum N_i \alpha_{ei}$, where N_i and α_{ei} are the concentration and the electronic polarizability of *i*th particle respectively. [47] The induced dipole moment from the electronic polarization is proportional to the applied electric field and has no dependence on the frequency. The time required to

induce the electronic polarization is ~ 10^{-15} sec, therefore this polarization mechanism is operative along the wide frequency range (up to 10^{15}Hz).

1.3.1.2 Orientation Polarization

Orientation polarization usually occurs in polar liquids, gases or polymeric materials where there are permanent dipoles with the freedom to rotate. The external electric field will align the existing randomly oriented dipoles to some direction and produce a polarization. It is operative up to the microwave frequency (10^8 Hz). The orientation polarization is strongly dependent on the temperature, as thermal energy is needed to overcome the resistance from neighboring molecules for alignment. This temperature dependence is a characteristic of the orientation polarization and helps it to differentiate from electronic and ionic polarizations, as the latter two types of polarization have no temperature dependence.

To calculate the orientation polarizability, several models have been developed. [47] The first model is called Langevin function, which is a function of the temperature (T), the dipole moment (μ) and the field strength (E). [48]In the situation where dipole moment is small and field strength is weak, or has high temperature, this model was developed by Debye and is approximated as: [49] [50]

$$a_o = \frac{\mu^2}{3KT} \tag{1.4}$$

In normal conditions, the contribution from the orientation polarization is larger than that from the electronic polarization.

1.3.1.3 Ionic Polarization

Ionic polarization exists where the electric field drags the charge center of positive ions away from that of negative ions yielding a net dipole in ionic solids. Ionic polarization is operative up to infra-red frequency (10^{12}-10^{13} Hz), because the alignment involves the displacement of the entire ions in the lattice and the response to the electric field becomes slower.

The ionic polarizability is expressed as: [47]

$$\alpha_i = \frac{q^2}{Y \cdot d_0} \tag{1.5}$$

Where, q is the electric charge (1.6×10^{-19}C), Y is Young's Modulus and d_0 is the equilibrium distance between atoms. In this case, we also only consider the ideal situation with symmetrical shape. For the high dielectric constant material dominated by the ionic polarization, the dielectric loss curve normally exhibits an abrupt loss peak and the conductivity is relatively large. One effective strategy to enhance the dielectric response in solids is through ion doping. For example, by doping the polyaniline with iodine, the polyaniline is oxidized and the dielectric constant can be increased to more than 10 times higher than the undoped one. [51]

1.3.1.4 Interface polarization

Interface polarization is present in the surfaces, gain boundaries and inter-phase boundaries, where dipoles can orient to certain degree under electric field and contribute to the total polarization of dielectric materials. The interface polarization is operative up to 10^4 Hz. The interface polarization has been accounted for the high dielectric response in many heterogeneous systems, especially the ferroelectric polymers and ceramics. [52-

[55]And the contribution of interface polarization to the total polarization of material is remarkable at low frequency range (Hz-KHz), that's why a lot of dielectric materials have very high dielectric constant at lower frequencies.

The interface polarization mechanism has been widely used in inorganic/organic nanocomposites in order to enhance the dielectric response. [52,55-59]And the degree of the polarization depends on the size and morphology of the crystalline domain, the defects and number of boundaries, as well as the difference in the conductivity between inorganic and organic materials.

Maxwell-Wagner polarization mechanism is generally used to explain the dielectric relaxation in polycrystalline materials. In addition, interface polarization is a very complicated mechanism and no satisfactory models have been determined to calculate the interface polarizability yet.

However, for amorphous solids, we will use the term of hopping polarization to describe this type of space charge polarization. In an amorphous solid, the localized charge can hop from one site to another site; therefore form the dipole moment by the transition between two different potential wells. Depending on the width and height of the potential barrier between two sites, the localized charge can hop or even tunnel between neighboring sites. The hopping polarizability is given as: [47]

$$\alpha_h = \frac{q^2 r^2}{3KT} \overline{P_0(A \to B) P_0(B \to A)} \tag{1.6}$$

In this equation, $\overline{P_0(A \to B) P_0(B \to A)}$ is an ensemble of the average product of two hopping probabilities (hop from site A to site B and hop from site B to site A); T is the temperature; K is the Boltzmann constant; r is the distance between A and B sites.

1.3.1.5 Hyperelectronic polarization

In addition to the above basic polarization mechanisms, another mechanism called hyperelectronic polarization has been found in some long polymeric molecules with an extensive electronic orbital delocalization by Pohl et al. [60,61] The hyperelectronic polarization is considered as the principle contributor to high dielectric constant in polyacene quinone radical (PAQR) polymers (e.g. 14000 at 100Hz for a PAQR polymer). Hyperelectronic polarization may due to the pliant interaction of charge pairs of excitons, located on long, polarizable polymers under a low frequency external electric field. The long-range displacement of charge pairs along the giant macromolecule will result in a strong polarization delocalized along the entire length or dimension of the macromolecule. The hyperelectronic polarization shows a non-linear dependence on the electric field and its magnitude is several orders larger than that of the electronic polarization, especially during the frequency range (KHz-MHz). We will give more details about this polarization mechanism later, as this is the major polarization mechanism we are trying to employ to create an all-organic high dielectric material. Scheme 1 shows a summary of polarization mechanisms and their response to frequency.

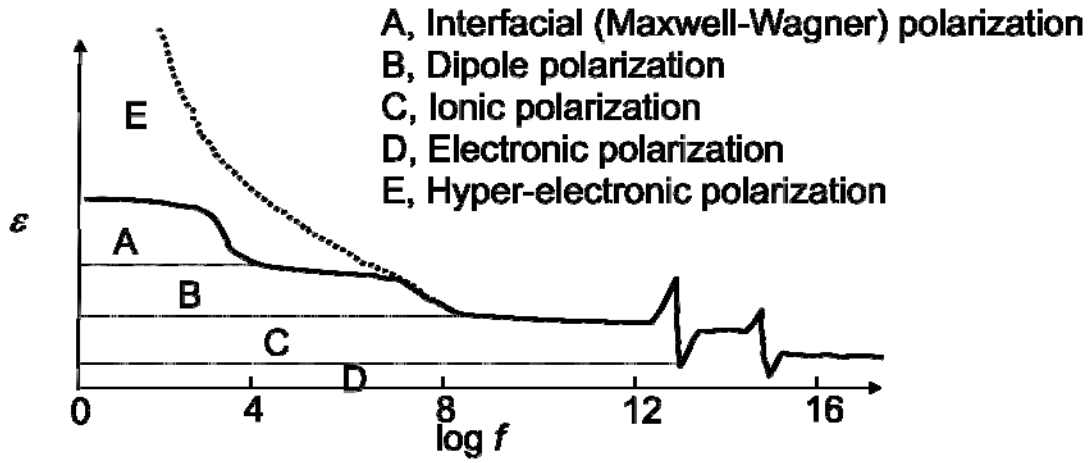

Scheme 1.1 Schematic diagram of polarization mechanisms and their frequency response.

1.3.2 Energy Transfer

Our major strategy is to use the polaron delocalization to enhance the dielectric response in hyperbranched or dendritic polymer systems. The understanding of the polaron formation and the delocalization in such systems will be very helpful to probe the hyperelectronic polarization contribution to the dielectric constant. Before talking about the energy transfer in conjugated polymers, we have to define some important terms first.

The first term is the exciton. One likely outcome of the light-polymer interaction will be the generation of molecular excitons. In this case, the electron and hole have strong interactions. There will be singlet excitons, biexcitons or triplet excitations and they can be distinguished by the exciton binding energy, which is defined as the energy difference between the optical transition and the energy of independent electron and hole in the polymer. A common exciton binding energy to most conjugated polymers is ~0.3 eV. Also depends on the material, the excited electron hole pairs can be called either

Frenkel exciton (localized on the same molecule) or Wannier exciton (localized over different molecules).

The second term is the polaron. A polaron is formed when the polymer absorbs a photon and results in strong electron-lattice interactions giving rise to lattice distortions, and creating an electron-hole pairs with sufficient separation distance. Based on the SSH Hamiltonian or other tight-binding Hamiltonians, polaron provides two energy levels located symmetrically about the center of the gap. The location of the polaron levels relative to the conduction band edge or valence band edge depends on the chain length.

The polaron delocalization in conjugate systems has a correlation with the excitation energy transfer (EET) process. [39,41,62-67]Excitation energy transfer generally takes place after the formation of an electronically excited state in a conjugated polymer. The polymer excited state is typically spatially delocalized along the polymer chain and the exciton is changing its spatial position and energy by transferring to other sites. This transfer may occur along a single polymer chain or hops between chains. If EET is very efficient, the exciton may travel over a substantial distance during its lifetime and as a result it may find some specific sites where it may become trapped or dissociated to form an electron-hole pair. Such a site could be a location on the polymer which significantly lowers the energy of the excited state (a trap), or even an energy accepting site of a different nature. Since conjugated polymers generally are associated with strong optical transitions, the main interaction between the donor and the acceptor in the energy transfer process is of Columbic nature. A Förster energy transfer process is a weak dipole-dipole interaction between the donor and the acceptor. Spectral overlap between donor emission and acceptor absorption spectra, distance between donor and acceptor, and their mutual

orientation are the factors controlling this type of energy transfer. In this case, the exciton hops between neighboring molecules or branches and results in an incoherent energy transfer. This process is very fast (~ ps) and can extend to long range (100 Å). The RET transfer rate is given by: [68]

$$k_T(r) = \frac{Q_D k^2}{\tau_D r^6}\left[\frac{9000(\ln 10)}{128\pi^5 N n^4}\right]\int_0^\infty F_D(\lambda)\varepsilon_A(\lambda)\lambda^4 d\lambda \tag{1.7}$$

Where Q_D is the quantum yield of donor in the absence of acceptor; k^2 is a relative orientation factor and is usually assumed to be 2/3; τ_D is the donor lifetime; r is the separation distance between donor and acceptor; N is Avogadro's number; n is the medium refractive index; $F_d(\lambda)$ is the corrected fluorescence intensity of the donor in terms of the normalized total intensity; $\varepsilon_A(\lambda)$ is the extinction coefficient of the acceptor at wavelength λ. By defining the Förster distance R_0 as the distance at which the probability of intermolecular energy transfer is equal to the relaxation of the donor by usual radiative and nonradiative ways, the EET rate is given as: [68]

$$k_T(r) = \frac{1}{\tau_D}\left(\frac{R_0}{r}\right)^6 \tag{1.8}$$

When the dipole-dipole interaction is strong enough, a Dexter energy transfer occurs instead by exchangin electron between the donor and the acceptor. The Dexter energy transfer mechanism requires the overlap between donor and acceptor spectrum, therefore, it operates very efficiently over short distance (e.g. 15-20 Å). The Dexter energy transfer rate is given as: [68]

$$k_T(r) = \frac{2\pi}{\hbar} Z^2 \int_0^\infty E_D(\lambda) A_A(\lambda) d\lambda \tag{1.9}$$

Where ħ is the reduced Planck's constant (6.582×10^{-16} eV s); $E_D(\lambda)$ is the donor emission intensity; $A_A(\lambda)$ is the extinction coefficient of the acceptor.

If we define L as the sum of the van Del Waals radii of the donor and acceptor, the energy transfer rate then becomes proportional to $e^{-2r/L}$.

The energy transfer rate is independent of the oscillator strength, but shows temperature dependence.

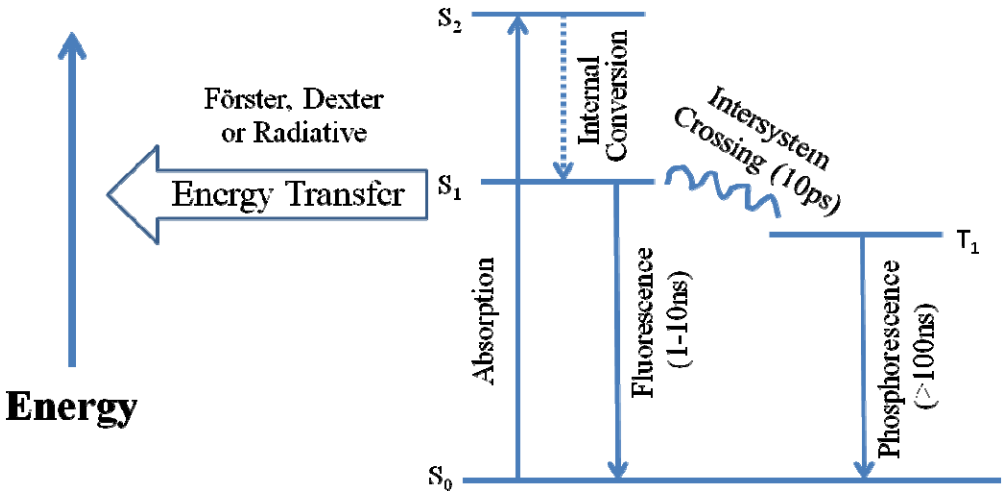

Scheme 1.2 Diagram of the energy transfer mechanism. [68]

1.3.4 Charge Transfer Mechanisms

The electrical properties of conjugated polymers, such as charge carrier mobility, have great influence on the dielectric properties of conjugated polymers. One fact is that the movement rate of charge carriers along the macromolecule will affect the response speed of dielectrics. As we require the dielectric loss to be small and the response to be quick at high frequency, therefore, the understanding of charge transfer is crucial in the design of high dielectric materials.

The investigation of charge transfer in conjugated polymers has been the research subject to many chemists and physicists in the last several decades due to its importance in the applications in polymer light emitting diodes (PLEDs), organic thin-film transistors (OTFTs) and organic photovoltaics (OPVs). [69-72] A series of techniques have been applied to characterize the charge transfer properties in conjugated polymers, such as time-of-flight (TOF), space-charge-limited current (SCLC) et al. The charge transfer mechanism depends on the factors including electrode type, the structure and property of the material, the field strength and temperature. Here, we mainly discuss the polaron hopping, polaron tunneling and Poole-Frenkel effects which are operative in our investigated dielectric materials.

1.3.4.1 Incoherent Polaron Hopping

Polaron hopping process is well known in non-crystalline materials, such as glass and disordered amorphous organic solid. [73-76] Actually, with the development of applications for conjugated polymers, more attention has been directed at developing the hopping model by adding more factors such as disorder to describe the experimental observations. In amorphous solids, the density of states (DOS) near the Fermi energy is localized due to the lack of long range order. When thermal energy is available and enough to overcome the potential wells between two localized state, the localized state will hop to the neighboring site and transport charge carriers through the material. In general, these localized states are close in energy levels, therefore, only small activation energy is required for the processing of hopping process and the hopping can occur at very low temperatures. Scheme 1.3 demonstrates a hopping process.

There are a variety of hopping regimes. Two popular ones are small polaron hopping and variable range hopping. Small polaron hopping occurs within a distance approximately one lattice constant. Whereas, the delocalized states will hop to a more distant neighboring site where less activation energy is required during variable range hopping process. Small polaron hopping theory was first established by Holstein by assuming uncorrelated carrier hops and the carrier mobility demonstrates simple activation type temperature dependence. [77,78] Then Emin extends the applicability of this model by considering the correlation between hops when the hopping rate is faster than lattice relaxation. [75,79,80] In this case, no clear active type variation of carrier mobility is shown. The nonadiabatic small hopping rate (W_{ij}) is given by Marcus theory: [81]

$$W_{ij} = \frac{J^2}{\hbar}\sqrt{\frac{\pi}{4E_a k_B T}}\exp(\frac{-E_a}{k_B T})\times\exp[-\frac{E_j - E_i}{2k_B T} - \frac{(E_j - E_i)^2}{16E_a k_B T}] \tag{1.10}$$

Here, $J=J_0 \exp(-r_{ij}/b)$ is the transfer integral between sites with a separation distance of r_{ij}; E_a is the activation energy; E_i, E_j are the energy level at i, j sites individually. The conductivity is expected to follow the relation: [81]

$$\log\sigma \propto T^{-1} \tag{1.11}$$

For variable range hopping, as the hopping polarons possess a wide range of relaxation times, the AC conductivity is frequency dependent. In this case, the conductivity is expected to follow Mott's Law: [82,83]

$$\sigma = \sigma_0 \exp(-\frac{A}{T})^{1/4} \tag{1.12}$$

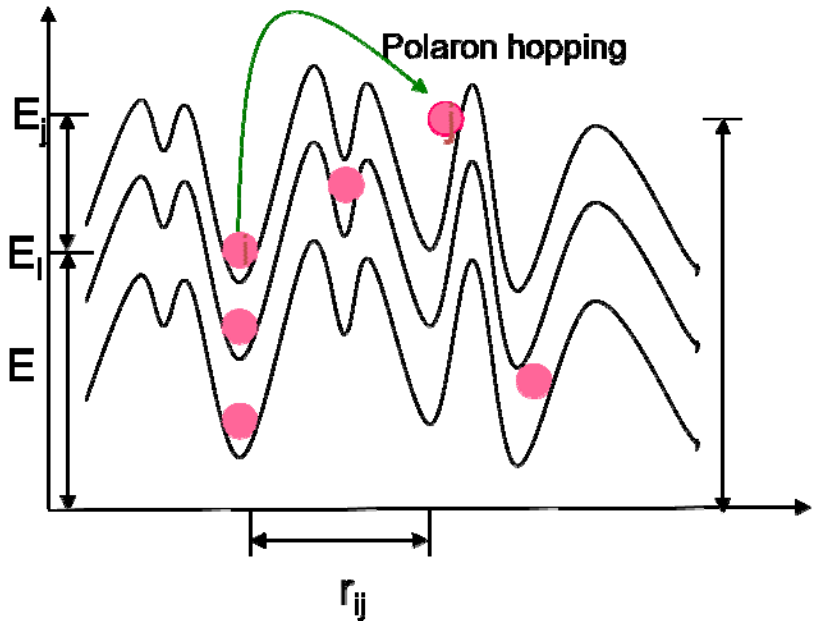

Scheme 1.3 Cartoon of polaron hopping process in amorphous solids

Polaron hopping has been found in various amorphous solids both experimentally and theoretically, such as pentacene, anthracence and copper phthalocyanine (CuPc). [74,84,85] The theory of polaron hopping is being kept updated upon the emergence of conflicts with some research data, especially for amorphous solids with high mobilities. Vidadi studied the CuPc monomer and suggested a hopping and band-type mechanism which contributed to high dielectric constant. [86] Also, Ahmad et al. studied the triclinic PbPc films sandwiched between gold electrodes and observed the evidence of variable-range hopping at low temperatures. [87]With the aid of ultrafast spectroscopy techniques, we proved that polaron hopping is a dominating charge transfer mechanism contributes to high dielectric response in hyper-branched CuPc dendrimers. [88]The details will be given in chapter 3.

1.3.4.2 Polaron Tunneling

The polaron tunneling mechanism is a quantum-mechanical effect in which electric field at the barrier is sufficiently high to reduce its width at Fermi level, thus the polaron can tunnel through a potential well even when its kinetic energy is less than the height of the barrier (Scheme 1.4). V.Babnar et al. suggested the polaron tunneling is one of the dominating charge transport mechanisms in CuPc, based on the observation of a high dc conducting component in the AC conductance. [89] For more details about the tunneling process, several reviews could be referred to. [81] Simmons has proposed a modified Fowler-Nordheim expression to describe the tunneling process as: [81]

$$J = \frac{e^3 V^2}{8\pi h \Phi d^2} \exp\left(-\frac{8\pi (2m)^{1/2} \Phi^{3/2} d}{3ehV}\right) \tag{1.12}$$

Where, e is the electron charge; V Φ is the barrier height; d is the tunneling distance ; m is the mass of free electron; h is Planck's constant, V is the electric field.

And the tunneling decay parameter is given as: [90]

$$\beta = \frac{4\pi (2m\phi)^{1/2}}{h} a \tag{1.13}$$

Here, a is a unitless parameter to describe the asymmetry of potental profile (a=1 for rectangular potential barrier); β is the tunneling decay parameter; m is the mass of free electron, Φ is the barrier height and h is Planck's constant.

π-conjugated polymers normally show a lower tunneling decay value (β ~ 0.2-0.6 Å-1) compared to saturated polymers due to π delocalization over the molecule. Therefore, more efficient tunneling should be expected. In hyperbranched or dendritic systems, the delocalization length is longer and due to the self-organization of macromolecules, the probability of polaron tunneling is estimated to be higher.

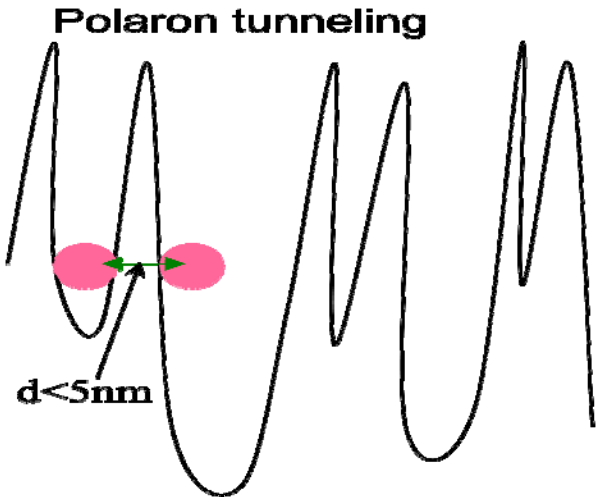

Scheme 1.4 Cartoon of polaron tunneling process in amorphous solids

Polaron tunneling may occur at low temperature when less thermal energy is available and contribute to the charge conduction under the situation that the distance between the neighboring sites is narrowed down to a critical value. In this case, the charge mobility shows a non-Arrhenius temperature dependence. For example, polaron tunnels in CuPc when the separation distance between two CuPc rings is ~5nm. [81]

1.3.4.3 Poole-Frenkel effect

Poole-Frenkel effect has been observed in many disordered molecules. [74,91-93] It refers to the activation energy of the electric conductivity or drift mobility is inversely proportional to the square root of the electric field strength E. The applied electric field assists in lowering the Coulomb potential barrier that a charge carrier needs to overcome before leaving the charge center traps (scheme 1.5). [94] The conductivity then shows a field dependence form: [95]

$$\sigma = \sigma_0 \exp(\beta_p E^{1/2} / 2KT) \tag{1.14}$$

$$\beta_p = 2(e^3 / 4\pi\varepsilon_0\varepsilon_r)^{1/2} \tag{1.15}$$

Where, σ_0 is the low field conductivity; β_p is the Poole-Frenkel field lowering coefficient; E is the applied electric field strength; ε_0 is the vacuum permittivity; ε_r is the high frequency dielectric constant; e is the unit of electronic charge.

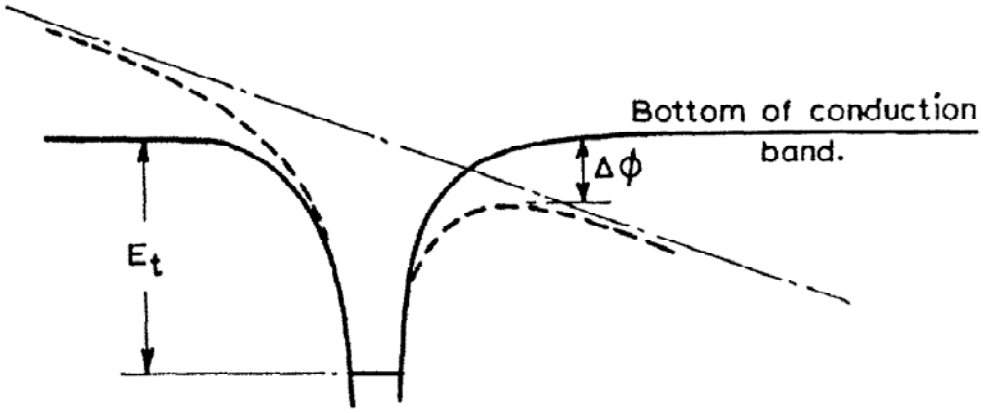

Scheme 1.5 Mechanism of Poole-Frenkel effect. The solid line represents the Coulomb potential barrier without applying electric field. The dotted line shows the lowering effect of electric field on the barrier. [95]

There are a lot of arguments surrounding the origin of Poole-Frenkel effect. [73] [81,95-100]One thing has to be pointed out is that sometime a negative electric field dependence is found in disordered polymers, which has been in debate during the last several decades. We are going to give more details in chapter 2.

1.4 Material Selection

Basically, there are two major directions toward creating high dielectric constant materials.

(1) Ceramics

One major area is directed at utilizing ferroelectric ceramics and a detailed review on the scientific and technical issues involving high k metal oxides has been conducted

by John Robertson. [7] A variety of inorganic high dielectric constant materials have been explored, which includes the $BaTiO_3$, [55,56,101-110] $CaCu_3Ti_4O_{12}$ [111-118] HfO_2, Al_2O_3 et al. For instance, a recent work by Thomas and his co-workers has obtained a dielectric constant ~ 40000 and a dielectric loss <0.07 at 1 KHz in a 30-80 nm size crystalline $CaCu_3Ti_4O_{12}$ powder. [114] Some efforts even extend to dope the ceramics with metal substitution or mix various components to form composite materials. For example, in a (Li, Fe)-doped NiO ceramics, a dielectric constant>100 could be obtained at 1 KHz at room temperature. [119]And high dielectric constant could be explained by Maxwell-Wagner (MW) interface polarization. However, the dielectric loss and dielectric dispersion are still huge. And the dielectric response in these materials relates closely to the homogeneity of the microstructure, the existence and amounts of defects, synthesis method, sintering temperature and crystalline size. In doped ceramics, the doping ratio is also a critical issue in controlling the dielectric loss in such kind composite materials. Moreover, low breakdown voltage, high leakage current in addition to high fabrication cost make the idea of replacing silicon oxide with ceramic high dielectrics less attractive. That's one of major impetus for researchers to look for other alternative high dielectric materials.

(2) Inorganic/Organic Nanocomposites

Organic dielectric materials normally have advantages as: high breakdown voltage, low dielectric loss, excellent processibility, good thermal property and stability, as well as low cost. But the dielectric constant is normally low (<3). Therefore, the driving force in this field is how to increase the dielectric constant in organic materials. One popular strategy is to introduce ceramic fillers into the polymer and try to combine the advantages

of both components. Typical fillers are $BaTiO_3$, $CaCu_3Ti_4O_{12}$ et al. [6,56,59,109,120-129] And host polymer matrix are likely to be ferroelectric polymers, such as poly(vinylidene fluoride) (PVDF) [122], Polyimide (PI), [9]Poly(vinylidene fluoride trifluoroethylene) [P(VDF-TrFE)], [52]poly(vinylidene fluoride trifluoroethylene-chlorofluoroethylene) [P(VDF-TrFE-CFE) or epoxy. [6,56,59]A recent review by Lu and Wong has been conducted on recent advances in high k nanocomposites materials for embedded capacitor applications.[124] Conductive filler/ polymer composite materials, considered as a percolation system, will achieve a very high dielectric constant by approaching the percolation threshold (f_c). The effective dielectric constant of the composite system will follow the power law: [130]

$$\frac{\kappa_{eff}}{\kappa_{matrix}} = \left| f_c - f \right|^{-s} \tag{1.3}$$

Here, K_{eff} is the effective dielectric constant, K_{matrix} is the dielectric constant of polymer matrix, f_c is the percolation threshold, f is the volume fraction of metal or inorganic fillers and s is a scaling constant (~1) and the selection of its value depends on the material properties, phase connectivity between filler and polymer as well as microstructure of composite. [131,132]Ten to a hundred fold enhancement has been observed in some percolative polymer composites. For example, the dielectric constant of polyimide is about 3.2, by adding 40 vol% calcium copper titanate (CCTO) filler by in situ polymerization, the CCTO/PI hybrid film shows a dielectric constant ~49.1 at 100Hz, about 15 times enhancement. [9] However, the dielectric constant drops to 20 and the dielectric loss is about 0.12 at 1MHz. Another recent work done in Deng's group has improved the dielectric constant of polymer matrix (PVDF) to 1700 at 100Hz with the blending of Bi_2S_3-$BaTiO_3$ filler at a concentration of 0.11, much higher than what has

been obtained previously in $BaTiO_3$/PVDF (<100), [133]CF-$BaTiO_3$/PVDF (~110) [58]and Ni-$BaTiO_3$/PVDF(800). [134]While, the dielectric constant drop to <60 and dielectric loss reaches ~0.5 at 1MHz. The major concern about the ceramic/polymer composite is the high dielectric loss due to high loading ratio of filler in order to obtain high dielectric constant. The high dielectric dispersion will also bring problem for high frequency applications. The enhancement in dielectric response is closely connected to the size and shape of the filler, the dispersion of filler into the polymer matrix and the adhesion property of the dielectric layer to the substrate of device, which creates a lot of technical barriers for practical applications.

The second way of utilizing percolation theory is to add metal fillers to polymer matrix. Various metal fillers, such as nickel (Ni), aluminum (Al), silver (Ag), carbon black and exfoliated graphite nanoplates have been used to prepare metal/polymer composites. [132,134-140]Lu et al reported an in-situ formed Al/high k epoxy composite having a dielectric constant ~ 90 and dielectric loss of 0.02 at 10 KHz with Al filler loading of 80wt%. By incorporating self-passivated Al filler into Ag/epoxy matrix, a dielectric constant of 150 at 10 KHz is obtained with the same weight percentage of Al filler loading as Al/epoxy composite. The high dielectric constant in the latter composite suggests that the dispersed silver nanoparticles have significant influence on dielectric enhancement. The dielectric loss in Al/Ag-epoxy composite is higher due to the conductive feather of Ag, but the dielectric loss is <0.1, which is tolerable for certain applications such as decoupling capacitors. [132]As no frequency dependence of dielectric response has been reported for these materials, so the applicability of such materials for high frequency applications is unknown yet. It should be noted that the coating of

insulating layer shell on the conductive filler core (for example, by self-passivation of Al to form Al_2O_3/Al core-shell structure) will prevent the direct contact between the fillers and effectively reduce the dielectric loss. In order to further reduce the filler concentration, a novel nanocomposites system has been suggested by replacing metal fillers with exfoliated graphite nanoplates (xGnP) because of their excellent electrical and thermal conductivity. [140] In addition, there is a tendency to form many parallel-board microcapacitors with low filler concentration due to its unique layered structure with a thickness in nm scale. [141]They found a high dielectric constant ~1000 at 1MHz with a filler loading of 3.12 vol% (270 times higher than PVDF matrix itself and previous reported metal/PVDF composite), and the dielectric constant at lower frequency (e.g. 100Hz) can go as high as 10^8. When the filler loading goes beyond the percolative stage (fc=1.01%), the dielectric dispersion is invisible during the wide frequency range (up to 10 MHz), even though the dielectric constant is <100. In this composite, Maxwell-Wagner-Sillars (MWS) polarization contributes substantially to the enhancement in dielectric constant. Although very high dielectric constant (~1000 at MHz frequency range) has been reported with low conductive filler loading (<5 vol %), the accompanied high dielectric loss as well as high conductivity (>0.01) still stand as barriers for the practical applications as embedded capacitors. Moreover, such composite systems easily become conductive once beyond percolation limit, therefore result in high leakage current. Recent advances in conductive filler/polymer composite have been achieved in the following areas: (1) Careful control in filler size and homogeneous dispersion in polymer matrix; (2) Creation of core-shell structured fillers via chemical or

photochemical routes; (3) Surface modification of fillers by adding surfactant, such as phosphate esters. A detailed discussion could be referred to the review by Lu et al. [124]

With the emergence of research on carbon nanotube since its discovery in 1991 by Sumio Iijima of the NEC Corporation, a variety of optical and electronic applications have been found or targeted for, such as solar cells, super capacitors, transistors and vessel for drug delivery. Several reviews have been conducted on the properties and applications of carbon nanotubes. [142-146]Carbon nanotubes (single wall or multi-wall) have been known to possess a couple of unique properties: good electrical and thermal property, high mechanical strength and large length to diameter aspect ratio (L/D) as well as tunable multi-functionality, which make them very attractive to high dielectric applications too. It has been shown that the dielectric constant can be greatly enhanced by adding a small amount of carbon nanotube dopants (doping ratio is in close proximity to the percolation threshold) into the non-conductive polymer matrix. Dang et al. have reported a high dielectric constant in MWCNT-poly(vinylidenefluoride) (PVDF) composites (600 at 1Kz), but the loss is quite high (i.e., far over 2) with a percolation threshold of 8 vol%, and large dielectric dispersion at low frequency range; [147]then Nan et al. published a recent work in fabricating a modified carbon nanotubes (MWCTs were coated with Polypyrrole) composite with a stable high dielectric constant (~44), low loss (<0.07) and large energy density (up to 4.95 J cm^{-3}). [148] The percolation threshold has been reduced to 0.005 vol% in a single wall nanotube/ epoxy composite. [149]However, in most cases, the percolation threshold cannot reach low enough due to the poor dispersion and aggregation of nanotubes. In addition, the poor thermal stability (e.g. glass transition temperature <200 °C) of polymer matrix poses a problem for the processing of carbon

nanotube/polymer mixture via conventional methods, such as hot molding and spin coating. To solve this problem, zhao et al. develops a scalable spray deposition technique, which is able to fabricate a multi-wall carbon nanotube / fluoropolymer perfluoro alkoxy (PFA) composite film with good thermal stability (stable up to 230°C) and high dielectric constant of 9000 at 10 KHz with a percolation threshold at 0.0043. [150] Moreover, three component dielectrics with carbon nanotube were synthesized, which shows a dielectric constant ~150 at 100 Hz while maintaining a low dielectric loss of 0.08. [151]The resulting enhancement of carbon nanotube/polymer composite can be explained by Maxwell-Wagner (MW) percolation theory. There is still a lot of work to do with carbon nanotube based composite for energy storage applications. A main issue is how to dramatically lower the dielectric loss while maintaining high dielectric constant. And several parameters will be optimized to maximize the potential of such systems: aspect ratio, functionality of carbon nanotube, filler loading level, solubility and the dispersion homogeneity.

(3) Organic Materials

Above, I have discussed about how to develop the inorganic/polymer composite materials for high dielectric constant applications. Actually, significant progress has been made in this aspect. However, no matter what kind of inorganic fillers have been used, the dielectric performance will be limited by the percolation theory and the dielectric loss is high due to the interface polarization. Therefore, the question is: can we find high dielectric constant in an all-organic system? The answer is yes.

Pohl et al found the existence of giant dielectric constant (60-300,000) in ekaconjugated polyacene quinine radical (PAQR) polymers and he named the space

charge polarization mechanism operative in such systems as hyperelectronic polarization. The mechanism of this polarization has been discussed in the early part of this chapter already. One good example is that the dielectric constant of polyacequinone radical polymer can achieve 240,000 at low frequency. However, the dielectric constant drops dramatically at high frequency. [61] In 2008, Zhang et al. observed a dielectric constant ~1,200,000 at 100 Hz in a PAQR synthesized by solid-state polymerization. [144] The dielectric loss is quite huge (~30). However, no frequency dependence has been reported, so we have no idea about high frequency dielectric properties. In addition, their work in HO-PAQR and RO-PAQR polymers found that the dielectric constant would be lowered by adding hydroxyl and alkoxyl function groups, which suggests that the planar conjugation of the associated π orbital plays an important role in achieving high dielectric constant in such PAQR systems. High dielectric constant is not only observed for PAQR polymers, other polymer materials such as copper phthalocyanine (CuPc) and P(VDF-TrFE) exhibited high dielectric constant too. For instance, Nalwa et al observed a dielectric constant as high as 10^5 in a KOH treated CuPc oligomers. [152]Since 1998, Zhang et al have found a very good dielectric response (k ~80) in an electron-irradiated P(VDF-TrFE) copolymer [153]and they have published dozens of papers about the high dielectric properties of P(VDF-TrFE) based composites. For example, by dispersing high k CuPc oligomers fillers in P(VDF-TrFE) matrix, the actuator composite shows a dielectric constant of 225 and dielectric loss of 0.4 at 1Hz. [54] The high dielectric loss is explained by long-range intermolecular polaron hopping. Several years later, Lu et al. reported a dielectric constant ~ 3000 and a dielectric loss <0.5 at 10 KHz in an in-situ polymerized polyaniline (PANI)/epoxy composite. [154]

In general, the concept of utilizing all-organic material for high dielectric applications is reasonable. The high breakdown strength and relatively low dielectric loss are obtainable. The cost can be remarkably reduced too. However, for high frequency applications, we would require the dielectric loss < 0.01 and low dielectric dispersion. From the previous investigation experience in triarylamine dendrimers and ladder oligomers using ultrafast spectroscopy techniques, we discovered that the polaron delocalization originating from intra-molecular charge transfer in dendrimers would substantially enhance their electronic and optical properties, here shown an example of triarylamine dendrimers with delocalized polaron. [39] The profound understanding of polaron delocalization leads to a proposed novel strategy of creating all-organic high dielectric constant materials, especially for high frequency applications. This strategy targets at hyper-branched and dendritic conjugated polymers. The rationales behind this novel design criterion are: (1) they may provide a substantially longer polaron delocalization length in 3D dimensions. And a longer delocalization length may increase the dielectric constant and avoid the anisotropy of dielectric response; (2) they may show ultrafast polaron delocalization due to intra-molecular charge transfer, which is able to produce a fast dielectric response at high frequencies; (3) their planar structure may facilitate the self-assembly of the molecular and avoid unfavorable movement along the chain due to increased rigidity and steric effect. PANI and its derivatives are appealing to researchers as one of most promising conductive polymers appropriate for various applications: OLED, sensor et al. And a significant improvement in the optical and electronic properties of hyper-branched polyaniline has been observed in comparison to that of linear polyaniline. Therefore, we synthesized a series of ion-doped hyper-

branched polyaniline and investigated their dielectric properties. [39]The dielectric constant of these hyper-branched polyanilines achieves ~200 at 1MHz, double than that of linear polyaniline. The polaron hopping processes in these branched polyaniline is dominated by the Marcus-Hush mechanism and the hopping energy is <0.1 eV. The enhancement in dielectric response is originated from the strong polaron delocalization and hyperelectronic polarization in these hyper-branched systems. Inspired by these findings and based on the understanding of polaron delocalization mechanisms, we selected copper phthalocyanine based hyper-branched polymer structure as the polymer matrix base for a detailed study and try to build up a structure-function relationship to help future design. We do find an impressive dielectric constant about 46 up to 1MHz in a hyper-branched copper phthalocyanine (HBCuPc) polymer compressed pellet. [88]The dielectric loss of such a dendrimer film can go as low as 0.002 at 1MHz with very small dielectric dispersion. The detailed results and discussion will be itinerated in later chapters and a brief review on CuPc material will be presented below.

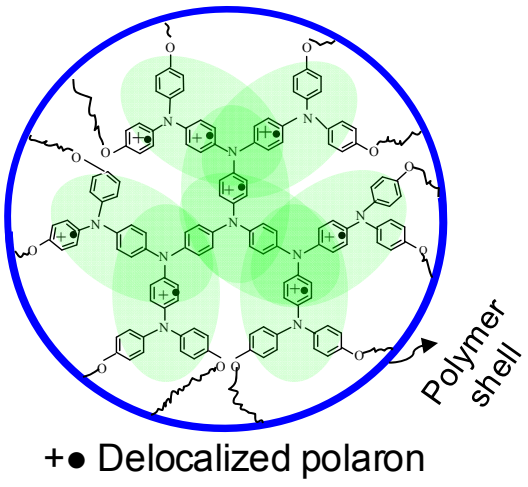

Scheme 1.6 An illustration of the concept of using polaron delocalization to enhance the dielectric response.

1.5 Copper Phthalocyanine Materials

Since the first synthesis in 1907, phthalocyanine based materials have been extensively investigated for numerous electronic and optical applications: field effect transistors, high energy density capacitors, dyes, pigments, catalysis, chemical sensors, photovoltaic cells, fuel cells, optical limiters, and photodynamic therapy of cancers. [54,81,155-162] The electronic and optical properties of phthalocyanine can be tuned by substituting the central metal atom, the axial and peripheral group; as well as adding dopants and varying the polymerization condition. A series of reports have been published regarding to the synthesis of phthalocyanine materials. [163-171]Phthalocyanine materials are highly conjugated aromatic macrocycles which contain thirty-eight delocalized π electrons in structure unit, as illustrated in Figure 1.3 [45]

Copper phthalocyanine (CuPc) has attracted our enthusiasm among other phthalocyanine materials due to its excellent thermal and chemical stability as well as unique electric properties. It has no dipole moment because it is symmetric, however, due to the delocalization within the phthalocyanine ring, a high electronic polarizability (1.2×10^{-22} cm^3) is obtained, which enables the enhancement of dielectric constant. [45,54,172-177]For example, Q.M. Zhang reported a high dielectric constant (>10,000) in an all-organic composite of CuPc oligomer/P (VDF-TrFE) polymer. The giant dielectric constant is due to the electron delocalization within the molecule. [54]Even a CuPc monomer can exhibit a dielectric constant ~ 5 and the dielectric dispersion is very low over a wide frequency range compared to other monomeric phthalocyanines (e.g. CoPc, FePc). For instance, Voet and Suriani reported a dielectric constant ~ 4.85 in a CuPc pellet. [178]

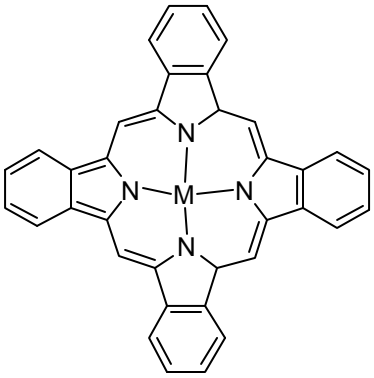

Figure 1.4 Molecular structures of phthalocyanine macrocycle (M=H or Metal).

The dielectric properties depends on the electrode material, synthesis, crystal structure (α or β phase), impurities, pressure, size and aggregation of CuPc particles. Due to the high conjugation and large planar structure feature of polymeric CuPc, it will show a higher dielectric constant and dielectric loss compared to monomer CuPc. For example, a dielectric constant ~46 was observed in a hyper branched copper phthalocyanine dendrimer as the π electrons are completely delocalized over the CuPc ring. [88] In addition, the dielectric response of polymeric CuPc is temperature and frequency dependent, but no clear tendency could be projected. For instance, a KOH treated poly-CuPc show a dielectric peak ($>10^5$) at 393K and 1 KHz, however, at room temperature, only a dielectric constant $<10^3$ was observed at the same frequency. [152]Moreover, it has been found that some poly-CuPc shows hyperelectronic polarization with intermediate dielectric constant at room temperature. Hence, it shows great potential in high dielectric constant applications.

1.5 Conclusion

In summary, I have gone through the fundamental theories necessary for the understanding of the experimental results I am going to discuss in the following chapters,

from chapter 3 to chapter 6. The aim of this dissertation is to discover the design criteria for an all-organic high dielectric constant material with high dielectric constant and low dielectric loss at high frequencies.

1.6 Dissertation Outline

The body of this dissertation is organized as follows:

In chapter 3, I will discuss the major findings from the investigation of the first series of hyperbranched copper phthalocyanine (HBCuPc) polymers. The dielectric measurement is carried out to characterize the dielectric properties of the HBCuPc polymer. Then we use the AC conductance measurement and time-of-flight (TOF) mobility measurement to probe the charge transfer mechanisms contributing the impressive dielectric response we observed in this hyperbranched polymer. In order to help the understanding of the charge transfer dynamics in both the ground and excited state, we also employed the steady-state and ultrafast spectroscopy techniques to study the optical properties of the HBCuPc polymers.

In chapter 4, I will talk about the synthesis and characterization of another novel hyperbranched copper phthalocyanine (HBCuPc-TPA-CN) polymer. We are interested in the study of the influence of the donor-acceptor strength on the dielectric properties of such kind systems. Also, we looked into the effect of the film substrate on the dielectric properties of the pristine films by means of the surface morphology characterization techniques such as scanning electron microscopy (SEM) and atomic force microscopy (AFM).

In chapter 5, I will focus on the relationship between the hyperbranched polymer architectures and their corresponding functions, aiming to define the design criteria of the

high dielectric hyperbranched polymer materials. For this purpose, a modified hyperbranched copper phthalocyanine polymer design will be presented and its electronic and optical properties will be discussed. In addition, a comparison will be drawn on these three series of hyperbranched copper phthalocyanine polymers trying to provide a clearer picture of the effective design. Furthermore, the optimization of the film preparation parameters such as the solvent and plasticizers will be useful to maximize the dielectric performance of the investigated hyperbranched copper phthalocyanine polymers.

In chapter 6, I will discuss the advantage of using the ultrafast up-conversion spectroscopy techniques as an effective approach to study the energy transfer dynamics in organic dendrimer systems. The fluorescence quenching dynamics of four generations of phosphorous dendrimer systems will be discussed in details.

Reference

(1) Dimitrakopoulos, C. D.; Purushothaman, S.; Kymissis, J.; Callegari, A.; Shaw, J. M. *Science* **1999**, *283*, 822-824.

(2) Homes, C. C.; Vogt, T.; Shapiro, S. M.; Wakimoto, S.; Ramirez, A. P. *Science* **2001**, *293*, 673-676.

(3) Carlson, C. M.; Rivkin, T. V.; Parilla, P. A.; Perkins, J. D.; Ginley, D. S.; Kozyrev, A. B.; Oshadchy, V. N.; Pavlov, A. S. *Applied Physics Letters* **2000**, *76*, 1920-1922.

(4) Scott, J. F. *Annual Review of Materials Science* **1998**, *28*, 79-100.

(5) Kotecki, D. E. *Integrated Ferroelectrics* **1997**, *16*, 1-19.

(6) Rao, Y.; Ogitani, S.; Kohl, P.; Wong, C. P. *Journal of Applied Polymer Science* **2002**, *83*, 1084-1090.

(7) Robertson, J. *European Physical Journal-Applied Physics* **2004**, *28*, 265-291.

(8) Pelrine, R.; Kornbluh, R.; Kofod, G. *Advanced Materials* **2000**, *12*, 1223-1225.

(9) Dang, Z. M.; Zhou, T.; Yao, S. H.; Yuan, J. K.; Zha, J. W.; Song, H. T.; Li, J. Y.; Chen, Q.; Yang, W. T.; Bai, J. *Advanced Materials* **2009**, *21*, 2077.

(10) Jiang, S. L.; Yu, Y.; Zeng, Y. K. *Current Applied Physics* **2009**, *9*, 956-959.

(11) Raval, H. N.; Tiwari, S. P.; Navan, R. R.; Mhaisalkar, S. G.; Rao, V. R. *IEEE Electron Device Letters* **2009**, *30*, 484-486.

(12) Khan, M. Z. R.; Hasko, D. G.; Saifullah, M. S. M.; Welland, M. E. *Journal of Physics-Condensed Matter* **2009**, *21*.

(13) Heeger, A. J. *Journal of Physical Chemistry B* **2001**, *105*, 8475-8491.

(14) Bredas, J. L.; Silbey, R.; Boudreaux, D. S.; Chance, R. R. *Journal of the American Chemical Society* **1983**, *105*, 6555-6559.

(15) Bredas, J. L.; Street, G. B.; Themans, B.; Andre, J. M. *Journal of Chemical Physics* **1985**, *83*, 1323-1329.

(16) Furukawa, Y.; Akimoto, M.; Harada, I. *Synthetic Metals* **1987**, *18*, 151-156.

(17) Hill, M. G.; Mann, K. R.; Miller, L. L.; Penneau, J. F. *Journal of the American Chemical Society* **1992**, *114*, 2728-2730.

(18) Tsumura, A.; Koezuka, H.; Ando, T. *Applied Physics Letters* **1986**, *49*, 1210-1212.

(19) Clark, J.; Chang, J. F.; Spano, F. C.; Friend, R. H.; Silva, C. *Applied Physics Letters* **2009**, *94*.

(20) Lu, K.; Guo, Y. L.; Liu, Y. Q.; Di, C. A.; Li, T.; Wei, Z. M.; Yu, G.; Du, C. Y.; Ye, S. H. *Macromolecules* **2009**, *42*, 3222-3226.

(21) Park, Y. D.; Lee, H. S.; Choi, Y. J.; Kwak, D.; Cho, J. H.; Lee, S.; Cho, K. *Advanced Functional Materials* **2009**, *19*, 1200-1206.

(22) Zhang, B. Z.; Zhao, X. Y. *Journal of Materials Science* **2009**, *44*, 2765-2773.

(23) Gao, M. M.; Yang, F. L.; Wang, X. H.; Zhang, G. Q.; Liu, L. F. *Electroanalysis* **2009**, *21*, 1035-1040.

(24) Krishna, J. B. M.; Saha, A.; Okram, G. S.; Purakayastha, S.; Ghosh, B. *Journal of Physics D-Applied Physics* **2009**, *42*.

(25) Chiang, J. C.; Macdiarmid, A. G. *Synthetic Metals* **1986**, *13*, 193-205.

(26) Huang, W. S.; Humphrey, B. D.; Macdiarmid, A. G. *Journal of the Chemical Society-Faraday Transactions I* **1986**, *82*, 2385.

(27) Macdiarmid, A. G.; Chiang, J. C.; Halpern, M.; Huang, W. S.; Mu, S. L.; Somasiri, N. L. D.; Wu, W. Q.; Yaniger, S. I. *Molecular Crystals and Liquid Crystals* **1985**, *121*, 173-180.

(28) Macdiarmid, A. G.; Chiang, J. C.; Richter, A. F.; Epstein, A. J. *Synthetic Metals* **1987**, *18*, 285-290.

(29) Nagamatsu, S.; Misaki, M.; Yoshida, Y.; Azumi, R.; Tanigaki, N.; Yase, K. *Journal of Physical Chemistry B* **2009**, *113*, 5746-5751.

(30) Wong, W. W. H.; Hooper, J. F.; Holmes, A. B. *Australian Journal of Chemistry* **2009**, *62*, 393-401.

(31) Zhao, Y.; Xie, Z. Y.; Qin, C. J.; Qu, Y.; Geng, Y. H.; Wang, L. X. *Solar Energy Materials and Solar Cells* **2009**, *93*, 604-608.

(32) Grell, M.; Bradley, D. D. C.; Ungar, G.; Hill, J.; Whitehead, K. S. *Macromolecules* **1999**, *32*, 5810-5817.

(33) Klaerner, G.; Miller, R. D. *Macromolecules* **1998**, *31*, 2007-2009.

(34) List, E. J. W.; Guentner, R.; de Freitas, P. S.; Scherf, U. *Advanced Materials* **2002**, *14*, 374-378.

(35) Pei, Q. B.; Yang, Y. *Journal of the American Chemical Society* **1996**, *118*, 7416-7417.

(36) Redecker, M.; Bradley, D. D. C.; Inbasekaran, M.; Woo, E. P. *Applied Physics Letters* **1998**, *73*, 1565-1567.

(37) Liu, C. Y.; Chen, S. A. *Macromolecular Rapid Communications* **2007**, *28*, 1743-1760.

(38) Kline, R. J.; McGehee, M. D. *Polymer Reviews* **2006**, *46*, 27-45.

(39) Yan, X. Z.; Pawlas, J.; Goodson, T.; Hartwig, J. F. *Journal of the American Chemical Society* **2005**, *127*, 9105-9116.

(40) Varnavski, O.; Yan, X. Z.; Mongin, O.; Blanchard-Desce, M.; Goodson, T. *Journal of Physical Chemistry C* **2007**, *111*, 149-162.

(41) Ramakrishna, G.; Bhaskar, A.; Bauerle, P.; Goodson, T. *Journal of Physical Chemistry A* **2008**, *112*, 2018-2026.

(42) Hagedorn, K. V.; Varnavski, O.; Hartwig, J.; Goodson, T. *Journal of Physical Chemistry C* **2008**, *112*, 2235-2238.

(43) Guo, M.; Varnavski, O.; Narayanan, A.; Mongin, O.; Majoral, J. P.; Blanchard-Desce, M.; Goodson, T. *Journal of Physical Chemistry A* **2009**, *113*, 4763-4771.

(44) Satoh, N.; Cho, J. S.; Higuchi, M.; Yamamoto, K. *Journal of the American Chemical Society* **2003**, *125*, 8104-8105.

(45) *Handbook of Low and High Dielectric Constant Materials and Their Applications*; Nalwa, H. S., Ed.; Academic Press: London, UK, **1999**; Vol. 1.

(46) Vouyovitch, L.; Alberola, N. D.; Flandin, L.; Beroual, A.; Bessede, J. L. *Ieee Transactions on Dielectrics and Electrical Insulation* **2006**, *13*, 282-292.

(47) *Dielectric Phenomena in Solids: With Emphasis on Physical Concepts of Electronic Processes* Kao, K. C., Ed.; Academic Press: London, UK, **2004**.

(48) Langevin, P. *Annales De Chimie Et De Physique* **1905**, *5*, 70-127.

(49) Debye, P. *Physikalische Zeitschrift* **1912**, *13*, 97-100.

(50) *Polar Molecules*; Debye, P., Ed.; Dover: New York, **1945**.

(51) Park, Y. W.; Moon, J. S.; Bak, M. K.; Jin, J. I. *Synthetic Metals* **1989**, *29*, E389-E394.

(52) Bai, Y.; Cheng, Z. Y.; Bharti, V.; Xu, H. S.; Zhang, Q. M. *Applied Physics Letters* **2000**, *76*, 3804-3806.

(53) Clayton, L. M.; Sikder, A. K.; Kumar, A.; Cinke, M.; Meyyappan, M.; Gerasimov, T. G.; Harmon, J. P. *Advanced Functional Materials* **2005**, *15*, 101-106.

(54) Zhang, Q. M.; Li, H. F.; Poh, M.; Xia, F.; Cheng, Z. Y.; Xu, H. S.; Huang, C. *Nature* **2002**, *419*, 284-287.

(55) Yao, S. H.; Dang, Z. M.; Jiang, M. J.; Bai, J. B. *Applied Physics Letters* **2008**, *93*.

(56) Benhamouda, A.; Fornies-Marquina, J. M.; Bouzit, N.; Bourouba, N. *European Physical Journal-Applied Physics* **2009**, *46*.

(57) Chen, Q.; Jin, L.; Weng, W. J.; Han, G. R.; Du, P. Y. *Surface Review and Letters* **2008**, *15*, 19-22.

(58) Dang, Z. M.; Fan, L. Z.; Shen, Y.; Nan, C. W. *Chemical Physics Letters* **2003**, *369*, 95-100.

(59) Dang, Z. M.; Yu, Y. F.; Xu, H. P.; Bai, J. *Composites Science and Technology* **2008**, *68*, 171-177.

(60) Hartman, R. D.; Pohl, H. A. *Journal of Polymer Science Part a-1-Polymer Chemistry* **1968**, *6*, 1135.

(61) Wyhof, J. R.; Pohl, H. A. *Journal of Polymer Science Part a-2-Polymer Physics* **1970**, *8*, 1741.

(62) Meisel, K. D.; Vocks, H.; Bobbert, P. A. *Physical Review B* **2005**, *71*.

(63) Susumu, K.; Frail, P. R.; Angiolillo, P. J.; Therien, M. J. *Journal of the American Chemical Society* **2006**, *128*, 8380-8381.

(64) Quemerais, P.; Fratini, S. *Modern Physics Letters B* **1997**, *11*, 1303-1312.

(65) Bagnich, S. A.; Im, C.; Bassler, H.; Neher, D.; Scherf, U. *Chemical Physics* **2004**, *299*, 11-16.

(66) Fishchuk, I.; Kadashchuk, A.; Devi, L. S.; Heremans, P.; Bassler, H.; Kohler, A. *Physical Review B* **2008**, *78*.

(67) Ranasinghe, M. I.; Hager, M. W.; Gorman, C. B.; Goodson, T. *Journal of Physical Chemistry B* **2004**, *108*, 8543-8549.

(68) J.R.Lakowicz; 2 ed.; Kluwer Academic/Plenum Publishers: New York, **1999**.

(69) Hallermann, M.; Haneder, S.; Da Como, E. *Applied Physics Letters* **2008**, *93*.

(70) Aziz, E. E.; Vollmer, A.; Eisebitt, S.; Eberhardt, W.; Pingel, P.; Neher, D.; Koch, N. *Advanced Materials* **2007**, *19*, 3257.

(71) Salikhov, R. B.; Lachinov, A. N.; Bunakov, A. A. *Physics of the Solid State* **2007**, *49*, 185-188.

(72) Tanaka, D.; Horike, S.; Kitagawa, S.; Ohba, M.; Hasegawa, M.; Ozawa, Y.; Toriumi, K. *Chemical Communications* **2007**, 3142-3144.

(73) Emin, D. *Phys Rev Lett* **2008**, *100*, 166602.

(74) Guo, M.; Yan, X. Z.; Goodson, T. *Advanced Materials* **2008**, *20*, 4167.

(75) Kreouzis, T.; Poplavskyy, D.; Tuladhar, S. M.; Campoy-Quiles, M.; Nelson, J.; Campbell, A. J.; Bradley, D. D. C. *Physical Review B* **2006**, *73*.

(76) Hultell, M.; Stafstrom, S. *Physical Review B* **2007**, *75*.

(77) Friedman, L.; Holstein, T. *Annals of Physics* **1963**, *21*, 494-549.

(78) Holstein, T. *Annals of Physics* **1959**, *8*, 343-389.

(79) Emin, D.; Holstein, T. *Annals of Physics* **1969**, *53*, 439.

(80) Emin, D.; Holstein, T. *Physical Review Letters* **1976**, *36*, 323-326.

(81) Gould, R. D. *Coordination Chemistry Reviews* **1996**, *156*, 237-274.

(82) *Electronic Processes in Non-Crystalline Materials*; Mott, N. F. D., E., Ed.; Clarendon Press: Oxford, **1979**.

(83) Petty, M. C. *Molecular Electronics: From Principles to Practice*; John Wiley & Sons Ltd.: Chichester, **2007**.

(84) Nelson, S. F.; Lin, Y. Y.; Gundlach, D. J.; Jackson, T. N. *Applied Physics Letters* **1998**, *72*, 1854-1856.

(85) Silinsh, E. A.; Klimkans, A.; Larsson, S.; Capek, V. *Chemical Physics* **1995**, *198*, 311-331.

(86) Vidadi, Y. A. R., L.D.; Chistyakov, E.A. *Sov. Phys. Solid State* **1969**, 173.

(87) Ahmad, K.; Pan, W.; Shi, S. L. *Applied Physics Letters* **2006**, *89*.

(88) Guo, M.; Yan, X. Z.; Kwon, Y.; Hayakawa, T.; Kakimoto, M. A.; Goodson, T. *Journal of the American Chemical Society* **2006**, *128*, 14820-14821.

(89) Bobnar, V.; Levstik, A.; Huang, C.; Zhang, Q. M. *Phys Rev Lett* **2004**, *92*, 047604.

(90) DiBenedetto, S. A.; Facchetti, A.; Ratner, M. A.; Marks, T. J. *Journal of the American Chemical Society* **2009**, *131*, 7158-7168.

(91) Bouhassoune, M.; van Mensfoort, S. L. M.; Bobbert, P. A.; Coehoorn, R. *Organic Electronics* **2009**, *10*, 437-445.

(92) Kazukauskas, V.; Pranaitis, M.; Cyras, V.; Sicot, L.; Kajzar, F. *Thin Solid Films* **2008**, *516*, 8988-8992.

(93) Nagata, Y.; Lennartz, C. *J Chem Phys* **2008**, *129*, 034709.

(94) Simmons, J. G. *Physical Review* **1967**, *155*, 657.

(95) Ieda, M.; Sawa, G.; Kato, S. *Journal of Applied Physics* **1971**, *42*, 3737.

(96) Hartke, J. L. *Journal of Applied Physics* **1968**, *39*, 4871.

(97) Hill, R. M. *Philosophical Magazine* **1971**, *23*, 59.

(98) Pautmeier, L.; Richert, R.; Bassler, H. *Synthetic Metals* **1990**, *37*, 271-281.

(99) Mark, P.; Hartman, T. E. *Journal of Applied Physics* **1968**, *39*, 2163.

(100) Gregg, B. A. *Journal of Physical Chemistry C* **2009**, *113*, 5899-5901.

(101) Wu, S. H.; Wang, S.; Chen, L. Y.; Wang, X. Y. *Journal of Materials Science-Materials in Electronics* **2008**, *19*, 505-508.

(102) Zhu, J. L.; Jin, C. Q.; Cao, W. W.; Wang, X. H. *Applied Physics Letters* **2008**, *92*.

(103) Bobade, S. M.; Gopalan, P.; Choi, D. K. *Japanese Journal of Applied Physics* **2009**, *48*.

(104) Fina, I.; Dix, N.; Laukhin, V.; Fabrega, L.; Sanchez, F.; Fontcuberta, J. *Journal of Magnetism and Magnetic Materials* **2009**, *321*, 1795-1798.

(105) Hiltunen, J.; Seneviratne, D.; Tuller, H. L.; Lappalainen, J.; Lantto, V. *Journal of Electroceramics* **2009**, *22*, 395-404.

(106) Jain, T. A.; Chen, C. C.; Fung, K. Z. *Journal of Alloys and Compounds* **2009**, *476*, 414-419.

(107) Qiao, L.; Bi, X. F. *Applied Physics a-Materials Science & Processing* **2009**, *95*, 733-738.

(108) Jayanthi, S.; Kutty, T. R. N. *Journal of Materials Science-Materials in Electronics* **2008**, *19*, 615-626.

(109) Park, J. M.; Lee, H. Y.; Kim, J. J.; Park, E. T.; Chung, Y. K. *IEEE Transactions on Ultrasonics Ferroelectrics and Frequency Control* **2008**, *55*, 1038-1042.

(110) Wada, N.; Hiramatsu, T.; Tamura, T.; Sakabe, Y. *Ceramics International* **2008**, *34*, 933-937.

(111) Onodera, A.; Takesada, M. In *9th International Russia-Commonwealth of Independent States-Baltic and States-Japan Symposium on Ferroelectricity*; Taylor & Francis Ltd: Vilnius, LITHUANIA, **2008**, p 239-245.

(112) Amaral, F.; Rubinger, C. P. L.; Valente, M. A.; Costa, L. C.; Moreira, R. L. *Journal of Applied Physics* **2009**, *105*.

(113) Ni, L.; Chen, X. M. *Solid State Communications* **2009**, *149*, 379-383.

(114) Thomas, P.; Dwarakanath, K.; Varma, K. B. R.; Kutty, T. R. N. *Journal of Thermal Analysis and Calorimetry* **2009**, *95*, 267-272.

(115) Prakash, B. S.; Varma, K. B. R. *Journal of Nanoscience and Nanotechnology* **2008**, *8*, 5762-5769.

(116) Jin, S. H.; Xia, H. P.; Zhang, Y. P. *Ceramics International* **2009**, *35*, 309-313.

(117) Smith, A. E.; Calvarese, T. G.; Sleight, A. W.; Subramanian, M. A. *Journal of Solid State Chemistry* **2009**, *182*, 409-411.

(118) Zhu, B. P.; Wang, Z. Y.; Zhang, Y.; Yu, Z. S.; Shi, J.; Xiong, R. *Materials Chemistry and Physics* **2009,** *113*, 746-748.

(119) Thongbai, P.; Yamwong, T.; Maensiri, S. *Applied Physics Letters* **2009**, *94*.

(120) Barber, P.; Houghton, H.; Balasubramanian, S.; Anguchamy, Y. K.; Ploehn, H. J.; zur Loye, H. C. *Chemistry of Materials* **2009**, *21*, 1303-1310.

(121) Dang, Z. M.; Lin, Y. Q.; Xu, H. P.; Shi, C. Y.; Li, S. T.; Bai, J. B. *Advanced Functional Materials* **2008**, *18*, 1509-1517.

(122) Deng, Y.; Zhang, Y. J.; Xiang, Y.; Wang, G. S.; Xu, H. B. *Journal of Materials Chemistry* **2009**, *19*, 2058-2061.

(123) Li, Y.; Pothukuchi, S.; Wong, C. P. *9th International Symposium on Advanced Packaging Materials: Processes, Properties and Interfaces, 2004 Proceedings* **2004**, 175-181.

(124) Lu, J. X.; Wong, C. P. *Ieee Transactions on Dielectrics and Electrical Insulation* **2008**, *15*, 1322-1328.

(125) Lu, J.; Moon, K. S.; Min, B. K.; Wong, C. P. *IEEE CPMT: International Symposium and Exhibition on Advanced Packaging Materials: Processes, Properties and Interfaces* **2006**, 88-92.

(126) Rao, Y.; Wong, C. P. *Journal of Applied Polymer Science* **2004**, *92*, 2228-2231.

(127) Takahashi, A.; Kakimoto, M.; Tsurumi, T. A.; Hao, J. J.; Li, L.; Kikuchi, R.; Miwa, T.; Oono, T.; Yamada, S. *Journal of Photopolymer Science and Technology* **2005**, *18*, 297-300.

(128) Lu, J. X.; Moon, K. S.; Xu, J. W.; Wong, C. P. *Journal of Materials Chemistry* **2006**, *16*, 1543-1548.

(129) Xu, J. W.; Wong, C. P. *54th Electronic Components & Technology Conference, Vols 1 and 2, Proceedings* **2004**, 496-506.

(130) Shen, Y.; Lin, Y. H.; Nan, C. W. *Advanced Functional Materials* **2007**, *17*, 2405-2410.

(131) Pecharroman, C.; Moya, J. S. *Advanced Materials* **2000**, *12*, 294-297.

(132) Lu, J.; Moon, K. S.; Wong, C. P. *Journal of Materials Chemistry* **2008**, *18*, 4821-4826.

(133) Kobayashi, Y.; Tanase, T.; Tabata, T.; Miwa, T.; Konno, M. *Journal of the European Ceramic Society* 2008, *28*, 117-122.

(134) Dang, Z. M.; Lin, Y. H.; Nan, C. W. *Advanced Materials* **2003**, *15*, 1625.

(135) Qi, L.; Lee, B. I.; Chen, S. H.; Samuels, W. D.; Exarhos, G. J. *Advanced Materials* **2005**, *17*, 1777.

(136) Xu, J. W.; Wong, C. P. *Applied Physics Letters* **2005**, *87*.

(137) Mdarhri, A.; Khissi, M.; Achour, M. E.; Carmona, F. *European Physical Journal-Applied Physics* **2008**, *41*, 215-220.

(138) Xu, H. P.; Dang, Z. M.; Jiang, M. J.; Yao, S. H.; Bai, J. *Journal of Materials Chemistry* **2008**, *18*, 229-234.

(139) Xu, J. W.; Wong, M.; Wong, C. P. *54th Electronic Components & Technology Conference, Vols 1 and 2, Proceedings* **2004**, 536-541.

(140) He, F.; Lau, S.; Chan, H. L.; Fan, F. *Advanced Materials* **2009**, *21*, 710.

(141) Stankovich, S.; Dikin, D. A.; Dommett, G. H. B.; Kohlhaas, K. M.; Zimney, E. J.; Stach, E. A.; Piner, R. D.; Nguyen, S. T.; Ruoff, R. S. *Nature* **2006**, *442*, 282-286.

(142) Avouris, P.; Freitag, M.; Perebeinos, V. *Nature Photonics* **2008**, *2*, 341-350.

(143) Sharma, P.; Ahuja, P. *Materials Research Bulletin* **2008**, *43*, 2517-2526.

(144) Zhang, J.; Zhu, D.; Matsuo, M. *Polymer* **2008**, *49*, 5424-5430.

(145) Kaushik, B. K.; Goel, S.; Rauthan, G. *Microelectronics International* **2007**, *24*, 53-63.

(146) Peng, C.; Zhang, S. W.; Jewell, D.; Chen, G. Z. *Progress in Natural Science* **2008**, *18*, 777-788.

(147) Dang, Z. M.; Wang, L.; Yin, Y.; Zhang, Q.; Lei, Q. Q. *Advanced Materials* **2007**, *19*, 852.

(148) Yang, C.; Lin, Y. H.; Nan, C. W. *Carbon* **2009**, *47*, 1096-1101.

(149) Bryning, M. B.; Islam, M. F.; Kikkawa, J. M.; Yodh, A. G. *Advanced Materials* **2005**, *17*, 1186.

(150) Zhao, X.; Koos, A. A.; Chu, B. T. T.; Johnston, C.; Grobert, N.; Grant, P. S. *Carbon* **2009**, *47*, 561-569.

(151) Yao, S. H.; Dang, Z. M.; Xu, H. P.; Jiang, M. J.; Bai, J. *Applied Physics Letters* **2008**, *92*.

(152) Nalwa, H. S.; Dalton, L. R.; Vasudevan, P. *European Polymer Journal* **1985**, *21*, 943-947.

(153) Zhang, Q. M.; Bharti, V.; Zhao, X. *Science* **1998**, *280*, 2101-2104.

(154) Lu, J. X.; Moon, K. S.; Kim, B. K.; Wong, C. P. *Polymer* **2007**, *48*, 1510-1516.

(155) Dimitrakopoulos, C. D.; Malenfant, P. R. L. *Advanced Materials* **2002**, *14*, 99.

(156) Dougherty, T. J. *Photochemistry and Photobiology* **1987**, *45*, 879-889.

(157) Shirota, Y. *Journal of Materials Chemistry* **2000**, *10*, 1-25.

(158) Perry, J. W.; Mansour, K.; Lee, I. Y. S.; Wu, X. L.; Bedworth, P. V.; Chen, C. T.; Ng, D.; Marder, S. R.; Miles, P.; Wada, T.; Tian, M.; Sasabe, H. *Science* **1996**, *273*, 1533-1536.

(159) Spikes, J. D. *Photochemistry and Photobiology* **1986**, *43*, 691-699.

(160) Wohrle, D.; Meissner, D. *Advanced Materials* **1991**, *3*, 129-138.

(161) Bao, Z.; Lovinger, A. J.; Dodabalapur, A. *Applied Physics Letters* **1996**, *69*, 3066-3068.

(162) Herron, N.; Stucky, G. D.; Tolman, C. A. *Journal of the Chemical Society-Chemical Communications* **1986**, 1521-1522.

(163) Kwon, Y.; Hayakawa, T.; Kakimoto, M. A. *Chemistry Letters* **2006**, *35*, 1306-1307.

(164) Chen, X. C.; Salmon, T. R.; McGrath, D. V. *Organic Letters* **2009**, *11*, 2061-2064.

(165) Cid, J. J.; Ehli, C.; Atienza-Castellanos, C.; Gouloumis, A.; Maya, E. M.; Vazquez, P.; Torres, T.; Guldi, D. M. *Dalton Transactions* **2009**, 3955-3963.

(166) Saydam, S.; Yilmaz, E.; Bagci, F.; Yaglioglu, H. G.; Elmali, A.; Salih, B.; Bekaroglu, O. *European Journal of Inorganic Chemistry* **2009**, 2096-2103.

(167) Makhseed, S.; Samuel, J. *Dyes and Pigments* **2009**, *82*, 1-5.

(168) Soares, A. R. M.; Tome, J. P. C.; Neves, M.; Tome, A. C.; Cavaleiro, J. A. S.; Torres, T. *Carbohydrate Research* **2009**, *344*, 507-510.

(169) Ahsen, V.; Yilmazer, E.; Ertas, M.; Bekaroglu, O. *Journal of the Chemical Society-Dalton Transactions* **1988**, 401-406.

(170) del Rey, B.; Keller, U.; Torres, T.; Rojo, G.; Agullo-Lopez, F.; Nonell, S.; Marti, C.; Brasselet, S.; Ledoux, I.; Zyss, J. *Journal of the American Chemical Society* **1998,** *120*, 12808-12817.

(171) Fox, J. M.; Katz, T. J.; Van Elshocht, S.; Verbiest, T.; Kauranen, M.; Persoons, A.; Thongpanchang, T.; Krauss, T.; Brus, L. *Journal of the American Chemical Society* **1999**, *121*, 3453-3459.

(172) Wang, J. W.; Wang, Y.; Wang, F.; Li, S. Q.; Xiao, J.; Shen, Q. D. *Polymer* **2009**, *50*, 679-684.

(173) Wang, Y.; Wang, J. W.; Wang, F.; Li, S. Q.; Xiao, J. *Polymer Bulletin* **2008**, *60*, 647-655.

(174) Bobnar, V.; Levstik, A.; Huang, C.; Zhang, Q. M. *Ferroelectrics* **2006**, *338*, 1523-1532.

(175) Shi, N.; Ramprasad, R. *Physical Review B* **2007**, *75*.

(176) Shi, N.; Ramprasad, R. *Applied Physics Letters* **2006**, *89*.

(177) Wang, J. W.; Shen, Q. D.; Bao, H. M.; Yang, C. Z.; Zhang, Q. M. *Macromolecules* **2005**, *38*, 2247-2252.

(178) Voet, A.; Suriani, L. R. *Journal of Colloid Science* **1952**, *7*, 1-10.

Chapter 2

Experimental Techniques

A series of optical and electronic techniques have been utilized to characterize the properties of polymer systems under investigation. In this chapter, a brief introduction to experiment principles, theories and general set-ups of some techniques will be laid out to provide a framework for understanding. More technical details will be elucidated in the experimental session of each chapter wherever it is used.

2.1 Capacitance Measurement

Dielectric constant is one of the key parameters in a high performance dielectric material. The dielectric properties can be characterized by directly measuring the magnitude and the phase of the current passing through the composite under a given AC voltage. It is related to the capacitance of the material. If we assume the material polarized by an AC sinusoidal field, the effect can be treated as a capacitor C in parallel with a conductor G (Figure 2.1). The complex electric impedance is given as:

$$Z^* = 1/(i\omega C^*) \tag{2.1}$$

And, the capacitance is expressed as:

$$C^* = (\varepsilon_r - i\varepsilon_i)\varepsilon_0 A/d \tag{2.2}$$

In above equations, ω is the angular frequency; ε_0 is the vacuum permittivity (8.8542×10^{-12} F/m); ε_r and ε_i are the real and imaginary part of dielectric constant

respectively; A is the contact electrode area and d is the thickness of the capacitor. Both ε_r and ε_i can be derived from the above and the complex dielectric constant then can be described as:

$$\varepsilon^* = \varepsilon_r - i\varepsilon_i \tag{2.3}$$

The loss tangent is given by:

$$\tan\delta = \frac{\varepsilon_r}{\varepsilon_i} \tag{2.4}$$

And the error for the measurement may be related to parameters which include the capacitance, the thickness of the dielectric sample and the area of the electrode.

$$(\frac{\Delta\varepsilon_r}{\varepsilon_r})^2 = (\frac{\Delta C}{C})^2 + (\frac{\Delta d}{d})^2 + (\frac{\Delta A}{A})^2 \tag{2.5}$$

The measurement accuracy is also affected by the shape and edge effect of the sample.

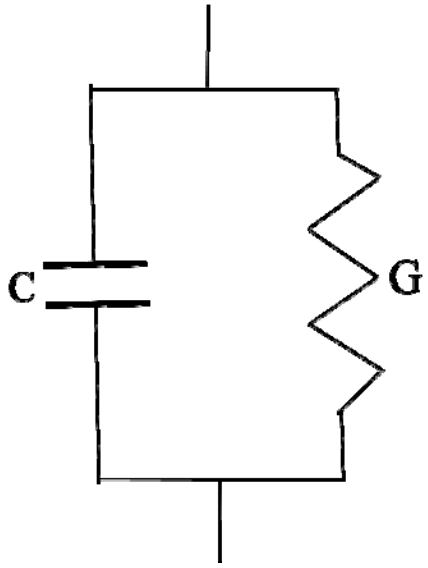

Figure 2.1 Equivalent circuit of the capacitance measurement

In our lab, HP LCR 4284A meter is connected with a 16451B dielectric test fixture (Figure 2.2) to directly record the variance of the capacitance and the dielectric loss of dielectric materials with the frequency. The applicable test frequency range is between 20Hz to 1MHz. The measurement range for the dielectric constant is 1 to 200,000 and the dielectric loss is 0.000001 to 9.99999. However, it depends on the measurement conditions. The measurement accuracy is pretty good in this set-up. For the dielectric constant measurement, the error is about ± 1%; and the dielectric loss measurement accuracy goes to ± (5%+0.005).

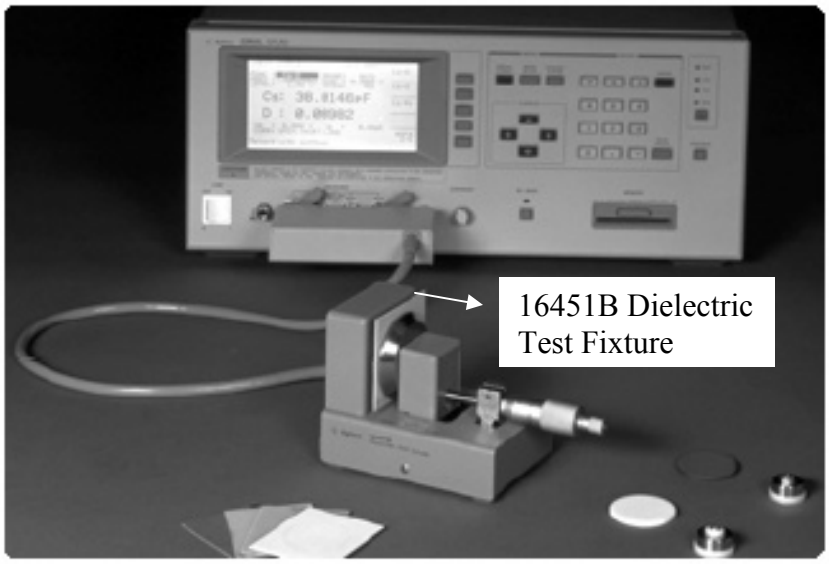

Figure 2.2 Dielectric experiment set-ups

In this set-up, the compressed pellets or pristine films of dielectric materials are inserted into two guarded electrodes with an effective electrode contact area (A) of 1.963×10^{-5} m^2. The thickness of the dielectric material will be characterized by the scanning electron microscopy (SEM) cross section measurement or the Dektak profiler. Once the thickness d is known, we can derive the dielectric constant from the capacitance by:

$$\varepsilon_r = \frac{Cd}{\varepsilon_0 A} \tag{2.6}$$

2.2 Steady-State Spectroscopy

UV-Vis absorption and steady-state fluorescence spectroscopy are two basic methods to characterize the optical properties of polymer materials. UV-Vis absorption follows a Beer-Lambert law: [1]

$$A = \varepsilon \cdot b \cdot C \tag{2.7}$$

Where, ε is the absorption coefficient, b is the light length and C is the concentration of absorbing materials. UV-vis spectrum will provide information about stable electronic states and inter-valence, as well as intra-molecular electronic coupling and polaron delocalization information.

The steady-state emission may yield some information on the intra-molecular relaxation to some extension. For example, the emission characteristics of triarylamine derivatives showed an intra-molecular interaction, which correlated to the interactions of the charge carrier and exciton. [2] These intra-molecular interactions can be detected through site-selective fluorescence spectroscopy that yields the true Stokes shift unsatisfied by spectra diffusion. The Stokes shift is therefore a measure of any relaxation which the molecule can undergo within its lifetime, such as the complex formation and energy transfer. [3] This measurement may give some information for the polaronic excitations and charge transfer.

2.3 Femtosecond Up-Converted Fluorescence Spectroscopy

Fluorescence up-conversion technique is used for measuring the intensity decays or anisotropy decays. It was already well established in the 70s and 80s. For example,

Lewis et al. used this technique to measure the emission lifetime of bacteriorhodopsin and they were able to resolve the lifetime at a time scale of ~ 15ps. [4] With its natural adaption to ultrafast process, it has become a very powerful tool for the study of ultra-fast excited state dynamics in a conjugated material, especially the one with very weak fluorescence and can hardly be detected by conventional steady-state fluorescence spectroscopy. [2,5-10] Among major advantages of this technique, the selective sensitivity to population dynamics of the fluorescent excited state makes this technique very popular. [11]

The fundamental theory about up-converted fluorescence lies in the fact that the emission from most materials is polarized upon light excitation. After the excitation, the randomly oriented absorption transition moments of the fluorophores in the ground state will orient towards the electric vector of the polarized light. Therefore, the process causes the depolarization of the emission. [3] There are several possible resources to contribute to the depolarization, such as rotational diffusion of fluorophores and resonance energy transfer (RET) processes. In general, the sample is excited with vertically polarized light. The direction of the polarizer can be aligned either parallel or perpendicular to the excitation and the intensity of emission detected will be called I_{par} and I_{per} respectively. The extent of polarization of the emission is described in terms of anisotropy (r). [3]

$$r = \frac{I_{par} - I_{per}}{I_{par} + 2I_{per}} \tag{2.8}$$

Actual emission intensity will be compensated by introducing a G factor, which is the ratio of the sensitivities of the detection system for vertically and horizontally polarized light. The anisotropy will then become: [3]

$$r = \frac{I_{par} - G \cdot I_{per}}{I_{par} + 2 \cdot G \cdot I_{per}} \tag{2.9}$$

For a single fluorophore oriented along the z-axis, the anisotropy value is 1. However, due to excitation photoselection of fluorophores in addition to the fact that the absorption and emission moments were not collinear in most cases, the anisotropy value is less than 0.4 for most fluorophores and depend on the excitation wavelength. In the absence of depolarizing processes, the fundamental anisotropy of a fluorophore is given by: [3]

$$r_0 = \frac{2}{5}\left(\frac{3\cos^2\beta - 1}{2}\right) \tag{2.10}$$

Rotation diffusion of fluorophore is a dominant cause of fluorescence depolarization. This depolarization mode is described in the simplest case for spherical rotors by the Perrin equation: [12]

$$\frac{r_0}{r} = 1 + \frac{\tau}{\theta} = 1 + 6D\tau \tag{2.11}$$

Where τ is the fluorescence lifetime; θ is the rotational correlation time and D is the rotational diffusion coefficient. If the correlation time is much larger than the lifetime ($\theta \gg \tau$), the measured anisotropy (r) is equal to the fundamental anisotropy (r_0). If the correlation time is much shorter than the lifetime ($\theta \ll \tau$), the anisotropy is zero.

Fluorescence resonance energy transfer (FRET) is another important process contributes to the depolarization. The description of this process is covered in chapter 1 already. In principle, the rate of energy transfer depends upon the extent of spectral overlap of the emission spectrum of the donor with the absorption spectrum of the acceptor, the quantum yield of the donor, the relative orientation of the donor and acceptor transition dipoles, and the distance between the donor and acceptor molecules. [3] The rate of energy transfer from a donor to an acceptor is given by: [3]

$$k_T = \frac{1}{\tau_D}(\frac{R_0}{r})^6 \tag{2.12}$$

Where τ_D is the decay time of the donor in the absence of acceptor; R_0 is the Förster distance and r is the donor-to-acceptor (D-A) distance. Anisotropy measurement has been applied to provide valuable information for the studies of exciton diffusion, [13] energy transfer [6] and excitation relaxation et al. [14]

Another widely used term is polarization, which is given by: [3]

$$r = \frac{I_{par} - I_{per}}{I_{par} + I_{per}} \tag{2.13}$$

Fluorescence quenching is an important aspect we have to mention. It refers to any process which decreases the fluorescence intensity of a sample. A variety of molecular interactions can result in quenching. These include excited-state reactions, molecular rearrangements, energy transfer, ground-state complex formation, and collisional quenching. There are two primary quenching phenomena we are interested in: static quenching occurs with the formation of a complex between the fluorophore and the quencher; collisional quenching (dynamic quenching) occurs when the quencher diffuse to the fluorophore during the lifetime of the excited state and the fluorophore returns to the ground state without emission of a photon after the contact. Collisional quenching of fluorescence is described by the Stern-Volmer equation: [3]

$$\frac{F_0}{F} = 1 + k_q \tau_0 [Q] = 1 + k_D [Q] \tag{2.14}$$

In this equation, F_0 and F are the fluorescence intensities in the absence and presence of quencher, respectively, k_q is the bimolecular quenching constant, τ_0 is the

lifetime of the fluorophore in the absence of quencher, and [Q] is the concentration of quencher. $K_q\tau_0$ is Stern-Volmer quenching constant.

Statistic quenching of fluorescence is given by: [3]

$$\frac{F_0}{F} = 1 + K_s[Q] \tag{2.15}$$

K_s is the association constant for complex formation. One possible way to distinguish the static quenching and collisional quenching is to measure the fluorescence lifetimes, as the lifetime doesn't decrease in static quenching. Other means will include the temperature dependence of quenching constant, examination of the absorption spectra of the fluorophore.

In many cases, the fluorophore can be quenching both by static quenching and collisional quenching, therefore, a modified Stern-Volmer equation is given to account for both effects: [3]

$$K_{app} = (\frac{F_0}{F} - 1)\frac{1}{[Q]} = (K_D + K_S) + K_D K_S[Q] \tag{2.16}$$

We are going to give more details about fluorescence quenching in chapter 6. In our set-up (Figure 2.3), a frequency-doubled light is generated from a mode-locked Ti-sapphire laser with a pulse width of ~55fs at a wavelength of 800nm. A filter F1 is used to attenuate the power of amplified pulses. The laser pulse is then directed to several lens and the nonlinear crystal to generate second or third harmonic (SHG or THG) signal. The set-up for second and third harmonic measurement will be different and the required signal depends on the excitation wavelength (e.g. a THG signal is used with an excitation wavelength of 273 nm). In our context, only SHG signal is used, so we will focus on

SHG set-up only unless specifying. The fundamental radiation is separated from SHG signal (400 nm) by the beam splitter (BS1). The gate beam is directed with several mirrors to retroreflector, which is connected to the optical delay line. After being reflected by retroreflector and pass through several mirrors, the gate pulse is finally projected into the nonlinear crystal NC. The sum frequency signal will be generated in nonlinear crystal by the interaction of both fluorescence from the sample and the gate radiation. In regards to the sample fluorescence, we should come back to the separated SHG signal. With the help of BS1, the SHG signal will be directed to excite the liquid sample, which is holding in a rotating cell to prevent possible photodegradation and other accumulative effects during the long exposure to femtosecond pulses. Berek's waveplate is used to control the polarization of excitation light, either vertical or horizontal to the input light source. The generated fluorescence of the sample is collected with an achromatic lens (A) and focus on NC to generate the sum frequency signal. Finally, this up-converted signal is dispersed using a monochromator and detected using a photomultiplier tube.

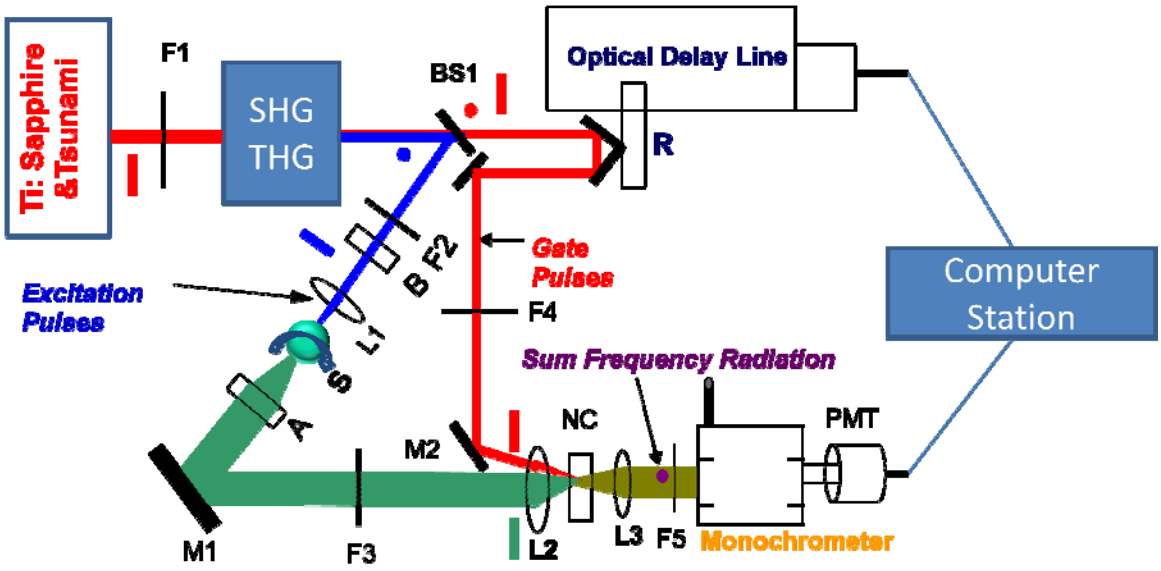

Figure 2.3 Femtosecond fluorescence up-conversion measurement set-up

2.4 Time-of-Flight Mobility Measurement

Mobility is an essential factor in understanding the nature of charge transfer process in conjugated polymers, which is closely relevant to the applications of many polymer electronic devices, such as organic photovoltaic cells, [15,16] organic light emitting diodes (OLED) [17,18] and organic field effect transistors (OFETs) [19,20] Charge carrier mobility is defined as the average velocity (υ) gained per unit field (E) and expressed as:

$$\mu = \langle \upsilon \rangle / E = (e/m)\tau \tag{2.17}$$

The mobility is proportional to the relaxation time (τ). In general, inorganic semiconductors have mobility several orders of magnitude higher than that of organic semiconductors. For instance, silicon shows 1500 $cm^2/V\bullet s$ and 1000 $cm^2/V\bullet s$ for the hole and electron mobility respectively at room temperature. However, the highest reported mobility for organic molecules, such as naphthalene diimide (NDI) has an electron mobility of 6.2 $cm^2/V\cdot s$ at a low humidity level. [21]

Several methods are available to measure the mobility of polymer systems via either a direct or indirect way. Popular straightforward ways to determine the mobility include the time-of-flight (TOF), the field effect transistor (FET/TFT) and the acousto-electric travelling wave (SAW) method. The indirect methods are based on the derivation of charge carrier mobility within the framework of model approximation on different transport mechanism, such as (1) the space charge limited current (SCLC); (2) the charge extraction by linearly increasing voltage (CELIV); (3) the xerographic discharge; (4) the hall effect. Several comprehensive reviews have been conducted to cover the basic principles and applications of these methods. [22-25]Each method has its own advantages as well as limitations. For example, pioneered by Kepler and LeBlanc in organic crystals since 1960, TOF has been widely used in low mobility polymers as a very straightforward and informative method. The mobility is a function of experimental parameters (the thickness of material, the applied voltage et al.) and the sign of charge can be easily switched by changing the polarity of applied voltage. But, this method is valid under the fulfillment of certain conditions: the dielectric relaxation time (τ_σ) must exceed the charge carrier transit time (t_{tr}) in order to maintain a constant electric field through the sample. Also, the measured mobility really depends on the geometry and fabrication process of the device, for example, the surface roughness and defects concentration of silicon wafer really matters. In the work we are going to talk, TOF is used to probe the charge transfer mechanisms in our proposed hyper-branched copper phthalocyanine based dendrimer systems. Hence, fundamental theories of TOF technique will be presented as follows.

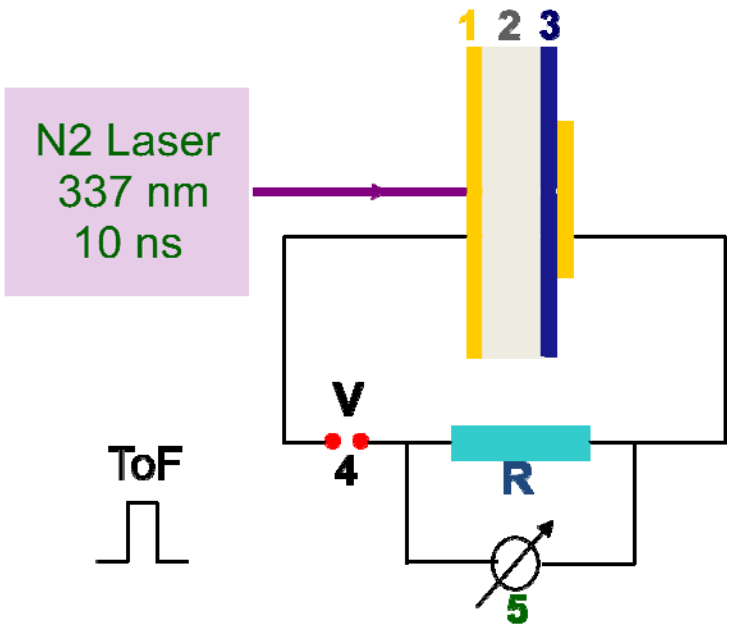

Figure 2.4 Time-of-flight (TOF) measurement set-up. 1. Gold electrode; 2. Si wafer (~500 µm thick); 3. Dendrimer film; 4. Applied voltage; 5. Par Model 164 boxcar integrator.

As shown in Figure 2.4 is the experiment set-up we used. TOF devices consist of layers of material (HBCuPc dendrimer) and charge carrier generation source (Si wafer) sandwiched between two electrodes (Au coating). A short laser pulse of 337nm with a pulse width of 10fs is used to photo-generate Gaussian shape of charge carriers from one side of Au electrode (the electrode should be semitransparent to allow the light to pass and reach the charge carrier generating layer). Dragged by the external applied electric field, the generated charge carriers drift through the material with certain thickness and arrive at the surface of the other electrode. A dispersive or non-dispersive transport is thus detected (Figure 2.5).

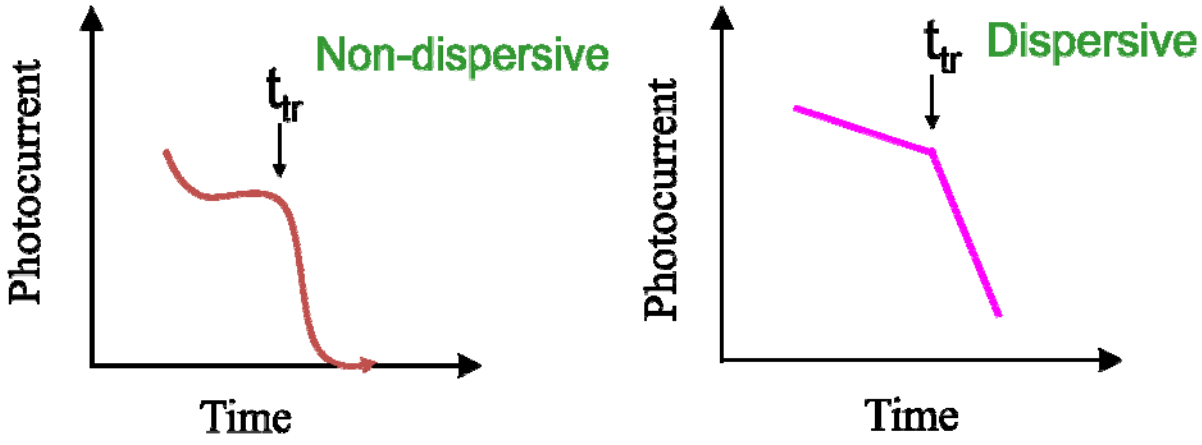

Figure 2.5 Illustration of (a) Non-dispersion and (b) Dispersive charge transport.

From the decay curve of transient photocurrent versus time, the mobility (μ) can be derived from the equation: [26]

$$\mu = \upsilon_d / E = d^2 / V t_{tr} \tag{2.18}$$

Here, d is the thickness of dendrimer film; E is the applied electric field; V is the applied voltage and t_{tr} is the transit time.

There are several different ways to determine the transit time and it does matter to the mobility of the material, as you can see from above equation, the mobility is inversely proportional to the transit time. One common way is to define the transit time as the time when the photocurrent drops to half of its plateau value. Then, it can be extrapolated from the intersection of two linear branches on the plot.

The charge carrier mobility is dependent on both the temperature and the applied electric field. And such dependence is very helpful in understanding the charge transfer mechanisms in investigated systems. There are several models involving in explaining

the different phenomena of the temperature and the electric field dependence of the mobility in disordered organics. Bässler and his co-workers have made a great contribution to this field. [27-41] He suggested a Bässler's Uncorrelated Gaussian Disorder Model (UGDM) to describe the mobility in a hopping system. In a typical hopping model, the movement of charge carriers is originated from thermally activated sites; hence strong temperature power law dependence in a relation of $\mu(T) \infty T^n$ with a common value of -3/2 is normally observed. The electric field dependence typically shows a Poole-Frenkel behavior ($\ln \mu(E) \infty \beta E^{1/2}$, where β is a coefficient) which arises from the theory of traping/detrapping in disordered materials. [42] In general, the mobility increases with the electric field. Whereas, weak electric field dependence was observed for some polymer systems and sometimes the coefficient even goes to a negative value. [26,33,43-47] For example, we observed negative electric field dependence in a HBCuPc dendrimer film and contribute this effect to the positional disorder in random organics. [26] The negative electric field dependence has brought a lot of debate in this field even though it bears on the fundamental nature of charge hopping transport in organic materials. Monte-Carlo simulations under the premise of Miller-Abrahams jump rate have produced the same effect in the framework of the Gaussian disorder model (GDM) by playing around the energetic and positional disorder. By extending this model by the introduction of a framework of effective medium approach (EMA), in addition to the consideration of polaron formation contribution, Bässler and his co-workers have suggested that the negative electric field dependence is an intrinsic property of disorder organics. [29]

2.5 Ultrafast Pump-Probe Transient Absorption Spectroscopy

Pump-probe transient absorption spectroscopy is useful to probe the excited state dynamics of organic materials. [48-50]The principle of this technique is simple: it requires at least two pulses from the same laser source. One is called the pump pulse. It perturbs the system and may lead to the energy or electron redistribution inside the molecule or the initiation of dissociation reactions. The other pulse is called a probe pulse. It passes the sample and the intensity of the probe is monitored as a function of time delay with respect to the pump pulse. The change in the absorption of the sample after the excitation (increase or decrease, even the appearance of a new absorption peak) may indicate the formation of the photochemical species, such as triplet states, charge complexes and excitons. The temporal behavior of the absorption spectra change could be probed by changing the time difference between the pump and the probe. The detected signal in the transient absorption measurement is the change in absorption (ΔA). The difference in absorption is a function of the time and wavelength evolution. In general, a 3D transient absorption spectrum will be obtained (e.g. Figure 2.6).

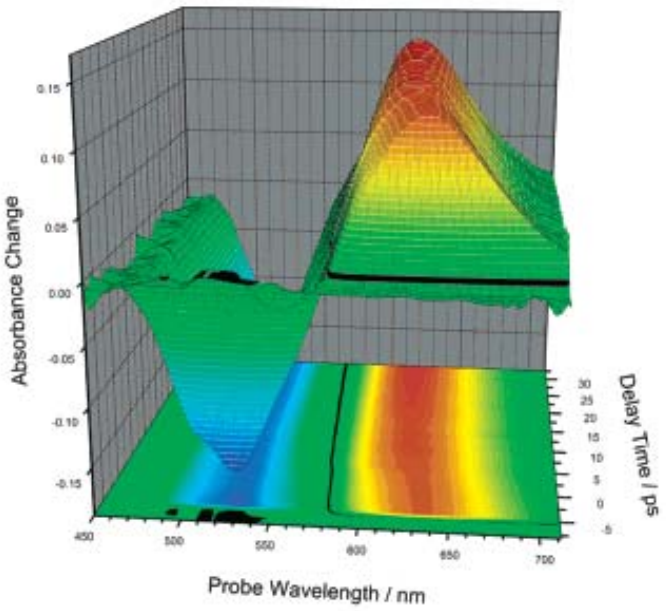

Figure 2.6 An example of transient absorption spectrum. [51]

In our system, as shown in Figure 2.7, with the input from a Millennia-pumped Ti: Sapphire oscillator (Spectra Physics, Tsunami), a pulse with a width of 100fs at 800nm is generated by a Nd:YLF(Evolution)-pump Ti:Sapphire regenerative amplifier (Spectra physics spitfire). A beam splitter is used to separate the pump and probe pulses with a ratio of 85: 15%. From the fourth harmonic of the idler beams, pump beam is produced by the optical parametric amplifier (OPA-800) and focus onto the sample cuvette. The probe beam is set to a delay by a computer controlled motion controller and projected onto a 2 mm sapphire plate to generate a white light continuum. The white light overlaps with the pump beam in a 2 mm sample quartz cuvette. The generated signal (ΔA, change in the absorption) is collected by a CCD detector (Ocean Optics). The data acquisition and analysis are operated by the software from Ultrafast Systems Inc.

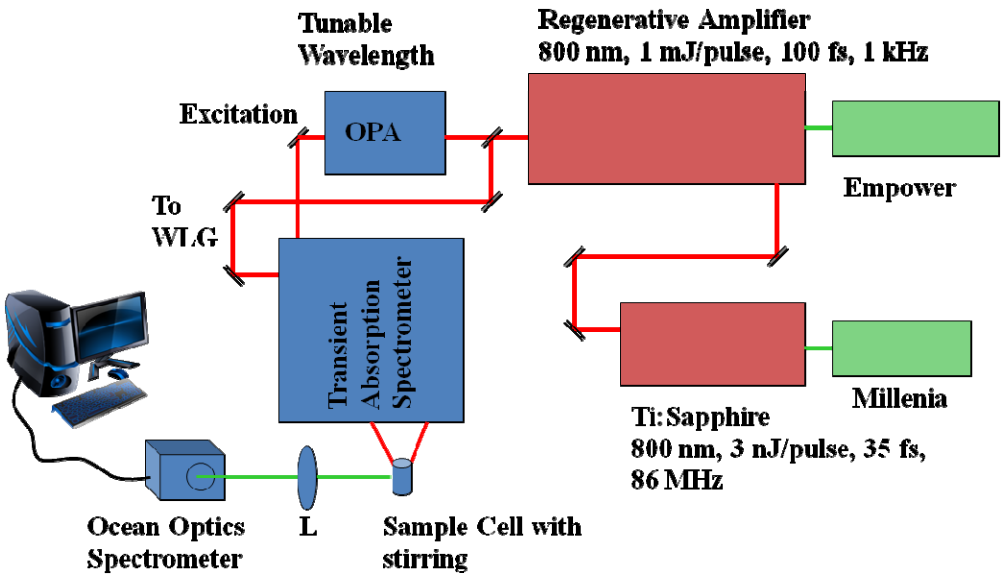

Figure 2.7 Illustration of pump-probe transient absorption measurement set-up.

Reference

(1) Ege, S. N. *Organic Chemistry : Structure and Reactivity*; 5th ed.; Charles Hartford: New York, **2004**.

(2) Yan, X. Z.; Pawlas, J.; Goodson, T.; Hartwig, J. F. *Journal of the American Chemical Society* **2005**, *127*, 9105-9116.

(3) Lakowicz, J. R.; 2 ed.; Kluwer Academic/Plenum Publishers: New York, **1999**.

(4) Hirsch, M. D.; Marcus, M. A.; Lewis, A.; Mahr, H.; Frigo, N. *Biophysical Journal* **1976**, *16*, 1399-1409.

(5) Goodson, T. *Annual Review of Physical Chemistry* **2005**, *56*, 581-603.

(6) Guo, M.; Varnavski, O.; Narayanan, A.; Mongin, O.; Majoral, J. P.; Blanchard-Desce, M.; Goodson, T. *Journal of Physical Chemistry A* **2009**, *113*, 4763-4771.

(7) Hagedorn, K. V.; Varnavski, O.; Hartwig, J.; Goodson, T. *Journal of Physical Chemistry C* **2008**, *112*, 2235-2238.

(8) Ranasinghe, M. I.; Hager, M. W.; Gorman, C. B.; Goodson, T. *Journal of Physical Chemistry B* **2004**, *108*, 8543-8549.

(9) Varnavski, O.; Goodson, T.; Sukhomlinova, L.; Twieg, R. *Journal of Physical Chemistry B* **2004**, *108*, 10484-10492.

(10) Varnavski, O. P.; Goodson, T.; Mohamed, M. B.; El-Sayed, M. A. *Physical Review B* **2005**, *72*.

(11) Glasbeek, M.; Zhang, H. *Chemical Reviews* **2004**, *104*, 1929-1954.

(12) Perrin, F. *Journal De Physique Et Le Radium* **1926**, *7*, 390-401.

(13) Cho, H. S.; Song, N. W.; Kim, Y. H.; Jeoung, S. C.; Hahn, S.; Kim, D.; Kim, S. K.; Yoshida, N.; Osuka, A. *Journal of Physical Chemistry A* **2000**, *104*, 3287-3298.

(14) Akimoto, S.; Yamazaki, T.; Yamazaki, I.; Osuka, A. *Chemical Physics Letters* **1999**, *309*, 177-182.

(15) Li, Y. F.; Zou, Y. P. *Advanced Materials* **2008**, *20*, 2952-2958.

(16) Zou, Y. P.; Gendron, D.; Badrou-Aich, R.; Najari, A.; Tao, Y.; Leclerc, M. *Macromolecules* **2009**, *42*, 2891-2894.

(17) Edman, L.; Summers, M. A.; Buratto, S. K.; Heeger, A. J. *Physical Review B* **2004**, *70*.

(18) Yang, C. M.; Liao, H. H.; Horng, S. F.; Meng, H. F.; Tseng, S. R.; Hsu, C. S. *Synthetic Metals* **2008**, *158*, 25-28.

(19) Klauk, H.; Zschieschang, U.; Pflaum, J.; Halik, M. *Nature* **2007**, *445*, 745-748.

(20) Piliego, C.; Jarzab, D.; Gigli, G.; Chen, Z. H.; Facchetti, A.; Loi, M. A. *Advanced Materials* **2009**, *21*, 1573.

(21) Shukla, D.; Nelson, S. F.; Freeman, D. C.; Rajeswaran, M.; Ahearn, W. G.; Meyer, D. M.; Carey, J. T. *Chemistry of Materials* **2008**, *20*, 7486-7491.

(22) *Organic Electronic Materials: Conjugated polymers and low molecular weight organic solids*; Farchioni, R.; Grosso, G., Eds.; Springer: New York, **2001**; Vol. 41.

(23) *Photoconductivity and Related Phenomena*; Dolezalek, F. K., Ed.; Elsevier, **1976**.

(24) Jaiswal, M.; Menon, R. *Polymer International* **2006**, *55*, 1371-1384.

(25) Arkhipov, V. I.; Heremans, P.; Bassler, H. *Applied Physics Letters* **2003**, *82*, 4605-4607.

(26) Guo, M.; Yan, X. Z.; Goodson, T. *Advanced Materials* **2008**, *20*, 4167.

(27) Fishchuk, I.; Arkhipov, V. I.; Kadashchuk, A.; Heremans, P.; Bassler, H. *Physical Review B* **2007**, *76*.

(28) Fishchuk, I.; Kadashchuk, A.; Bassler, H. *Physica Status Solidi C - Current Topics in Solid State Physics, Vol 5, No 3* **2008**, *5*, 746-749.

(29) Fishchuk, I.; Kadashchuk, A.; Bassler, H.; Abkowitz, M. *Physical Review B* **2004**, *70*.

(30) Fishchuk, I.; Kadashchuk, A.; Bassler, H.; Nespurek, S. *Physical Review B* **2003**, *67*.

(31) Fishchuk, I.; Kadashchuk, A. K.; Bassler, H. *Molecular Crystals and Liquid Crystals* **2005**, *426*, 71-80.

(32) Fishchuk, I.; Kadashchuk, A. K.; Vakhnin, A.; Korosko, Y.; Bassler, H.; Souharce, B.; Scherf, U. *Physical Review B* **2006**, *73*.

(33) Hertel, D.; Bassler, H.; Scherf, U.; Horhold, H. H. *Journal of Chemical Physics* **1999**, *110*, 9214-9222.

(34) Arkhipov, V. I.; Bassler, H.; Wolf, U.; Barth, S. *Conjugated Polymer and Molecular Interfaces* **2002**, 613-650.

(35) Arkhipov, V. I.; Emelianova, E. V.; Heremans, P.; Bassler, H. *Physical Review B* **2005**, *72*.

(36) Arkhipov, V. I.; Heremans, P.; Emelianova, E. V.; Adriaenssens, G. J.; Bassler, H. *Journal of Physics-Condensed Matter* **2002**, *14*, 9899-9911.

(37) Emelianova, E. V.; van der Auweraer, M.; Bassler, H. *Journal of Chemical Physics* **2008**, *128*.

(38) Hertel, D.; Bassler, H. *Chemphyschem* **2008**, *9*, 666-688.

(39) Mozer, A. J.; Sariciftci, N. S.; Pivrikas, A.; Osterbacka, R.; Juska, G.; Brassat, L.; Bassler, H. *Physical Review B* **2005**, *71*.

(40) Nikitenko, V. R.; von Seggern, H.; Bassler, H. *Journal of Physics-Condensed Matter* **2007**, *19*.

(41) Pautmeier, L.; Richert, R.; Bassler, H. *Synthetic Metals* **1990**, *37*, 271-281.

(42) *Electrical Transport in Solids*; Kao, K. C.; Hwang, W., Eds.; Pergamon Press: Oxford, **1981**.

(43) Kageyama, H.; Ohnishi, K.; Nomura, S.; Shirota, Y. *Chemical Physics Letters* **1997**, *277*, 137-141.

(44) Mozer, A. J.; Sariciftci, N. S. *Chemical Physics Letters* **2004**, *389*, 438-442.

(45) Mozer, A. J.; Denk, P.; Scharber, M. C.; Neugebauer, H.; Sariciftci, N. S.; Wagner, P.; Lutsen, L.; Vanderzande, D.; Kadashchuk, A.; Staneva, R.; Resel, R. *Synthetic Metals* **2005**, *153*, 81-84.

(46) Kreouzis, T.; Poplavskyy, D.; Tuladhar, S. M.; Campoy-Quiles, M.; Nelson, J.; Campbell, A. J.; Bradley, D. D. C. *Physical Review B* **2006**, *73*.

(47) Mohan, S. R.; Joshi, M. P.; Singh, M. P. *Chemical Physics Letters* **2009**, *470*, 279-284.

(48) Medina, A. S.; Claessens, C. G.; Rahman, G. M. A.; Lamsabhi, A. M.; Mo, O.; Yanez, M.; Guldi, D. M.; Torres, T. *Chemical Communications* **2008**, 1759-1761.

(49) Ramakrishna, G.; Bhaskar, A.; Goodson, T. *Journal of Physical Chemistry B* **2006**, *110*, 20872-20878.

(50) Ishii, K.; Iwasaki, M.; Kobayashi, N. *Chemical Physics Letters* **2007**, *436*, 94-98.

(51) Lor, M.; Viaene, L.; Pilot, R.; Fron, E.; Jordens, S.; Schweitzer, G.; Weil, T.; Mullen, K.; Verhoeven, J. W.; Van der Auweraer, M.; De Schryver, F. C. *Journal of Physical Chemistry B* **2004**, *108*, 10721-10731.

Chapter 3

Hyper-branched Copper Phthalocyanine for High Frequency Applications

3.1 Introduction

Recent interests in the use of novel polymeric materials for high dielectric constant effects have increased owing to their possible application in high-energy density and pulsed capacitors. [1] In particular, materials which demonstrate desired dielectric properties at high operational frequencies (>1 kHz) are highly sought after. Existing polymeric dielectrics, such as ceramic-polymers [2,3] and metal-polymeric composites, [4] typically exhibit a strong interfacial polarization (Maxwell-Wagner effect), and this effect results in a strong dispersion of the dielectric constant. Phthalocyanine (Pc) materials have been well studied for applications in solar cells, fuel cells, optical-limiting materials, gas sensors and field-effect transistors. [5-14] More recently there have been interests in applications for high dielectric constant material for capacitors. [15,16] For example, polymeric materials mixed with phthalocyanine (Pc) tetramers have been reported with good dielectric response which is heavily related to a the space charge effect. [12] However, the dielectric loss of these percolative systems is generally large, [2-4,12] and efforts are still necessary to improve the stability and flexibility of these systems. The use of Pc systems is an intriguing approach, and Pc polymer coated nanoparticles have been prepared and suggested as good candidates for dielectric applications. [17] Pc oligomers treated with base

(KOH) have shown a large dielectric response at lower frequency, and this was explained under the Maxwell-Wagner-Sillars model. [18] While many of these reports present exciting avenues toward creating large dielectric responses in primarily organic materials, there has not been much attention to the intrinsic high frequency dielectric response of all-organic systems. Also, in spite of the fact that numerous reports have demonstrated the dielectric performance of CuPc polymers, the understanding of the electronic and optical behavior in hyperbranched polymers is limited, which is essential in the development of new materials. Moreover, our previous experience in the study of triarylamine-based dendrimers and ladder oligomers using the ultra-fast spectroscopy suggested a coherent energy migration process occurred and polaron delocalization states were possible.[19] In this chapter, we report a strategy towards utilizing an organic multi-chromophore structure such as a Pc dendritic system to create a high dielectric constant material. Because of the long-range and fast polaron delocalization we find that the hyperelectronic polarization dominates the large dielectric response.

3.2 Experimental Section

Materials. All reagents were supplied by Aldrich Chemical Co. unless stated otherwise. Dimethyl sulfoxide (DMSO) and N, N-dimethylacetamide (DMAc) were dried with calcium hydride and then distilled under reduced pressure. All other chemicals were regent grade and were used as received unless otherwise stated.

Synthesis. Preparation of 1, 2-bis (3,4-dicyanophenoxy) benzene monomer. The 1, 2-bis (3, 4-dicyanophenoxy) benzene monomer was first synthesized by dissolving 6.27 g (40mmol) 4-nitrophthalonitrile and 2.20 g (20mmol) catechol in 60 mL DMSO. Then 11.04 g (0.08 mL) potassium carbonate was added into the above mixture in a flask.

After stirring at room temperature for 48 hours, the reaction mixture was poured into 1000 mL of water. The crude product was collected by filtration, washed with water, and dried under vacuum. The pure product was obtained by recrystallization using methanol. The white powdery product was dried in vacuum, producing 4.21 g of 1, 2-bis (3, 4-dicyanophenoxy) benzene. This base-catalyzed nucleophilic aromatic nitro displacement of 4-nitrophthalonitrile with catechol can yield the corresponding oxygen substituted phenyl phthalonitrile ether in a yield of 78%. Melting point (mp):191 °C (measured by DSC, lit. 188-189 °C). Figure 3.1 shows ^{1}H and ^{13}C NMR spectrum of the monomer 1, 2-bis (3, 4-dicyanophenoxy) benzene in DMSO. ^{1}H NMR (ppm): .08-6.93 (d, 2H); 6.70-6.99 (d, 2H); 6.41-6.53(s, 4H); 6.31-6.41 (d, 2H). (Figure 3.1-a): ^{13}C NMR (ppm): 160.1; 144.6; 136.1; 126.8; 123.3; 121.8;121.5; 116.6; 115.8; 115.2 ; 108.6. (Figure 3.1-b): IR (KBr, cm^{-1}): 3433, 3082, 2923, 2852, 2360, 2239, 2230, 1587, 1566, 1486, 1455, 1416, 1384, 1286, 1257, 1244, 1180, 1103, 951, 901, 873, 852, 795, 775, 669, 525. (Figure 3.2)

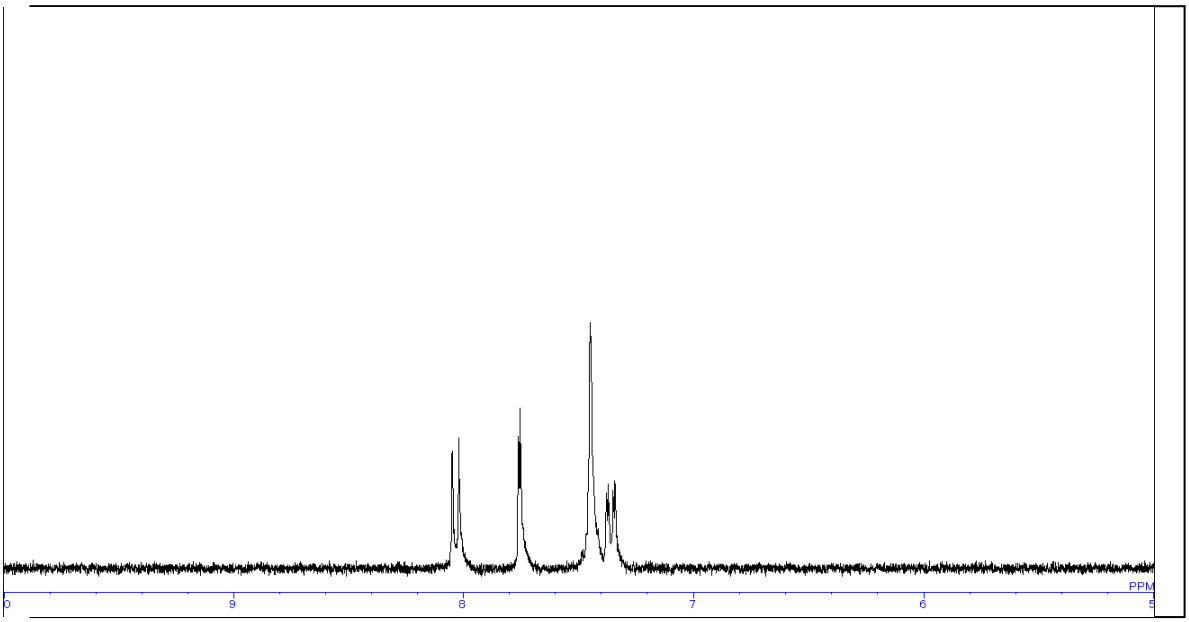

(a)

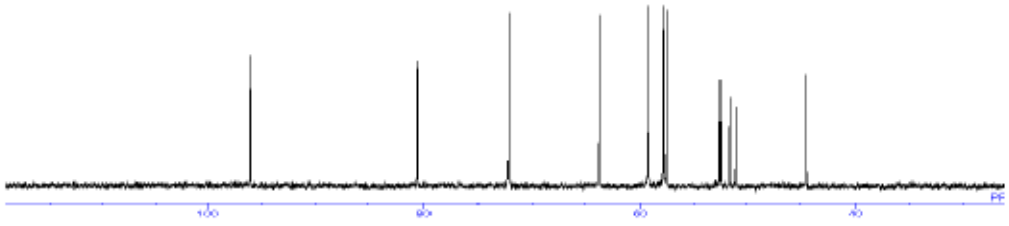

(b)

Figure 3.1 (a) Synthesis Protocol and ^{1}H NMR spectrum; (b) ^{13}C NMR spectrum of 1, 2-bi (3, 4-dicyanophenoxy) benzene in DMSO.

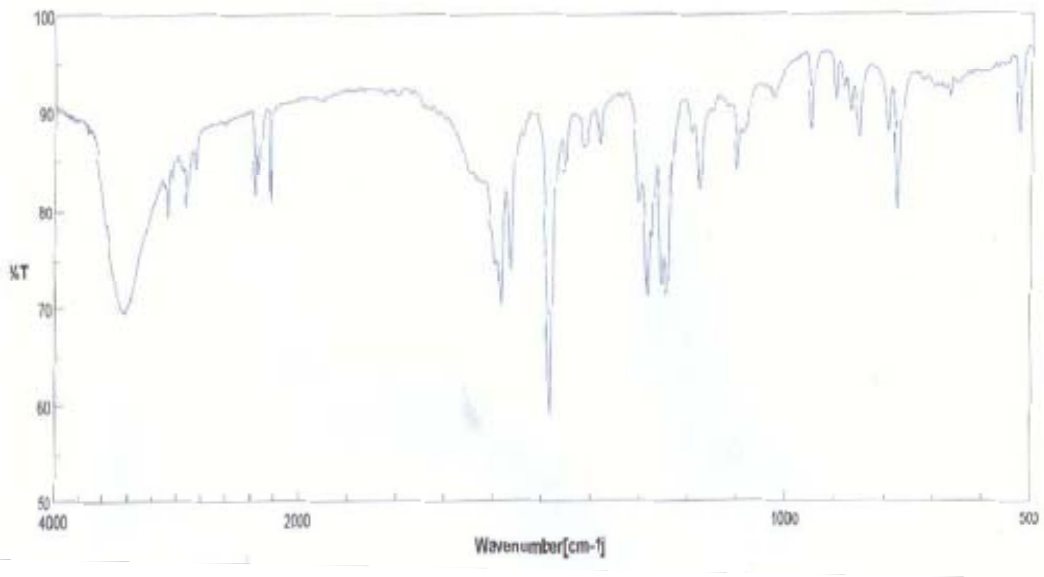

Figure 3.2 IR spectrum of 1, 2-bi (3, 4-dicyanophenoxy) benzene.

Preparation of CN-ended hyperbranched copper phthalocyanine (HBCuPc). The novel hyperbranched phthalocyanine (HBCuPc) was synthesized by a copper fusion technique consisting of 1, 2-bis (3, 4-dicyanophenoxy) benzene in dimethylacetamide

(DMAC). To a flask, 1.08g (3mmol) of 1, 2-bis (3, 4-dicyanophenoxy) benzene and 0.09 g (1mmol) of CuCl were dissolved in 40 mL of DMAc and then the mixture was stirred at 160 °C for 20 hrs. The extent of the cyclotetramerization reaction was monitored in real time by the increase of the absorption extinction coefficient of the products in comparison to the absorption of copper phthalocyanine complex. The reaction mixture was poured into 800 mL of water. The crude product was collected by filtration, washed with water, and dried in vacuum. After refluxing in methanol twice, the product was filtrated and washed using cold methanol for three times. The dark blue powdery product was dried in vacuum, affording 0.98 g of hyperbranched CuPc with a yield of 67%. The final structure of the HBCuPc was determined by ^{1}H-NMR, ^{13}C-NMR, IR, UV-Vis, TGA and GPC spectra respectively (Fig 3.3-3.7).

^{1}H NMR (ppm): 8.10-6.92 (d); 6.75-6.61 (q); 6.65-6.61(q); 6.45-6.21(q). (Figure3.3):

IR (KBr, cm^{-1}): 3222, 3065, 2231, 1771, 1717, 1607, 1588, 1565, 1489, 1454, 1402, 1361, 1309, 1255, 1217, 1183, 1092, 1049, 950, 881, 838, 770, 746, 674, 643, 553, 524. (Figure 3.4);

TGA: 418 °C (10% weight loss) (Figure 3.5);

GPC: Mw=3120, Mn=2380, Mw/Mn=1.31 (Figure 3.6).

Content of CuPc unit in HBCuPc was calculated as 15% based on the following observation. CuPc itself has ε of 281.2. If the monomer ideally reacted with CuCl, the structure of the product is shown as below and ε value of CuPc unit in this structure was calculated as ε=205. However, ε value of HBCuPc obtained in this work was found by

UV-Vis spectra (Figure 3.7) as ε=31. Therefore, CuPc unit content in HBCuPc was obtained by the equation:

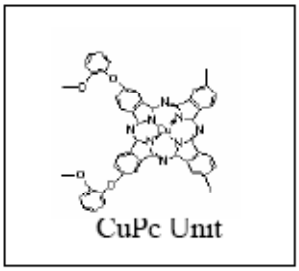

$$\text{CuPc Unit Contents in HBCuPc (\%)} = \frac{\text{HBCuPc } \varepsilon}{\text{CuPc unit } \varepsilon} \times 100$$

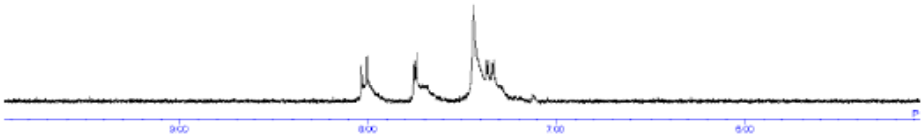

Figure 3.3 ^{1}H NMR spectrum of HBCuPc polymer.

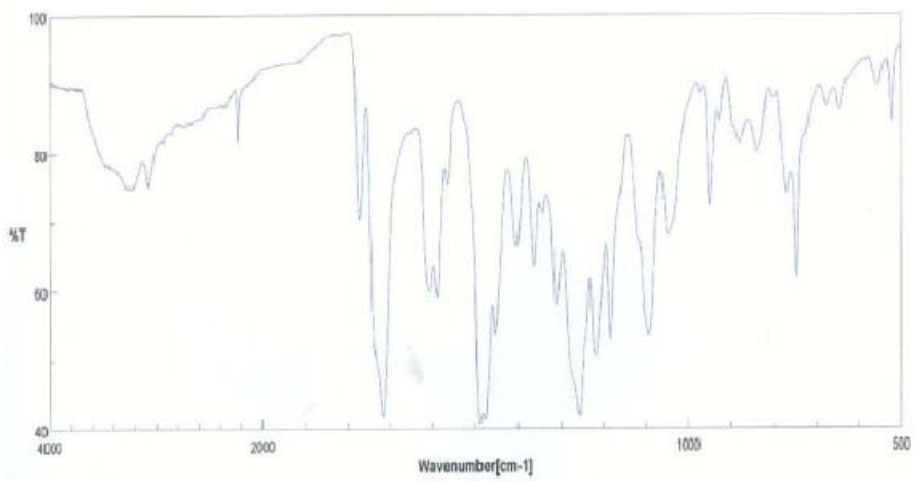

Figure 3.4 IR spectrum of the HBCuPc polymer.

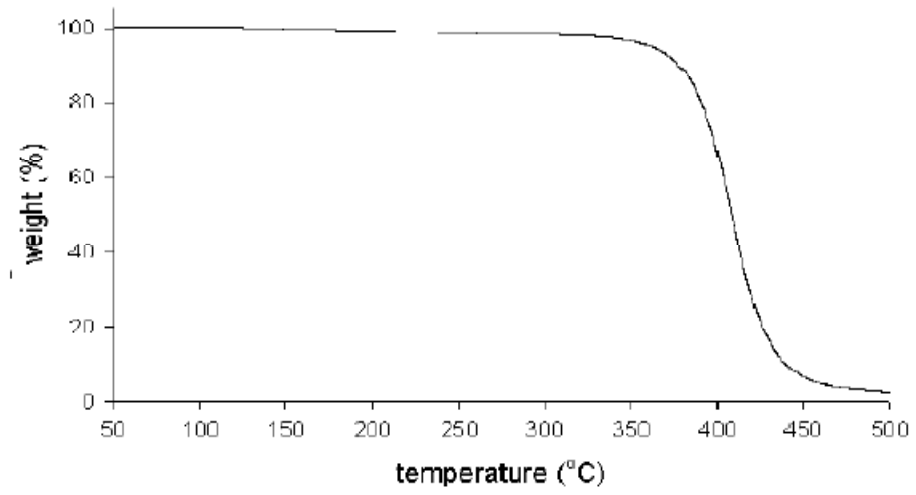

Figure 3.5 TGA curve of the HBCuPc polymer.

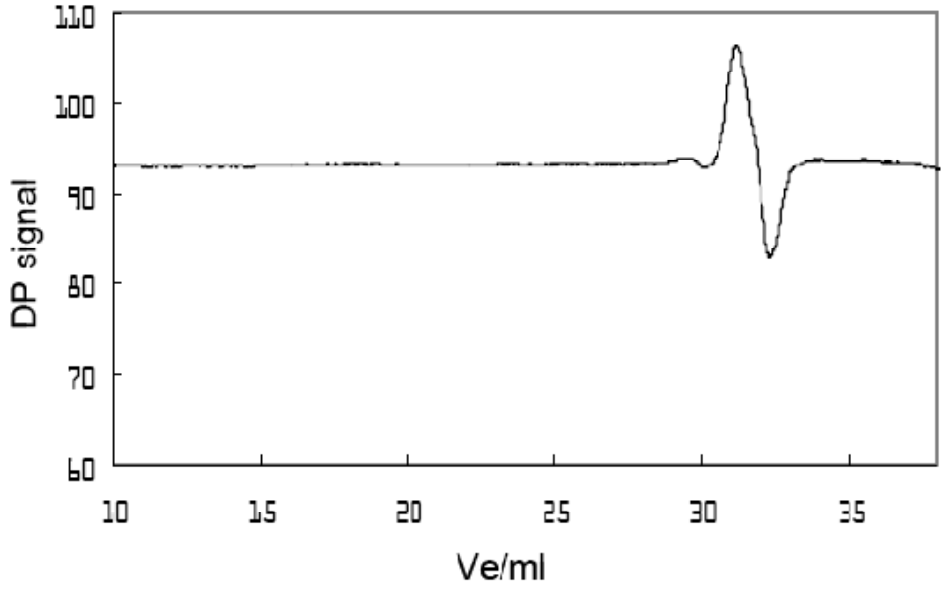

Figure 3.6 GPC curve of the HBCuPc polymer.

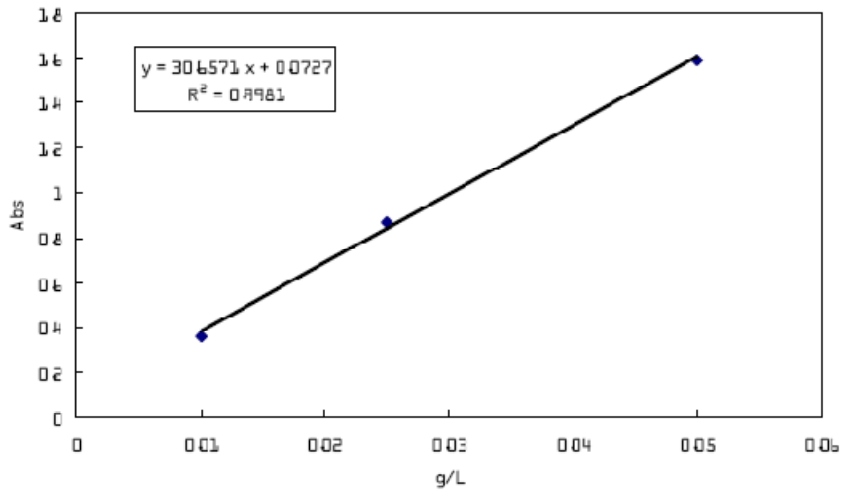

Figure 3.7 ε of the HBCuPc polymer.

Preparation of dielectric pellets and casting films of the HBCuPc polymer. The compressed pellets of HBCuPc dendrimer with varying thickness were prepared by using a hydraulic presser with a pressure of 12,000 psi for 3 mins from grindered polymer powder. The HBCuPc pristine films were prepared by dissolving a certain amount of the polymer powder to 0.5mL DMAc solutions first, and then stirred the solution for 10hrs, followed by the grinding or sonication for extra 10 mins. The pristine films made on Al foil substrates were dried in air, followed by the heat treatment under vacuum for 12 hrs in order to evaporate the solvent.

Techniques. Infrared (IR) spectra were recorded on a Shimadzu FTIR-8100 Fourier transform infrared spectrophotometer. NMR spectra were recorded on a JEOL JNM-AL 300 MHz spectrometer. Thermo gravimetric analysis (TGA) was carried out with a Seiko TG/DTA 6200 at a heating rate of 10 °C/min under air. Gel permeation chromatography (GPC) was performed on a Shodex RI-71 refractive index detector. Dimethylformamide (DMF) containing 0.01 Mol of lithium bromides was used.

Dielectric measurements were carried out by a 4284A HP LCR meter (20Hz-1MHz) with an HP 16451B dielectric fixture. A contacting electrode method was used. The capacitance (C_p) and dielectric loss (tanδ) were directly recorded from the instruments. The dielectric constant was determined by the equation $\varepsilon = \frac{C_p d}{\varepsilon_0 A}$. Here ε_0 is the dielectric permittivity of the vacuum (8.85 x 10^{-12} F/m); A is the area of the electrode and d is the thickness of the film.

Ultraviolet (UV)-visible absorption spectra were recorded with an Agilent Technologies 8453 spectrophotometer. Steady-state fluorescence measurements were performed on a Fluomax-2 fluorimeter. The solvent for all spectroscopic measurement is DMAc.

Time-resolved polarized fluorescence measurements were carried out on a femtosecond fluorescence up-conversion set-up. The detailed description of the set-up has been itinerated in chapter 2. In brief, the HBCuPc polymer/DMAc solution was excited with frequency-doubled light from a mode-locked Ti-sapphire laser with a pulse width of ~ 55fs at a wavelength of 820nm. The polarization of the excitation beam for the anisotropy measurements was controlled with a Berek compensator. The sample cell was 1mm thick and was held in a rotating holder to avoid possible photodegradation and other accumulative effects. The fluorescence emitted from the sample was collected with achromatic lens and directed parallel or perpendicular to a nonlinear crystal of β-barium borate. After passing through a motorized optical delay, the rest of the fundamental light mixed with the emission from the sample in another nonlinear crystal to generate sum frequency signal. This up-conversion signal was dispersed using a monochromator and detected using a photomultiplier tube (R 1527P, Hamamatsu City, Japan).

Time-of-flight mobility measurement: The HBCuPc polymer/ DMAC solution was cast onto silicon wafer (~500μm). Then it was sandwiched between gold electrodes using vacuum deposition. A 337nm N_2 laser pulse of 10 ns duration was used to excite the transient current. An electric field was applied across the sample by applying a potential difference between the electrodes. The experimental set-up could be referred to chapter 2.

3.3 Results and Discussion

The structure of the HBCuPc polymer under investigation in this work is illustrated in scheme 3.1. The cyano end-group is attached to the copper phthalocyanine polymer in order to enhance its polarity and solubility.

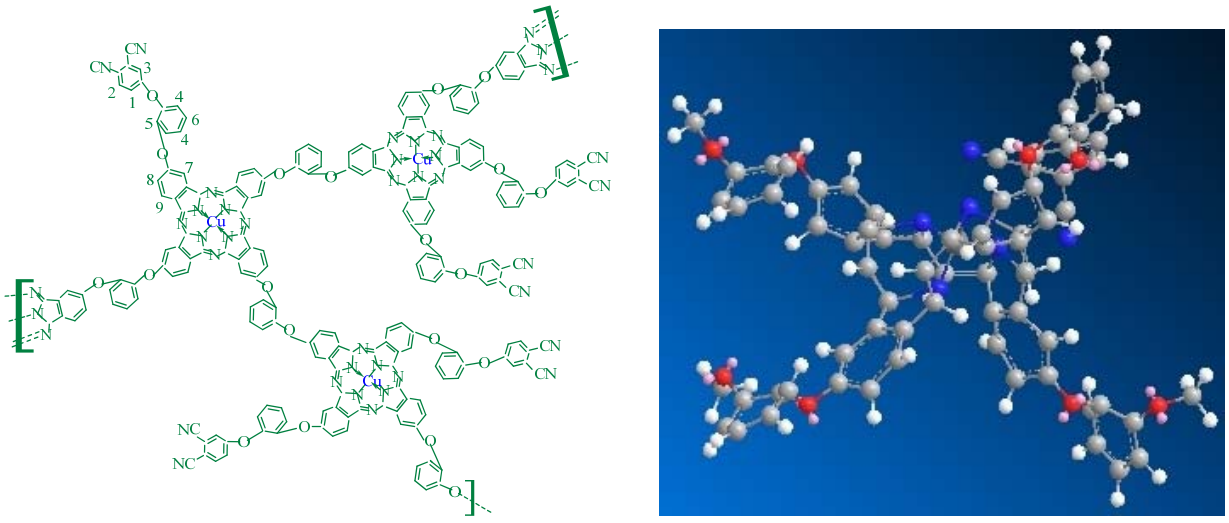

Scheme 3.1 the structure of the HBCuPc dendrimer

As shown in Figure 3.8 is the dielectric response of a compressed pellet of the HBCuPc. The thickness of the compressed pellet was ~76 μm. An impressive dielectric response of ~46 is obtained even at frequencies up to 1 MHz. This value is significant and is larger than that observed for the CuPc complex which was only 5.3 at 50 KHz. [1]

The comparison of the dielectric response between HBCuPc polymer and CuPc monomer is clearly illustrated in Figure 3.9. It can also be noted in Figure 3.8 that the dispersion of the dielectric constant is very small. This result suggests a major improvement over what has been reported in the past with Pc related materials. For example, in the case of the oligomers of Pc, the dielectric dispersion is very large where the dielectric response drops by 3 orders of magnitude over a similar frequency range as that seen in the result of Figure 3.8. [18] Very small dispersion in an organic material has been also observed in $Co(acac)_2$-cured-expoy resin material; however, the dielectric response at these higher frequencies in this material was relatively small (~6 at 1 MHz). [2] It has been suggested that for these systems such a small dispersion may be a result of the formation of large polar moieties. [3] From our measurements of the previous similar systems, we find that this may also be the case for the HBCuPc system where a long-range polaron delocalization in the branched structure gives rise to a small dispersion at high frequencies. [19,20]

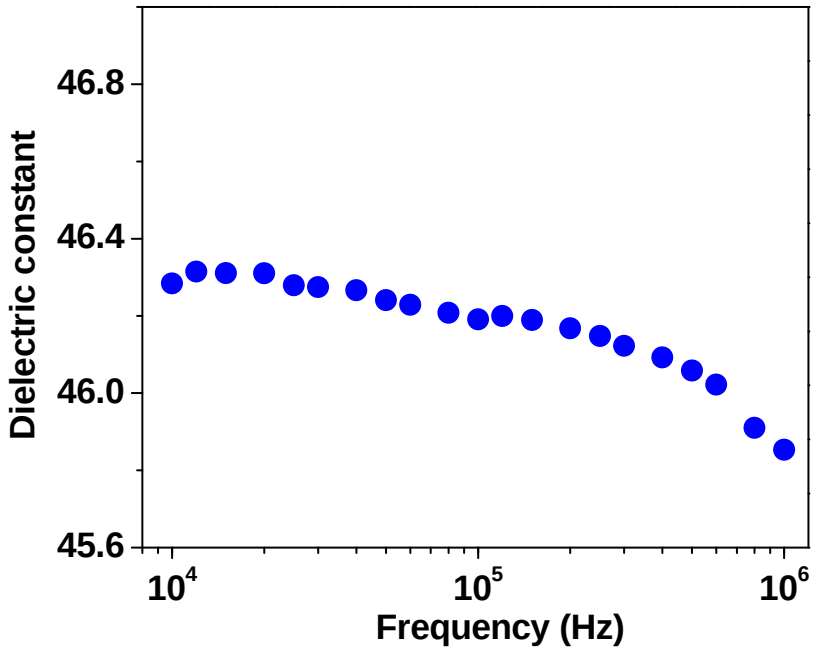

Figure 3.8 the dielectric dispersion of HBCuPc polymer compressed pellet with a thickness of 76 µm.

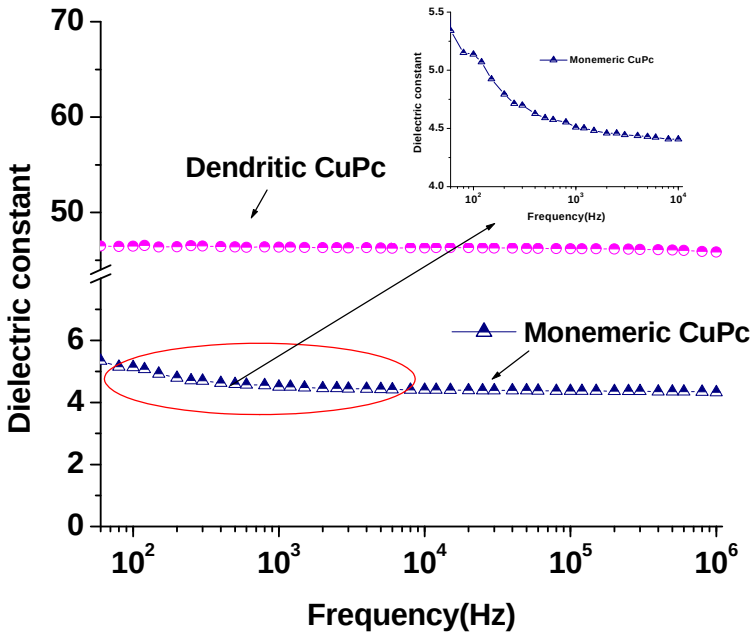

Figure 3.9 the dielectric constant of HBCuPc polymer compressed pellet as compared to that of CuPc monomer.

As shown in Figure 3.10 is the dielectric loss of HBCuPc polymer pellet. The previous results for Pc related polymers and oligomers had shown losses (tanδ) up to 0.7 for the polymer composite and above 1.0 for the Pc oligomers. [12,18,21] And even a CuPc monomer shows a dielectric loss up to 0.3. However, in our system, the dielectric loss is <0.003 at frequencies lower than 10 KHz. Then, it increases towards higher frequency and achieves a dielectric loss ~0.01 at 1MHz. The dielectric response we have found with this HBCuPc dendrimer present a major improvement which we attribute to the long-range interactions in the hyperbranched structure.

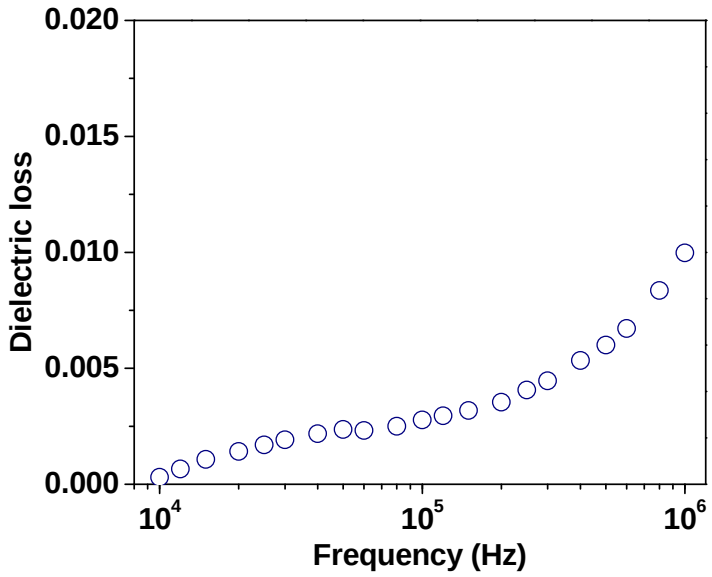

Figure 3.10 the dielectric loss of HBCuPc dendrimer compressed pellet with a thickness of 76 μm.

To probe the transport mechanism which yields this impressive dielectric response in the HBCuPc system, we carried out the analysis of the AC conductance. The AC conductance was analyzed by the expression given as $\sigma_{AC} = \varepsilon_0 \varepsilon_r \tan\delta\omega$, where ε_0 is the permittivity of the vacuum, ε_r is the real part of the dielectric constant, tanδ is the

dielectric loss, and ω is the angular frequency. Measurements with the AC conductivity of the HBCuPc samples showed a frequency dependent conductivity which could be fitted by a power law given as $\sigma_{AC} = A + B\omega^s$, where *A* and *B* are constants related to the DC (zero frequency conductivity) and *s* is a fitting parameter. The AC conductance of the pressure compressed pellet with a thickness of 76 μm showed the super-linear power law dependence with an *s* value of ~1.70 (Figure 3.11). It has been suggested that the *s* parameter may give an indication of the charge transport mechanism in the system. For example, a value of the *s* parameter of 1.75 was obtained for a metallorgano Pc film. [14,22] Moreover, low temperature measurements of CuPc oligomers have found a superlinear dependence too. [21] The explanation common to both of these cases in regards to the transport mechanism was heavily based on polaron tunneling in the system. However, for this situation the tunneling of polarons occurs on a relatively short length scale (short range interactions). [14,22] For the case of the compressed pellet sample of the hyperbranched Pc system, the contribution from a polaron tunneling mechanism is reasonable in describing the transport properties. It should be mentioned that in the case of the dendritic structure we have found that the interactions may extend over a number of repeat units and thus over larger length scales.[23] This effect may be sensitive to the macromolecular order exhibited in the dendritic system which may be a function of the fabrication (packing) of the solid-state system (compressed pellet or thin film).

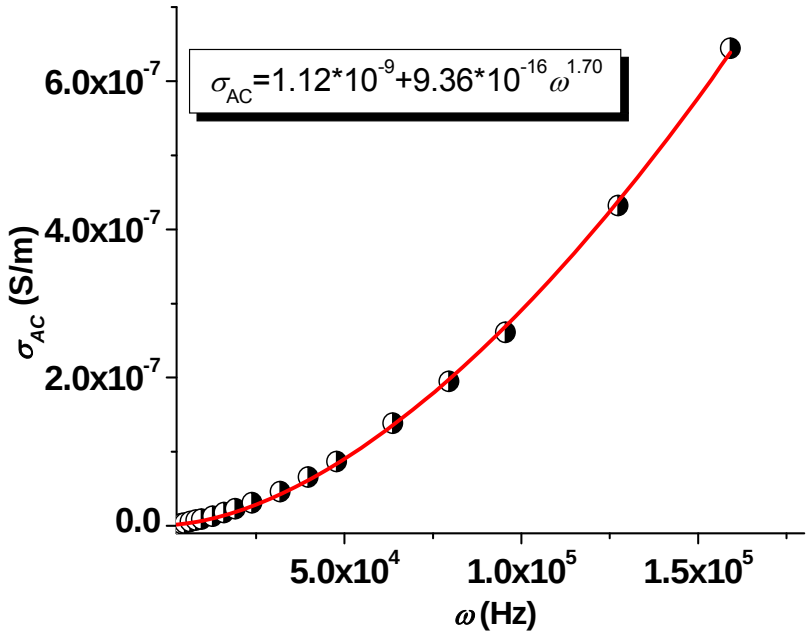

Figure 3.11 the AC conductance of HBCuPc polymer compressed pellet with a thickness of 76 µm.

In order to check if there is a thickness dependence of the dielectric performance for the HBCuPc polymer compressed pellet, we carried out the dielectric measurement on HBCuPc pellets with various thicknesses. Figure 3.12 shows an example of the dielectric dispersion of a compressed pellet with a thickness ~16 µm. The dielectric constant of this pellet can go up to 76 at lower frequencies; however, it drops quickly to ~11 at 1MHz and shows a typical dielectric dispersion of CuPc based polymers. The high dielectric constant in this thin pellet should be related to the space charge, which can also be supported by the Ac conductance analysis of this thin HBCuPc dendrimer pellet. As you can see in Figure 3.13, a large DC component with a value of 2.0×10^{-5} S/m is present in this thin pellet, 4 orders of magnitude higher than that in 76 µm thick pellet. This high DC component may suggest that there is a substantial contribution from space charge. Moreover, the AC conductance shows a power law dependence (an s value ~0.8) in this

thin dendrimer pellet, which may be related to polaron hopping charge transfer mechanisms.

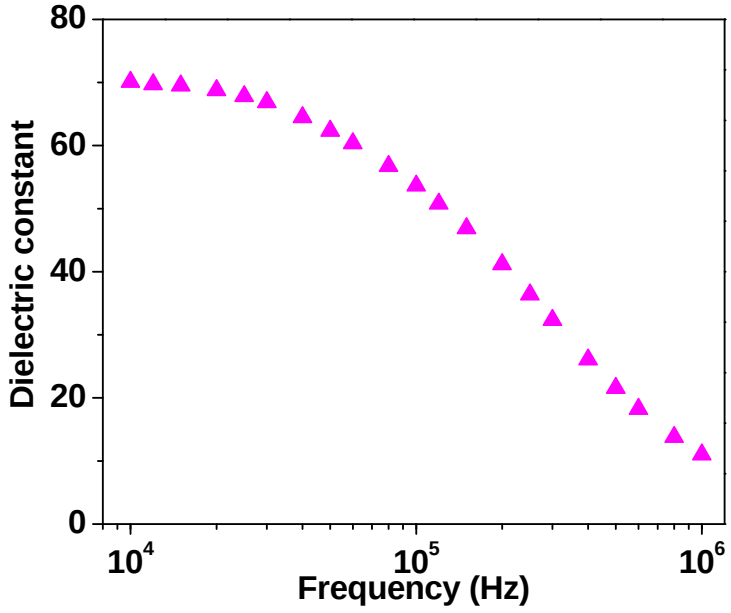

Figure 3.12 the dielectric dispersion of HBCuPc dendrimer compressed pellet with a thickness of 16 µm.

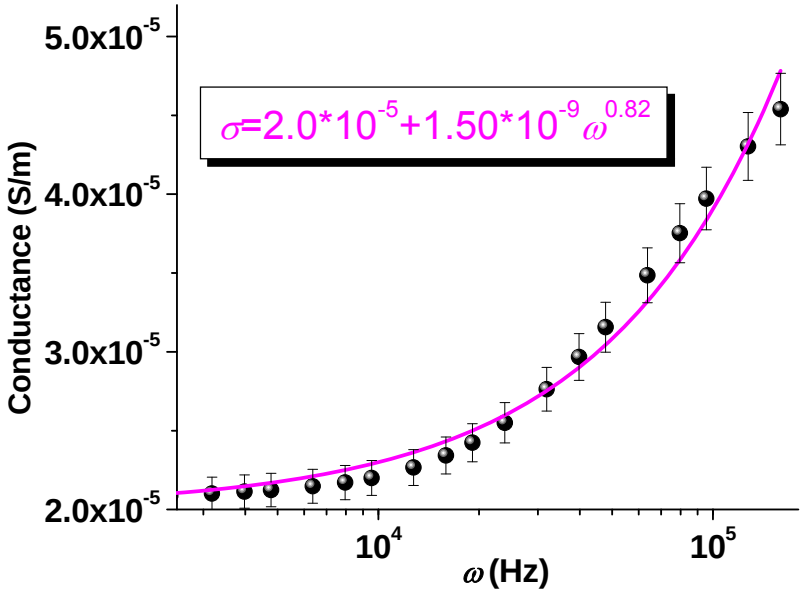

Figure 3.13 AC conductance of HBCuPc dendrimer compressed pellet with a thickness of 16 µm.

The thickness dependence may be related to the crystalline size and the packing of the HBCuPc powders. Other unknown factors, such as electrode edge effect, environment may do the contribution too. But in our previous investigations, we found that the conductance was proportional to the inverse of sample thickness in hyper-branched polyaniline sample and no double-layer capacitor effect was observed. Therefore, the impressive dielectric response we have observed should be the intrinsic behavior of HBCuPc polymer.

To probe the importance of the morphology of the system once fabricated in the solid-state, we also carried out measurements of films of various thicknesses and concentrations of the branched Pc system. Shown in Figure 3.14 is the dielectric response for a pristine film of the HBCuPc coated on an Al substrate. This system also showed a very small dispersion and the dielectric constant was close to ~15 at 1MHz. A very small dielectric loss (on the order of 0.001) was obtained at high frequencies (Figure 3.14). Compared to TiO_2 functionalized polystyrene nanocomposites (ε_r= 6~10), [24] the dielectric performance of the hyperbranched Pc films meets the stiff requirements for gate dielectrics and of organic transistor applications.

Our measurements of different film's AC conductance showed no apparent thickness dependence. The AC conductance (σ_{AC}) of this pristine film exhibited a behavior which can be fitted by a power law with an *s* value in the range of ~0.8 (Figure 3.15). This value for *s* suggests that the dominant mechanism of transport is a polaron hopping mechanism and may be related to the disordered dielectric effects in the system. [25]From our results on this and similar systems we have found that the polaron hopping can be relatively fast. [19] For example, with the use of time-resolved spectroscopy we have

found that the hopping time can be as fast as ~1 ps. [19] Such a fast hopping would suggest a relatively strong long range interaction of the branched structure and this is an intrinsic effect. It is interesting to note that this was not the case for the compressed pellet samples of the hyperbranched Pc, where a value of *s* greater than unity was obtained and this may be related to the fabrication procedure used to make the samples.

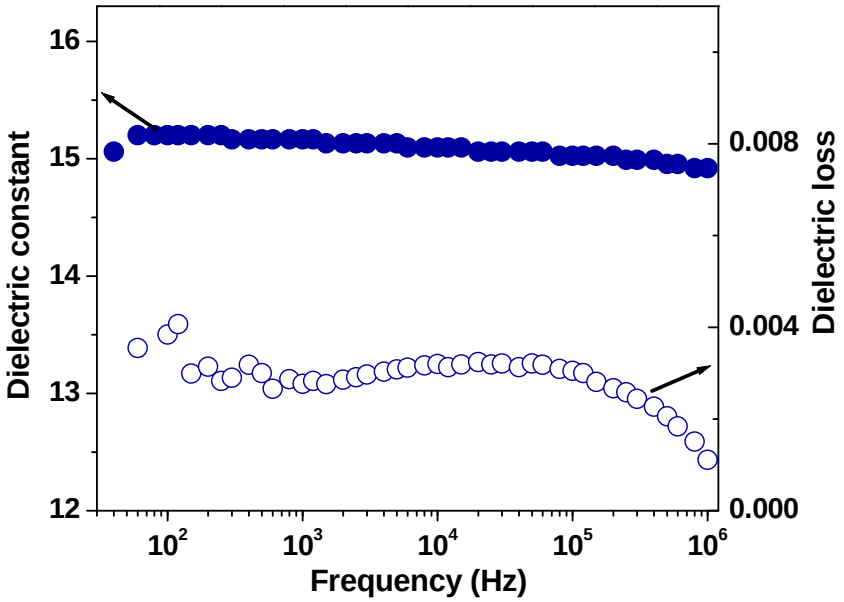

Figure 3.14 the dielectric response of HBCuPc dendrimer casting film with a thickness of 10 µm.

In order to probe the electronic properties of this dendrimer, we carried out time-of-flight measurements to investigate the electron mobility. HBCuPc dendrimer was first dissolved in DMAc solution at a concentration of 1mg/mL, then the HBCuPc/DMAc solution was drop-cast on a silicon wafer with a thickness of 500 µm. After drying in a vacuum oven at 120°C for several hours, a dendrimer film with a thickness ranging between 4 to 5 µm was obtained using a surface profiler. Other details of the procedure are elaborated in the experiment section.

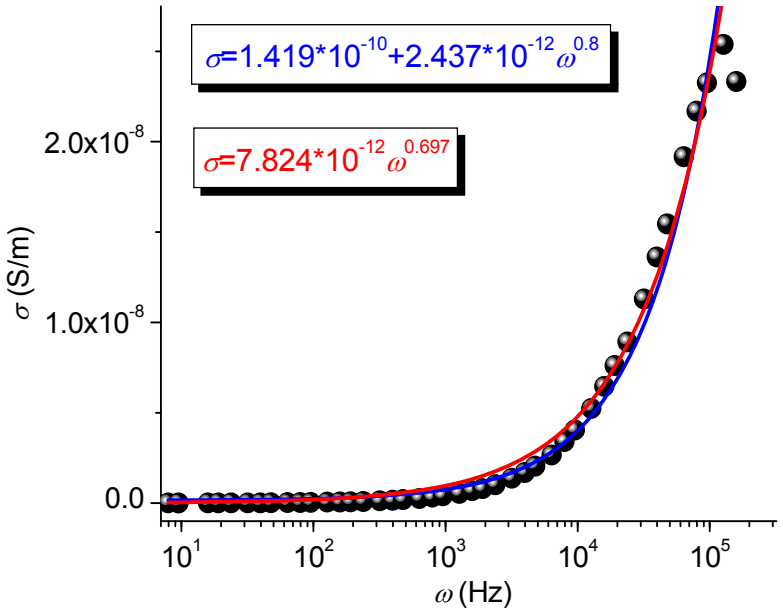

Figure 3.15 AC conductance of HBCuPc dendrimer casting film with a thickness of 10 µm.

A typical transient current at an applied field of 5V at several different temperatures is depicted in Figure 3.16 plotted on a linear scale. The transient current signals at room temperature follow a plateau region after a fast decay, then slowly tail off. This shows the characteristics of non-dispersive charge carrier transport. However, upon lowering the temperature, an apparent transition from non-dispersive to dispersive charge carrier transport occurs, which indicates that the disorder increases as temperature increases in this dendrimer system and agrees well with the disorder formalism predication by Bässler and co-workers. [26] The dispersive charge transport may originate from the hopping between localized states. This agrees with the observation in the ultrafast depolarization and fluorescence dynamics (see below).

For these typical transient curves, the mobility can be calculated by equation 3.1.

$$\mu = \frac{d^2}{t_{tr} \cdot V} \tag{3.1}$$

In equation 3.1, μ is the mobility, d is the thickness of the film, t_{tr} is the charge carrier transit time and V is the applied electric field. A significant charge carrier mobility in the order of 10^{-4} $cm^2/V \cdot s$ can be obtained, which is within the same order compared to the value observed for CuPc crystalline film by Micielski W. et al.[1] The investigation of HBCuPc morphology by using TEM (Figure 3.17) showed aggregates formed by large spherical crystalline domain of ~62 nm, which may help to rationalize the high charge carrier mobility in this hyperbranched system. The fast displacement of charge carriers and large carrier mobility also support the high dielectric response observed at high frequency in this polymer system.

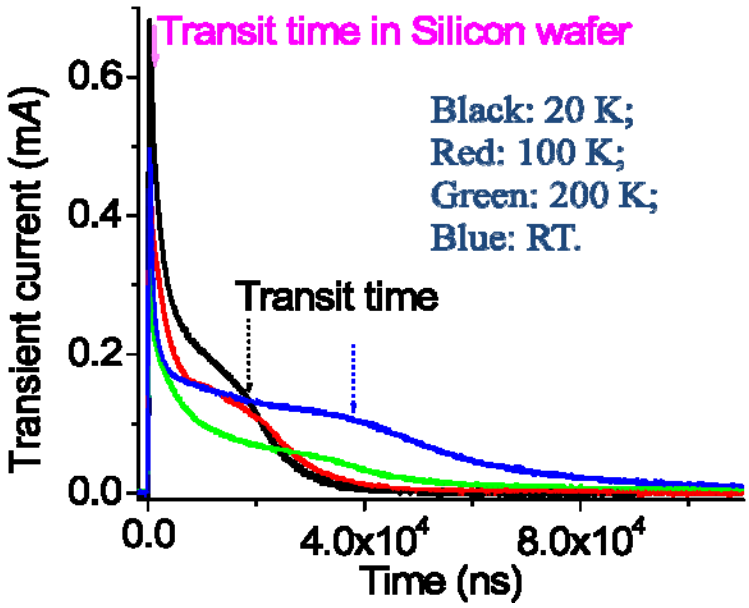

Figure 3.16 the transient current of the HBCuPc polymer/Silicon film with an applied electric field of 5V at various temperatures. *The sharp peak indicates electron transport in silicon wafer.

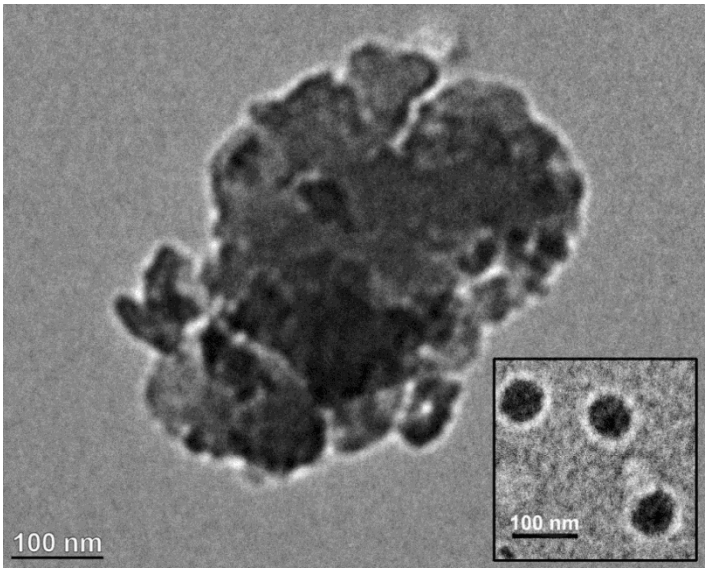

Figure 3.17 TEM image of the HBCuPc polymer

As supported by previous experimental results of the charge transport in disordered organics, the mobilities are usually low (with a magnitude between 10^{-7} $cm^2/V \cdot S$ and 10^{-10} $cm^2/V \cdot S$) and strongly temperature and electric-field dependent in the case of a hopping dominated charge transport. [27-30] And generally, the transport of charge carriers in polymers is slower than that in crystalline molecules. [31] However, the electron mobility in this novel dendrimer system is actually high. Thus we looked into the temperature and electric-field dependence. In Figure 3.18, the temperature dependence of the mobility is illustrated. The measurements have been carried out at an electric field of 5V. Generally, at high temperatures, thermal excitation of the carriers to the band edges is possible for a Pc semiconductor and extended-state conductivity can occur. At low temperature less thermal energy is available and polaron hopping may dominate. [26] Thus, a high mobility at higher temperature is typically observed in contrast to this negative temperature dependence observed in this dendrimer system. This non-Arrhenius behavior may be suggested to originate from positional dielectric disorder. [32] When the

temperature is decreased, due to the self-organization of the CuPc planar structures, a tighter stacking of the CuPc rings may become possible, which may shorten the hopping distance of the polaron between the CuPc rings in the system. Also, when the distance between CuPc rings becomes short enough (<5Å), polaron tunneling may occur at a very low temperature. [14]

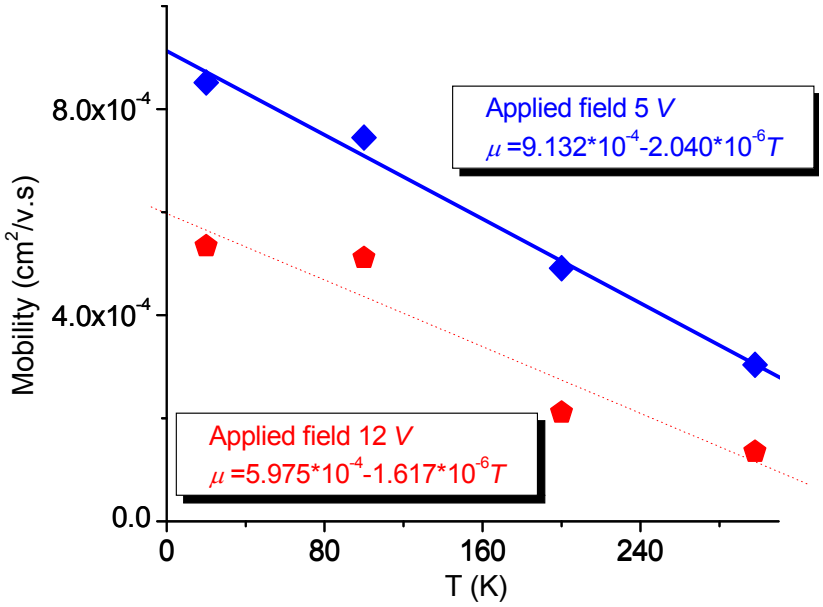

Figure 3.18 the temperature dependence of charge carrier mobility at an applied voltage of 5V.

This also provides support that a super-linear power law relationship of AC conductance is obtained with an s value of 1.7 in a HBCuPc dendrimer compressed pellet with a thickness of 76 μm, as shown in Figure 3.11. Vidadi et al. has suggested a charge transport mechanism dominated by polaron hopping and band-type mechanisms in CuPc film with an s value of 1.75. [22]

If the temperature dependence is replotted in an Arrhenius format, as illustrated in the Figure 3.19, as the temperature decreases, the mobility increases and obeys the $\mu \propto 1/T$ relation, a characteristic of non-Arrhenius behavior, but it tends to saturate at

lower temperatures, such as a dispersive transport regime. There is a weak temperature dependence of the mobility, because when the temperature decreased from 200K to 20K, only a three-fold increase was observed. Extrapolating to the limit $1/T \rightarrow 0$ based on the fitting, μ_0 with a value of 2.27×10^{-4} $cm^2V^{-1}s^{-1}$ is found with 5V applied field. The weak temperature dependence may indicate that the polaron tunneling becomes more dominant at low temperature, because less hopping sites will be available once the system disorder is reduced at lower temperature.

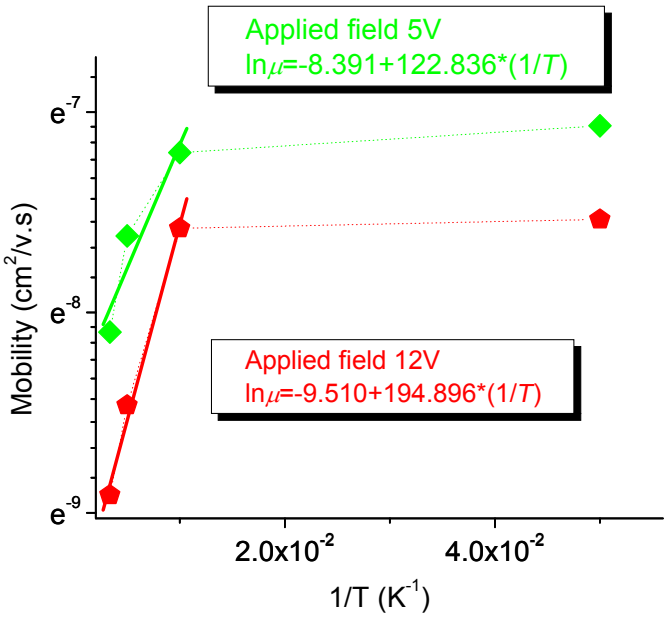

Figure 3.19 the Arrhenius plot of the charge carrier mobility at two different applied electric field, 5V and 12V respectively.

Furthermore, if we look at the activation energies derived from the fitting of data in Figure 3.19 at two different applied field, we can find that the activation energy decreases at low electric field (with a value of 0.0106 eV at 5V and a value of 0.0168eV at 12V respectively). This decrease in activation energy indicates more hopping sites will be available at low electric field, therefore a high mobility should be expected at low

electric field. The low activation energy may also suggest that the polaron formation contribution should be considered in combination with energetic and positional disorder suggested by Bässler and co-workers, [26] because polaron has a strong effect on the low temperature activation energy relaxation in disordered organic materials. [33]

Shown in Figure 3.20 is the applied field strength dependence of the charge mobility in the dendrimer film with a thickness of ~4μm. It is apparent that the mobility dependence on the electric field follows a relation of $\mu \propto E^{1/2}$, a typical Poole-Frenkel-like behaviour. [34] The slope of the electric field dependence decreases with the increasing of temperature (from 20 K to RT, the slope drops from -1.41578 to -1.7867), which indicates that the mobility becomes a less strongly positive function of field and satisfies the prediction from disorder formalism. [26] As the typical Poole-Frenkel dependence of the mobility on the electric field has no correlation with the electrode type, thus may be associated with the charge carriers and the positional disorder of hopping sites, which has been found in other organic materials, such as polythiophenes. [34] In contrast to the observed field dependence characteristic in the phthalocyanine monomer film, a negative dependence occurs, which has been found in various disordered organic materials. [34-36 37] In addition, numerous Monte Carlo simulations of charge transport have reproduced such effect based on a Gaussian disorder model (GDM). [26,35] Currently, there are several major arguments surrounding this negative field dependence. [34,38,39] One argument states that the negative dependence occurs due to the limitation of TOF technique, for example, the dielectric relaxation time is longer than the injected carrier transit time, and a prerequisite for TOF application is no longer satisfied. [38] However, this explanation contradicts to some experimental results. Herein, Cordes et al. draw the conclusion that this effect can

be attributed to the predominance of diffusion at low field. [39] Another explanation was given by H. Bässler and his co-workers. [34] They found that this effect is an inherent property of the hopping transport in disordered solids by extending the disorder model within the framework of an effective medium approach (EMA), in addition to the consideration of polaron formation contribution. We infer that the hyperelectronic polarization diminishes in a weak field and there is a larger degree of positional disorder at high electric field in this dendrimer system.

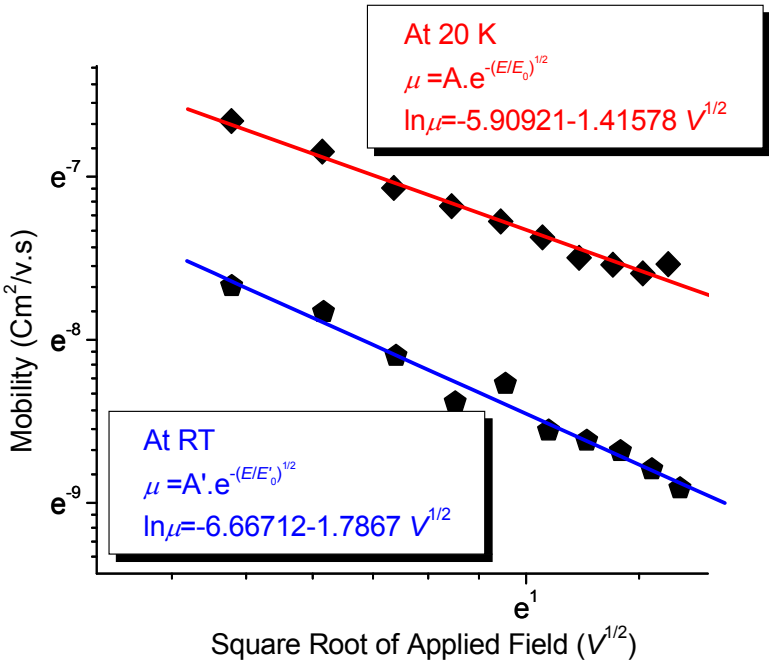

Figure 3.20 charge carrier mobility versus square of electric field strength at different temperature.

The TOF signals of the novel HBCuPc dendrimer show characteristics of Gaussian transport, as described by Bassler's uncorrelated Gaussian disorder model (UGDM). In this model, the zero field mobility μ *(0, T)* and the field activation of the mobility γ *(0, T)* have $1/T^2$ temperature dependence and can be expressed as:

$$\mu(0,T) = \mu_0 \times \exp(-2/3(\sigma/k_BT)^2) \quad (3.2)$$

$$\gamma(0,T) = C((\sigma/k_BT)^2 - \Sigma^2) \quad (3.3)$$

Where σ is the width of the Gaussian distribution of hopping sites, C and Σ are the parameters of the model. From the fitting, we obtained a value of 2.627×10^{-8} $cm^2V^{-1}s^{-1}$ for μ_0, which is comparable to that for HBCuPc with a value of 2.8×10^{-8} $cm^2V^{-1}s^{-1}$. [40] In addition, a weak energetic disorder in this organic system was found. Also, earlier reports of simulations of charge transport also supported the fact that the negative electric field dependence occurs at strong positional disorder and weak energetic disorder in a disordered organic solid system. [36] As the positional disorder increases at lower field, faster paths are opening and charge transport occurs within a percolation type cluster of hopping sites with a relatively small hopping distance, which results in a larger probability of charge hopping. The negative electric field dependence in combination with Non-Arrhenius temperature dependence is in agreement with the Ac conductance analysis of this dendrimer system.

In order to have a better understanding of the charge transport mechanisms in this novel dendrimer system, we also carried out steady-state adsorption and emission spectroscopy. Figure 3.21 shows the absorption and emission spectra of HBCuPc solution. Four main UV-Vis adsorption bands are observed. The strong adsorption peaks are dominated by Soret bands, Q and B band. The absorption at 336 nm is assigned to B band (π-π* transitions of the macrocycle). Precedent to B band peak, other two absorption peaks in UV range may be assigned to N (305 nm, d-π) and C (259 nm, d-π*) bands, respectively. A strong Q-band adsorption peak is observed at 678nm and

attributed to the π-π* transition on the phthalocyanine macrocycle, similar to published spectroscopic features of CuPc rings. [41-43] Accompanying to the Q-band, there is a relatively weak peak, seen as a shoulder, appears at 624nm may be assigned to metal-to-ligand charge transfer. [43]

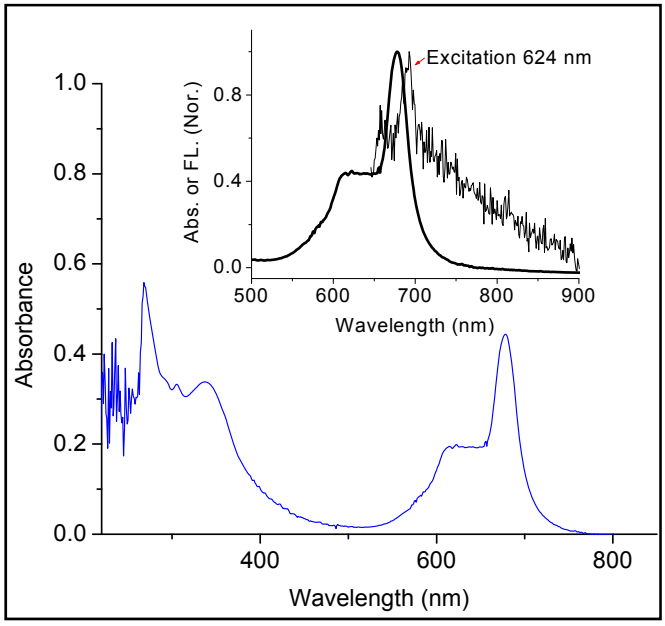

Figure 3.21 UV-Vis and steady state emission spectra of HBCuPc polymer

When excited at 624nm, a weak emission peak was observed which confirms our assignment of metal-to-ligand charge transfer to the band at 624nm in this polymer. Moreover, no emission is observed at an excitation in higher energy bands. For example, when excited at B band or at 400 nm, no emission was observed by the steady state measurement. It's interesting to note that the emission spectrum at 624 nm is not exhibiting mirror symmetry to the adsorption spectrum. This distortion may indicate a symmetry breaking after the excitation, which agreed to the observation of femtosecond fluorescence dynamics illustrated in Figure 3.22. The results show that the fluorescence

decay of this polymer possesses two components, including a fast component on a time scale of 120 fs, which is within the range of the IRF. Initially, the fluorescence decays fast with an anisotropy residue of 0.2, which indicated the symmetry breaking in the delocalized system and the excitation was transferred to other rings. Otherwise, we should expect a residue value of 0.1 in this planar structure, with the exciton located on one ring. In addition, it provides evidence to the electron hopping process suggested in this dendrimer system, because the breaking in symmetry could possibly induce more traps to form. The slow component was on a time scale of 3 ps, comparable to many exciton hopping processes observed and which may be attributed to electron hopping process between neighboring CuPc rings in the excited states. All above characteristics shown in HBCuPc dendrimer spectra indicate non-radiative relaxation pathways, for instance, ring-to-ring charge transfer or ring-to-metal charge transfer process involved. [19,44]

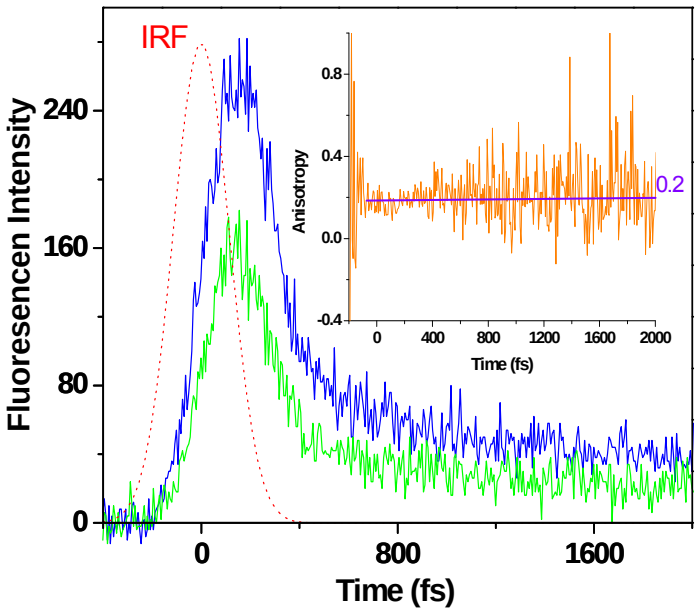

Figure 3.22 B-band fluorescence dynamics and fluorescence anisotropy (inset) of HBCuPc polymer at an excitation of 400 nm.

Moreover, we investigated the Q-band fluorescence dynamics at an excitation of 400nm (Figure 3.23). Similar to B-band fluorescence dynamics, there exist two decay components from the best fit of the fluorescence. The fast component is in a time scale of 194fs and may be related to a relaxation from Q_y to Q_x. The slow component is in a time scale of 14ps, which may correlates to a hopping process or solvation induced intramolecular vibrational energy redistribution. As we observe a component related to the hopping process in both B band and Q band emissions, we can conclude that there is a fast electron hopping process in the HBCuPc dendrimer system. It may be related to the fast hopping of the exciton in microwave region, which can explain the fast dielectric response exhibited in this dendrimer system.

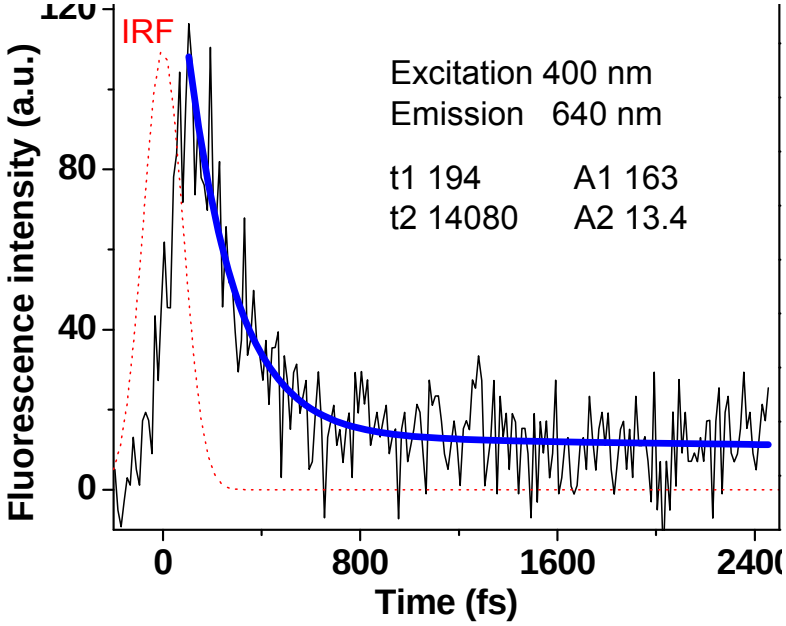

Figure 3.23 Q-band fluorescence dynamics of HBCuPc polymer at an excitation of 400 nm.

We also made effort to obtain low loss dielectric nano-composites by incorporating high dielectric constant of $BaTiO_3$ into HBCuPc polymer. The dielectric constant of the $BaTiO_3$/HBCuPc polymer nanocomposites was found to be greater than 9 in a wide frequency range and the dielectric loss (<0.03 at high frequencies) tended to decrease with the increasing ratio of the HBCuPc polymer in the nanocomposites (Figure 3.24). In comparison to the dielectric loss of pure $BaTiO_3$ nanoparticles, it was reduced to a ratio of 1/10. In addition, the incorporating of epoxy into the nanocomposites seemed to be able to reduce the dielectric loss further. In this case, the particle size and morphology of $BaTiO_3$ nanoparticles would be a dominating factor. The surface modification of nanoparticles will be one efficient strategy to create high dielectric constant, low dielectric loss nanocomposites as well. A great deal of effort has been carried out to optimize the composition of nanocomposites to enhance their performance.

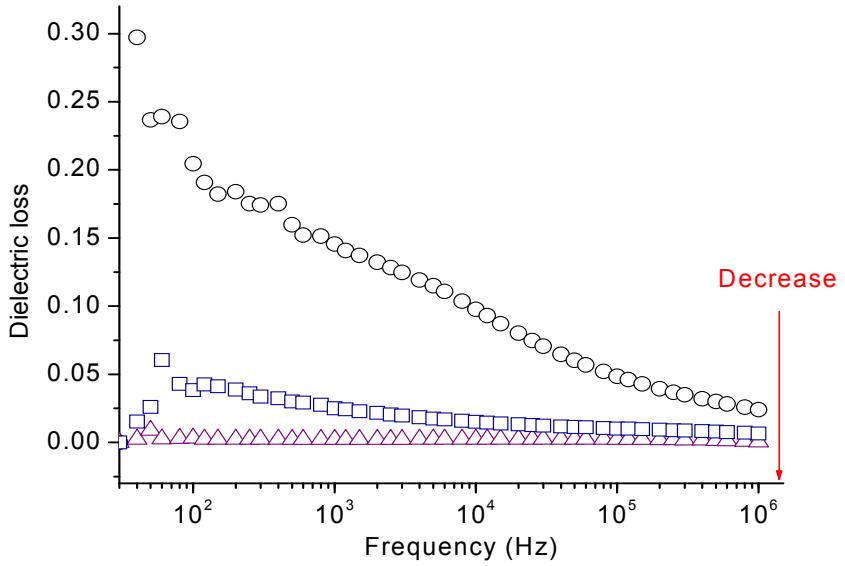

Figure 3.24 Dielectric loss of pure $BaTiO_3$ (○), HBCuPc dendrimer/ $BaTiO_3$ (100/80 Vol%) nanocomposites (□) and HBCuPc dendrimer/ $BaTiO_3$/Epoxy (100/50/80 Vol%, Δ).

3.4 Conclusion

In conclusion, we have found a novel organic branched Pc polymer system which shows impressive dielectric properties with very low loss at high operational frequencies. Compared to the percolative systems, this hyperbranched polymer system shows very low loss at higher frequencies and a small dispersion, as well as improved stability and flexibility. Measurements were carried out with both pressure compressed pellets and thin films of the Pc polymer system. The mechanism for this impressive high-frequency response with relatively small dispersion is suggested to be due to a long range polaron hopping mechanism accompanied by strong intramolecular interactions in the branched system. Moreover, we have observed non-Arrhenius and Poole-Frenkel behavior in this polymer system. The non-dispersive to dispersive transformation occurred when the temperature decreased, due to the self-organization of CuPc rings, creating more polaron hopping, as well as polaron tunneling pathways. The time-of-flight measurements demonstrated a fast movement of the carriers in the system (under sub microsecond with a low drain voltage) and the significant carrier mobility ($\sim 10^{-4}$ $cm^2V^{-1}s^{-1}$), may provide strong evidence to the strong and fast dielectric response in this dendrimer system. The impressive dielectric response in this dendrimer system can be attributed to polaron hopping and tunneling charge transport mechanisms.

Reference

(1) *Handbook of Low and High Dielectric Constant Materials and Their Applications*; Nalwa, H. S., Ed.; Academic Press: London, UK, **1999**; Vol. 1.

(2) Rao, Y.; Ogitani, S.; Kohl, P.; Wong, C. P. *Journal of Applied Polymer Science* **2002**, *83*, 1084-1090.

(3) Bai, Y.; Cheng, Z. Y.; Bharti, V.; Xu, H. S.; Zhang, Q. M. *Applied Physics Letters* **2000**, *76*, 3804-3806.

(4) Xu, J. W.; Wong, C. P. *Applied Physics Letters* **2005**, *86.*

(5) Dimitrakopoulos, C. D.; Malenfant, P. R. L. *Advanced Materials* **2002**, *14*, 99.

(6) Dougherty, T. J. *Photochemistry and Photobiology* **1987**, *45*, 879-889.

(7) Shirota, Y. *Journal of Materials Chemistry* **2000**, *10*, 1-25.

(8) Perry, J. W.; Mansour, K.; Lee, I. Y. S.; Wu, X. L.; Bedworth, P. V.; Chen, C. T.; Ng, D.; Marder, S. R.; Miles, P.; Wada, T.; Tian, M.; Sasabe, H. *Science* **1996**, *273*, 1533-1536.

(9) Spikes, J. D. *Photochemistry and Photobiology* **1986**, *43*, 691-699.

(10) Wohrle, D.; Meissner, D. *Advanced Materials* **1991**, *3*, 129-138.

(11) Bao, Z.; Lovinger, A. J.; Dodabalapur, A. *Applied Physics Letters* **1996**, *69*, 3066-3068.

(12) Zhang, Q. M.; Li, H. F.; Poh, M.; Xia, F.; Cheng, Z. Y.; Xu, H. S.; Huang, C. *Nature* **2002**, *419*, 284-286.

(13) Herron, N.; Stucky, G. D.; Tolman, C. A. *Journal of the Chemical Society-Chemical Communications* **1986**, 1521-1522.

(14) Gould, R. D. *Coordination Chemistry Reviews* **1996**, *156*, 237-274.

(15) Wang, J. W.; Shen, Q. D.; Bao, H. M.; Yang, C. Z.; Zhang, Q. M. *Macromolecules* **2005**, *38*, 2247-2252.

(16) Guo, M.; Yan, X. Z.; Kwon, Y.; Hayakawa, T.; Kakimoto, M. A.; Goodson, T. *Journal of the American Chemical Society* **2006**, *128*, 14820-14821.

(17) Li, L. T., A.; Hao, J.; Kikuchi, R.; Hayakawa, T.; Tsurumi, T.A.; Kakimoto, M.A. *IEEE Trans. Compon. Packag. Technol.* **2005**, 754.

(18) Nalwa, H. S.; Dalton, L. R.; Vasudevan, P. *European Polymer Journal* **1985**, *21*, 943-946.

(19) Yan, X. Z.; Pawlas, J.; Goodson, T.; Hartwig, J. F. *Journal of the American Chemical Society* **2005**, *127*, 9105-9116.

(20) Yan, X. Z.; Goodson, T. *Journal of Physical Chemistry B* **2006**, *110*, 14667-14672.

(21) Bobnar, V. L., A.; Huang, C.; Zhang, Q.M. *Condens. Matter. Mater. Phys.* **2005**, 041202(R).

(22) Vidadi, Y. A. R., L.D.; Chistyakov, E.A. *Sov. Phys. Solid State* **1969**, 173.

(23) Ranasinghe, M. I. V., O. P.; Pawlas, J.; Hauck, S. I.; Louie, J.; Hartwig, J. F.; Goodson, T., III. *J.Am.Chem.Soc.* **2002**, 6520.

(24) Maliakal, A. K., H.; Cotts, P. M.; Subramoney, S.; Mirau, P. *J.Am.Chem.Soc.* **2005**, 14655.

(25) *Electronic Processes in Non-Crystalline Materials*; Mott, N. F. D., E., Ed.; Clarendon Press: Oxford, **1979**.

(26) Bässler, H. *Phys. Status Solidi B* **1993**, 15.

(27) Fishchuk, I.; Kadashchuk, A.; Bassler, H.; Nespurek, S. *Physical Review B* **2003**, *66.*

(28) Hertel, D.; Bassler, H.; Scherf, U.; Horhold, H. H. *Journal of Chemical Physics* **1999**, *110*, 9214-9222.

(29) Arkhipov, V. I.; Bassler, H. *Physica Status Solidi a-Applied Research* **2004**, *201*, 1152-1186.

(30) Wang, L. F., D.; Basu, A.; Dodabalapur, A. *J.Appl.Phys.* **2007**, 054515.

(31) Hertel, D. S., U.; Bässler, H. *Adv. Mater.* **1998**, 1119.

(32) Mozer, A. J.; Sariciftci, N. S.; Pivrikas, A.; Osterbacka, R.; Juska, G.; Brassat, L.; Bassler, H. *Physical Review B* **2005**, *71*.

(33) Arkhipov, V. I. E., E.V.; Kadashchuk,A.; Blonsky,I.; Nešpůrek, S. Weiss, D.S.; Bässler, H. *Phys.Rev.B* **2002**, 165218.

(34) Kažukauskas, V. P., M.; Čyras, V.; Sicot, L.; Kajzar, F. **2007**, 247-251.

(35) Borsenberger, P. M. P., L.; Bässler, H. *J.Phys.Chem* **1991**, 5446.

(36) Fishchuk, I.; Kadashchuk, A.; Bassler, H.; Abkowitz, M. *Physical Review B* **2004**, *70*.

(37) Peled, A. S., L.B. *Chem. Phys. Lett.* **1988**, 422.

(38) Juška, G. G., K.; Arlauskas, K.; Österbacka,R.; Stubb, H. *Phys.Rev.B* **2002**, 233208.

(39) Cordes, H. B., S.D.; Kohary,K.; Thomas,P.; Yamasaki, S.; Hensel,F.; Wendorff, J.H. *Phys.Rev.B* **2001**, 094201.

(40) Mahapatro, A. K. G., S.; *J.Appl.Phys.*, **2007**, 034318.

(41) Ambily, S. M., C.S. *Thin Solid Films* **1999**, 284-288.

(42) Berkovits, V. L. Z., A.V.; Kazanskii,A.G.;Kolos'ko,A.G.; Ramsh,S.M.; Terukov, E.I.; Fenukhin,A.V.Ulin, V.P.Yure,T.A.; Kleider, J.P. *Phys.Solid State* **2007**, 272-276.

(43) Henriksson, A. R., B.; Sundbom, M. *Theoret. Chim.Acta (Berl.)* **1972**, 303-313.

(44) Knupfer, M. S., T.; Peisert, H.; Fink, J. *Phys.Rev.B* **2004**, 165210.

Chapter 4

Effect of Donor and Acceptor Strength in Hyperbranched Pc Polymers for High Dielectric Applications

4.1. Introduction

High energy density and low loss tangent capacitors powered at high frequency are essential electronic components for many pulsed power device applications, which include pulsed laser, defibrillators and display devices.[1,2] Therefore, high dielectric constant materials with high breakdown field, low dielectric loss, and low dielectric dispersion are strongly needed. The traditional high dielectric constant materials for high energy density capacitors are ceramics (e.g. $BaTiO_3$, $CaCu_3Ti_4O_{12}$).[3-8] They can achieve very high dielectric constant at low frequency (1-100KHz). However, they suffer from problems such as poor processibility and large impact from defects. In order to avoid or mitigate these limitations, many efforts have been devoted to introduce inorganic fillers (e.g. Al, $BaTiO_3$) or conductive fillers (e.g. conductive polymers, carbon nanotubes) into the polymers. [9-23] For example, Rao et al. developed a high dielectric constant (~150 at 10 KHz) lead-magnesium niobate-lead titanate (PMN-PT) /$BaTiO_3$/epoxy nanocomposite with ceramic filler loading up to 85% by volume.[24] The required high filler concentration in order to achieve high dielectric constant will result in high dielectric loss and relatively low breakdown voltage in these polymer-ceramic composites, as well as some technical

barriers such as poor dispersion of the fillers in the polymer matrices and poor compatibility with organic substrates.[25] To overcome the limitations of ceramic/organic composites, considerable efforts have been taken recently. For instance, Dang et al. reported a giant dielectric permittivity ~400 at 100 Hz in a functionalized carbon nanotube/poly(vinylidene fluoride) (PVDF) nanocomposite with the conductive filler loading of 8 vol%.[14] In comparison to polymer-ceramic systems, the required loading of conductive fillers for a similar value of dielectric constant has been greatly lowered down. Whereas, the dielectric loss was extremely high (tanδ=~2) and the dielectric properties of the composite was still constrained by the percolation theory. Therefore, an all-organic material with high dielectric constant have inspired a great interest in the exploration of their usage especially for catering to the miniaturization and cost-saving demand of next generation electronics. In fact, a number of organic materials have shown high dielectric constant.[26-31] For instance, PVDF/poly(p-chloromethyl styrene) (PCMS) grafted copper phthalocyanine (CuPc) (PCMS-g-CuPc) all-organic composite showed a dielectric constant of 325 at 100Hz due to the Maxwell-Wagner-Sillars polarization mechanism.[28] Also, thiourea (TU) - graft- cyanoacrylate/ PVDF composites possessed a dielectric constant ~ 54 up to 100MHz.[31] A common disadvantage of above materials is the high dielectric dispersion and large loss tangent, e.g. TU-graft-cyanoacrylate/PVDF composite had a loss tangent ~0.03. These will lead to thermal effect and perhaps thermal failure. Hence, it necessitates the research on high dielectric constant and low dielectric loss all-organic materials.

Recently, we demonstrated that high dielectric constant and low loss are attainable by using polaron delocalization in hyperbranched polymer systems.[1,2,32] For

example, a high dielectric constant (>46) and low dielectric loss (~0.001) were observed in a hyper-branched copper phthalocyanine dendrimer with very small dielectric dispersion.[1] The charge transfer mechanism for this impressive dielectric performance was related to a long range polaron hopping process accompanied by strong inter-molecular interactions in the branched systems. And the high electron mobility (~10^{-4} $cm^2V^{-1}s^{-1}$) in addition to the non-Arrhenius and Poole-Frenkel behavior observed from time-of-flight measurement provided a convincing proof for the strong and fast dielectric response found in this hyperbranched copper phthalocyanine system.[32] Moreover, ultrafast delocalization and electron hopping are evidenced from femtosecond up-conversion fluorescence measurement, which were suggested to be able to enhance the dielectric response in hyperbranched systems in comparison to their linear analogues.[2,32]

Hence, in this chapter, the design, synthesis and characterization of functionalized hyperbranched copper phthalocyanine (HBCuPc-TPA-CN) polymer are reported. In this polymer, the electron donating group of triphenylamine (TPA) was functionalized into the hyperbranched copper phthalocyanine architecture due to its excellent thermal and electrochemical stability, electron donating ability in addition to its good film-forming properties.[33-38] In addition, previous investigations in triarylamine dendrimers and ladder systems have found that highly delocalized radical cations could be formed in an electron rich hyperbranched system, which will result in strong interactions over relatively large molecular distance.[39,40] CuPc has recently emerged as a versatile block for novel electron accepter units. [41-43]Therefore, we are interested in the understanding of the influence of the interaction strength of the donor-acceptor in hyperbranched systems and the formed intermediate charge pairs on the optical and electronic properties of the HBCuPc-TPA-

CN polymers. The conclusion will be made based on the comparison between the HBCuPc-TPA-CN polymer and the previously investigated HBCuPc polymer.

4.2 Experimental Section

Materials. All reagents were purchased from Aldrich Chemical Co. and used as received unless stated. Both dimethyl sulfoxide (DMSO) and N, N-dimethylacetamide (DMAc) were dried with calcium hydride and distilled under reduced pressure.

Synthesis of the monomer (bis((3,4-dicyanophenoxy)phenyl)phenylamine). Scheme 4.1 summarizes the synthesis of compounds 1-3. In general, Aniline was first coupled with 4-iodoanisole to produce bis(4-methoxyphenyl)phenylamine(1), followed by the demethylation reaction by BBr_3 to yield bis(4-hydroxyphenyl)phenylamine (2). Finally, the coupling reaction of bis(4-hydroxyphenyl)phenylamine and 4-nitrophthalonitrile was carried out in DMSO to form bis((3,4-dicyanophenoxy)phenyl)phenylamine.[44,45]

Preparation of bis(4-methoxyphenyl)phenylamine (1). A mixture of 10 g (107.37 mmol) of aniline, 2.13 g (21.48 mmol) of copper (I) chloride, 54.22 g (966.39 mmol) of potassium hydroxide, 3.87 g (21.48 mmol) of 1,10-phenanthroline, and 56.28 g (230.86 mmol) of 4-iodoanisole were dissolved in 250 ml of m-xylene at 180 °C under nitrogen atmosphere and stirred for 72 hr. Then the reaction mixture was cooled down to the ambient temperature, dissolved in 300 mL of methylene chloride, washed with 3 × 300 mL of water, and dried by magnesium sulfate. After that, the solvent was removed under reduced pressure, and the residue was purified by the flash chromatography (40 × 150 mm column, SiO_2, CH_2Cl_2/hexane, 1:10). The 9.52 g (31%) of bis(4-methoxyphenyl)phenylamine was collected as a yellow solid.

R_f = 0.5 (SiO_2, CH_2Cl_2/hexane, 1:10);

^{1}H NMR (300 MHz, DMSO-d6): δ= 7.19 (t, 2H, *J* = 8.63, 15.97 Hz), 6.99 (d, 4H, *J* = 8.99 Hz), 6.89 (d, 4H, *J* = 8.99 Hz), 6.84-6.76 (m, 3H)

^{13}C NMR (75 MHz, DMSO-d6) δ=155.5, 148.3, 140.2, 128.8, 126.2, 120.1, 119.8, 114.8, 55.1

FT-IR (KBr, cm^{-1}): 3034, 2954, 2911, 1592, 1478, 1440, 1321, 1278, 1244, 1168, 1083, 993, 913, 813, 759, 716, 590, 521

Anal. Calcd for $C_{20}H_{19}NO_2$: C, 78.66; H, 6.27; N, 4.59. Found: C, 78.87; H, 6.26; N, 4.86.

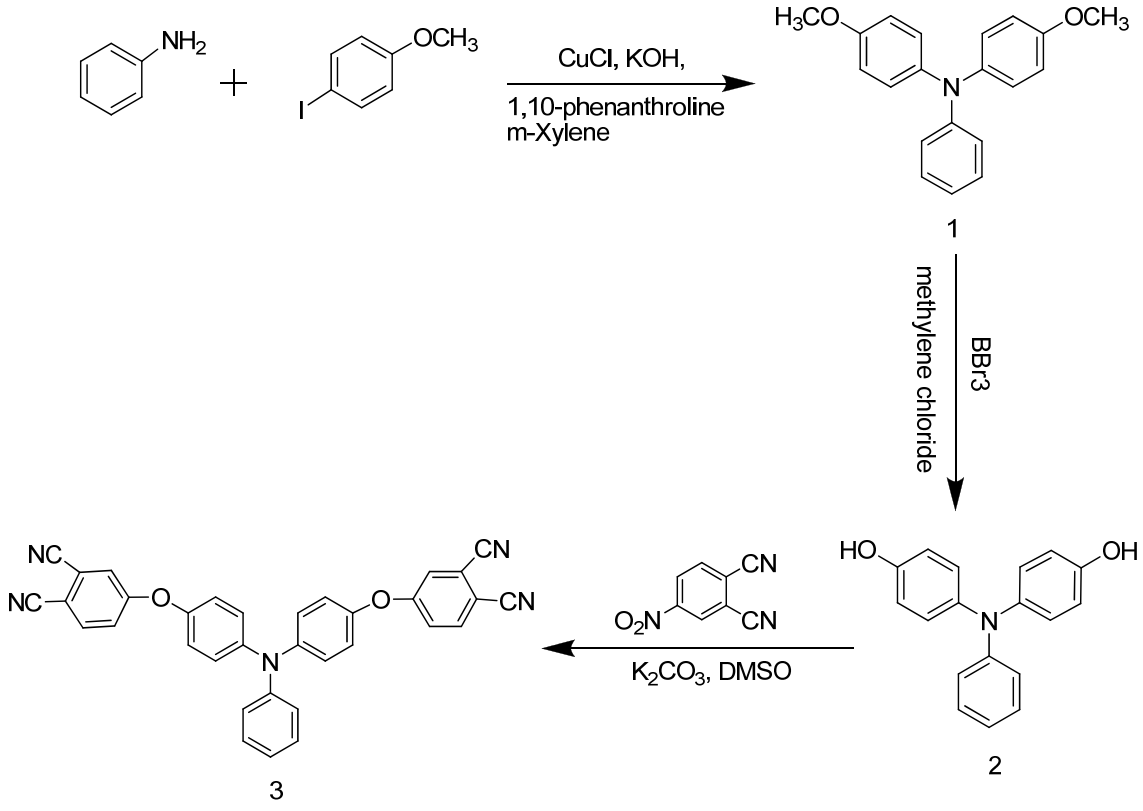

Scheme 4.1 Synthesis of bis((3,4-dicyanophenoxy)phenyl)phenylamine monomer (3).

Preparation of bis(4-hydroxyphenyl)phenylamine (2). To a stirred solution of 5 g (16.37 mmol) of bis(4-methoxyphenyl)phenylamine in 75 mL of chloroform at 0 °C

under nitrogen atmosphere, 130.99 mL (130.99 mmol) of 1M BBr_3 in methylene chloride was added dropwise. After 1hr at 0 °C, the reaction mixture was kept at 0 °C for 1 hr, then was heated up to room temperature and stirred for 5 hr. After cooling back to 0 °C, methanol was added slowly to the reaction mixture. And the solvent was removed under reduced pressure, diluted with 500 mL of ethyl acetate, washed with 3 × 300 mL of a saturated aqueous sodium bicarbonate solution, and dried by magnesium sulfate. Finally, the residue was purified by the flash chromatography (40 × 150 mm column, SiO_2, EtOAc/hexane, 1:3) and 4.12 g (91%) of green bis(4-hydroxyphenyl)phenylamine was obtained.

R_f = 0.2 (SiO_2, CH_2Cl_2/hexane, 1:3)

^{1}H NMR (300 MHz, DMSO-d6) δ= 9.20-9.08 (br, 2OH), 7.13 (t, 2H, *J* = 7.34, 15.97 Hz), 6.90 (d, 2H, *J* = 8.81 Hz), 6.76-6.67 (m, 7H)

^{13}C NMR (75 MHz, DMSO-d6) δ=153.9, 148.9, 138.7, 128.8, 127.0, 119.1, 118.3, 116.1, 115.5

FT-IR (KBr, cm^{-1}): 3538, 3061, 1595, 1438, 1312, 1250, 1164, 1078, 1011, 914, 811, 726, 695, 593, 517

Anal. Calcd for $C_{18}H_{15}NO_2$: C, 77.96; H, 5.45; N, 5.05. Found: C, 77.14; H, 5.43; N, 5.32.

Preparation of bis((3,4-dicyanophenoxy)phenyl)phenylamine (3).

To a flask, 4 g (14.42 mmol) of bis(4-hydroxyphenyl)phenylamine, 6.24 g (36.06 mmol) of 4-nitrophthalonitrile, and 9.97 g (72.12 mmol) of K_2CO_3 were dissolved in 80 mL of DMSO at room temperature under nitrogen atmosphere and stirred for 48 hr. Then, the mixture solution was cooled down to 0 °C, and water was added to generate the solid.

The precipitate was collected by the filtration, and rinsed with cold methanol. Yellow powder of 5.52 g (72%) of bis((3,4-dicyanophenoxy)phenyl)phenylamine was obtained after the purification by the recrystallization using methanol and ethyl acetate.

R_f = 0.4 (SiO_2, EtOAc/hexane, 1:2)

^{1}H NMR (300 MHz, DMSO-d6) δ=8.09 (d, 2H, *J* = 8.63 Hz), 7.77 (d, 2H, *J* = 2.57 Hz), 7.44 (dd, 2H, *J* = 2.57, 8.63 Hz), 7.36 (t, 2H, *J* = 7.34, 15.97 Hz), 7.17-7.03 (m, 11H)

^{13}C NMR (75 MHz, DMSO-d6) δ=161.1, 148.8, 146.8, 144.6, 136.0, 129.5, 125.2, 123.7, 123.2, 122.2, 121.7, 121.3, 116.5, 115.6, 115, 2, 107.9

FT-IR (KBr, cm^{-1}): 3428, 3040, 1592, 1498, 1414, 1276, 1205, 1086, 951, 840, 721, 644, 590, 524

Anal. Calcd for $C_{34}H_{19}N_5O_2$: C, 77.12; H, 3.62; N, 13.23. Found: C, 76.83; H, 3.54; N, 13.30.

Synthesis of the HBCuPc-TPA-CN Polymer. The HBCuPc-TPA-CN polymer was synthesized by a copper fusion method, [46,47] as shown in Scheme 4.2. To a flask, 2 g (3.78 mmol) of bis((3,4-dicyanophenoxy)phenyl)phenylamine was dissolved in 5 ml of DMAc at 160 °C under nitrogen atmosphere. Then 112.17 mg (1.13 mmol) of copper(I) chloride was added into the flask and the mixture was stirred for 8h. DMAc solvent was used to dilute the reaction mixture to 5 wt%. The mixture was poured into 1000 mL of water. The crude product was collected by the filtration, dried under vacuum, dispersed in methanol, and refluxed for 6h. The precipitate was then filtered, dried under vacuum, dissolved in DMAc, and stirred for 6h. After the filtration, the filtrate was poured into methanol and the precipitated polymer was filtered off, and dried under vacuum. A 780

mg of HB-CuPc-TPA was obtained as a dark blue solid. The final structure was characterized by ^{1}H NMR, FT-IR and DI-Mass spectra. The HBCuPc-TPA-CN dendrimers with varying molecule weight were synthesized and the sample under this investigation has a molecule weight (Mw) of 20,000.

^{1}H NMR (300 MHz, THF-d8): broad aromatic protons from δ= 6.5-8.0

FT-IR (KBr, cm^{-1}): 3650, 3037, 1735, 1592, 1402, 1312, 1230, 1160, 1092, 1011, 890, 748, 572; Anal. Found: C, 72.85; H, 3.61; N, 13.55.

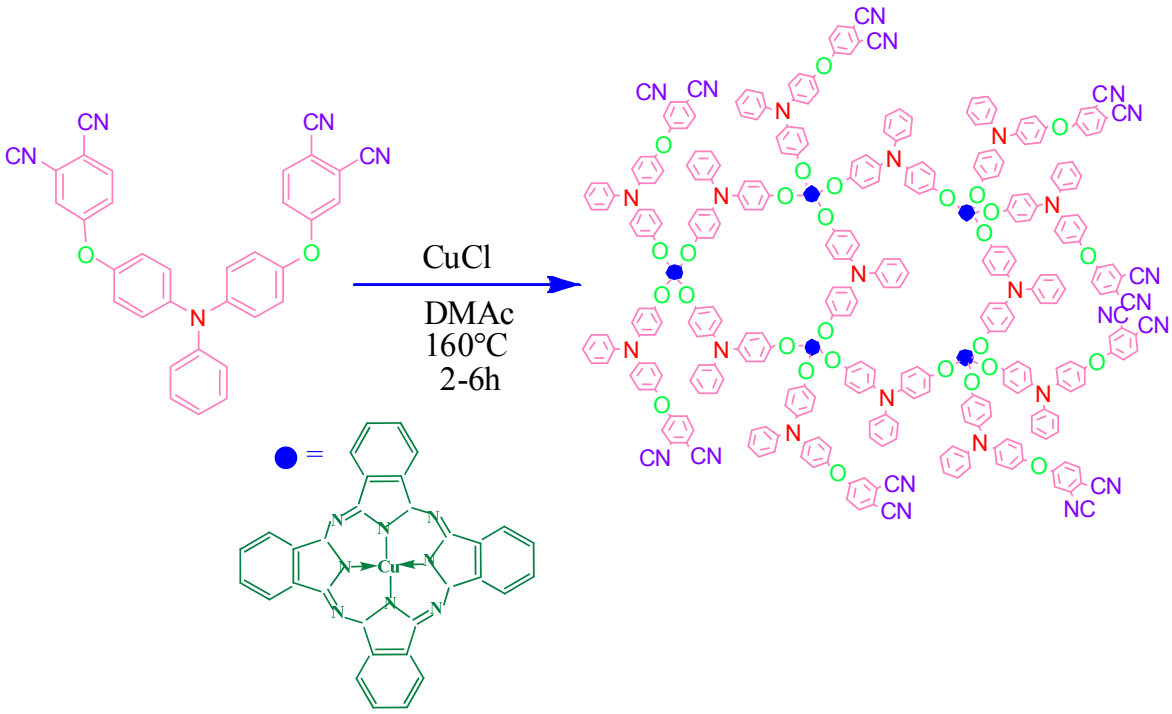

Scheme 4.2 Synthesis of CN- ended HBCuPc-TPA dendrimer

Preparation of casting films of the HBCuPc dendrimer. A small amount of dark blue HBCuPc-TPA-CN powder was grindered in a pestle for 10 mins. Then the powder was poured into a vial filled up with 0.5 mL DMAC solution. The mixture was stirred on a hot plate for 10 hrs. Heat was supplied at the first 3 hrs to dissolve the

phthalocyanine powder. The formed homogeneous gel solution from the mixture was sonicated for extra 10 mins to break down the polymer aggregates. Both alumina foil and indium tin oxide (ITO) glass were used as the substrate. For the ITO glass substrate, several steps of cleaning process were followed to avoid the contamination and the film was coated on the conductive side of the ITO glass. The prepared films were dried in air for one day and followed by continuous heat treatment in vacuum for another 14 hrs to evaporate all the solvents.

Steady-State Spectroscopy Techniques. Ultraviolet (UV)-visible absorption spectra were recorded with an Agilent Technologies 8453 spectrophotometer. Steady-state fluorescence measurements were performed on a Fluomax-2 fluorimeter. The solvent for all spectroscopic measurement is DMAc.

Dielectric Measurement. Dielectric measurements were carried out with a 4284A HP LCR meter (20Hz-1MHz) connected with an HP 16451B dielectric fixture. A contact electrode method was used. The capacitance (C_p) and dielectric loss (tanδ) were directly recorded from this instrument. The dielectric constant was determined by the equation $K = \frac{C_p d}{\varepsilon_0 A}$. Here ε_0 is the dielectric permittivity of the vacuum (8.85 x 10^{-12} F/m); A is the area of the electrode (m^2) and d is the thickness of the film (m). The film thickness was obtained by scanning electron microscopy (SEM) cross section measurement and Dektak surface profiler and the results were in good agreement with each other.

Time-Resolved Fluorescence Decay and Anisotropy Measurement. Time-resolved polarized fluorescence measurements were carried out on a femtosecond fluorescence up-conversion set-up. The detailed description of the set-up has been

itinerated elsewhere.[39,40] In brief, the HBCuPc-TPA-CN polymer/DMAc solution was excited with frequency-doubled light from a mode-locked Ti-sapphire laser with a pulse width of ~ 55fs at a wavelength of 820nm. The polarization of the excitation beam for the anisotropy measurements was controlled with a Berek compensator. The sample cell was 1mm thick and was held in a rotating holder to avoid possible photodegradation and other accumulative effects. The fluorescence emitted from the sample was collected with achromatic lens and directed parallel or perpendicular to a nonlinear crystal of β-barium borate. After passing through a motorized optical delay, the rest of the fundamental light mixed with the emission from the sample in another nonlinear crystal to generate sum frequency signal. This up-conversion signal was dispersed using a monochromator and detected using a photomultiplier tube (R 1527P, Hamamatsu City, Japan).

The measured fluorescence decay was calculated according to the expression: $r(t) = \frac{I_{par} - GI_{per}}{I_{par} + 2GI_{per}}$. Here, I_{par} and I_{per} are the intensities of fluorescence polarized vertically and horizontally to the polarization of excited light respectively. The G factor accounts for the varying sensitivities for the detection of emission at vertically and horizontal polarization configurations and is 1.01 in our case. The standard for obtaining G factor in the experiment was the perylene dissolved in cyclohexane solution.

Pump Probe Transient Absorption Measurements. Transient absorption measurement was used to investigate the excited state dynamics of the phthalocyanine polymer at different excitation wavelengths and the description of the system has been provided elsewhere.[48] Briefly, the pump beam was produced by the OPA-800C. The pump beams used in the present investigation were obtained from the fourth harmonic of the idler beams and were focused onto the sample cuvette. The probe beam was delayed

with a computer controlled motion controller and then focused into a 2 mm sapphire plate to generate white light continuum. The white light was then overlapped with the pump beam in a 2 mm quartz cuvette containing the sample and the change in the absorbance for the signal was collected by a CCD detector (Ocean optics). Data acquisition was controlled by the software from Ultrafast Systems Inc. For this measurement, we used the pump power of 250 nJ per pulse and the kinetics was found to be independent of pump-power for all the investigated phthalocyanine polymers. Magic angle polarization was maintained between the pump and probe using a wave plate. The pulse duration was obtained by fitting the solvent response, which was 130 fs. The sample was stirred with a rotating magnetic stirrer and no photodegradation of the sample has been observed.

4.3 Results and Discussion

4.3.1 Dielectric Response

Dielectric behaviors of the HBCuPc-TPA-CN polymer cast films with different thickness and substrate were studied and compared. The tests showed very good reproducibility. In addition, these dielectric films showed very good thermal stability in the room temperature, as there is no visible deviation in the dielectric response after one year. Figure 4.1 shows the dielectric properties of the HBCuPc-TPA-CN polymer film with a thickness of ~10 μm as a function of the frequency. It can be observed that the frequency dependence of the dielectric constant was weak in the HBCuPc-TPA-CN polymer film, similar to that in the previously investigated HBCuPc polymer film.[1] The dielectric constant of the HBCuPc-TPA-CN polymer film at 1MHz was ~11, which is a distinct improvement over previously investigated triphenylamine based polyamides (~3-4) and CuPc monomer (~5) systems.[8,34] This enhancement may be contributed by the

ultrafast delocalization of the rigid macrocycles of CuPc rings within the hyperbranched architecture. And the increased delocalization length in hyperbranched polymer in relative to that of the monomer may play an important role too. As to the comparison of the dielectric constant values between the HBCuPc-TPA-CN and HBCuPc polymers, a relatively lower dielectric constant in the former film was possibly due to the inhibition of the face-to-face packing because of the tetrahedral shape of triphenylamine moiety. Besides, the formation of a charge transfer complex between the TPA donor and the CuPc acceptor may result in a low polaron hopping activation energy and an increase in the effective hopping distance. The dielectric loss decreased sharply from 0.28 at 1 KHz with the increase of the frequency, which is mainly due to the strong ionic polarization in the system.

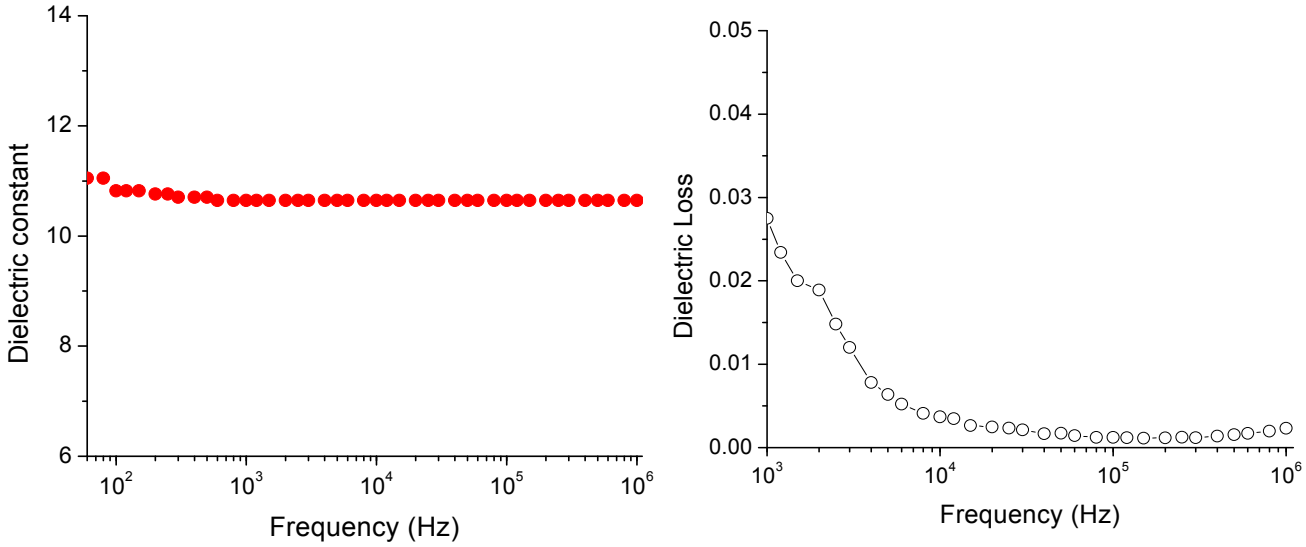

Figure 4.1 a) Dielectric response and b) dielectric loss curves of HBCuPc-TPA-CN polymer pristine film with a thickness of 10µm.

Between the frequency ranges from 10 KHz to 1MHz, the dielectric loss dissipation was mitigated and it reached 0.0025 at 1MHz. As the exciton traps induced by the TPA donor may immobilize a considerable amount of charge carriers and cause a delay in the response to the re-arrangement of the dipole orientation at low frequencies. The flexible rotation due to the TPA moiety in combination with the steric effect will affect the electron transport properties of the HBCuPc-TPA-CN polymer system and relatively smaller electron mobility should be expected.

4.3.2 Charge Transport Mechanisms

An effective transport of charge carrier in the hyperbranched polymer system will enable the improvement in the dielectric response. The knowledge in the operative charge transfer mechanisms in the hyperbranched polymer system is crucial to the development of the high dielectric materials. The Ac properties in the HBCuPc-TPA-CN dendrimer may provide important information about the electronic conduction processes, which can be inferred from the type of conductivity (σ) dependence on the angular frequency (ω).[49-51] The hopping conduction mechanism has been observed in various CuPc based materials. For example, Sadaoka and Sakai observed a power law conductivity dependence ($\sigma \propto \omega^n$) not only for compressed powders but also for thin films of CuPc monomers and concluded that the hopping was a major conduction process in CuPc.[51] Vidadi et al. also suggested for a CuPc film that the charge carrier transport was dominated by hopping in the low temperature and high frequency region.[52] Although the AC conductance of CuPc materials has been well studied, few reports are available for hyperbranched or dendritic CuPc macromolecules. Here, measurement of the AC conductance as a function of the angular frequency was conducted on the HBCuPc-TPA-

CN polymer and a power-law relationship was observed. From the fitting of the Ac conductance ($\sigma_{AC} = A + B\varpi^{s}$), a super-linear power law was found as:

$$\sigma = 3.5116\times10^{-9} + 6.6447\times10^{-17}\omega^{1.58} \quad (4.1)$$

Or, $$\sigma = 2.5005\times10^{-16}\omega^{1.48867} \quad (4.2)$$

A value of s= 1.48-1.58 for the exponent of the σ (ω) function was determined for the HBCuPc-TPA-CN polymer films at frequencies of 20 Hz- 1 MHz. Identical conclusion was made to that drawn from the HBCuPc polymer in our earlier work, polaron hopping conduction is the major charge carrier transport mechanism operative in the HBCuPc-TPA-CN polymer film. No visible change in the conductivity with frequency up to 10 KHz, which is typical for hopping conduction. But more charge carriers may be available to "hop" by tunneling upon further increase in the frequency, which explains the increase of the bulk conductivity above 10 KHz. In this case, both polaron hopping and polaron tunneling mechanisms are in effect. Actually, we have found a super-linear power law dependence (yielding an s value ~1.7) in previously investigated HBCuPc polymer pressed pellet, but a linear power law dependence (s: ~0.7-0.8) was followed in the cast film of the HBCuPc polymer.[1] Beyond that, the AC conductance of this novel polymer system is ten-fold of that in the HBCuPc system, which may suggest the existence of a stronger dipole orientation in this novel system due to the introduction of electron rich TPA units.[53] In addition, the diffusion process is dominant in such kind of molecular materials, and then the conduction is dependent on the barriers that originate from the lattice relaxation as well as the intermolecular interaction. The formation of $CuPc^{\bullet-}$-$TPA^{\bullet+}$ charge transfer states with stronger electron coupling hence resulted in high AC conductance in HBCuPc-TPA-CN polymer.

Furthermore, the high AC conductance in this HBCuPc-TPA-CN polymer film may suggest that there exists more delocalization states; Whereas, the comparatively low dielectric constant may indicate a shorter delocalization length for polarons in HBCuPc-TPA-CN system as compared to that in the HBCuPc system. That is to say, the introduction of TPA moiety into hyper-branched CuPc structure possibly interrupts the conjugation along the branch. The difference in the dielectric properties of above two hyperbranched phthalocyanine systems may support the concept of utilizing the longer delocalization length in hyperbranched systems to enhance the dielectric response of organic materials. It also suggests that one critical factor is the balance between the amount of delocalization states and the delocalization length, as well as disorder. [2,54,55] Martens and Brom has suggested that the electronic delocalization is dominated by an inter-grain charge transfer process.[56] With the possibility to form more charge transfer states, more delocalization sites will be available in the HBCuPc-TPA-CN polymer. But if there are some defects along the boundary between the donor and the acceptor, the enhancement in the dielectric constant may be limited.

To confirm the dielectric performance in such a hyper-branched system and optimize the preparation conditions, other casting films of HBCuPc-TPA-CN polymer were prepared. The thickness effect has been eliminated by keeping the films at the same thickness (~10μm). We found out that the films prepared from sonicated solutions have smaller dielectric dispersion, while maintaining the similar dielectric performance. The alleviated dielectric dispersion may be related to the reduced amount of crystalline nano domains of HBCuPc-TPA-CN particle and induced disorder in this system.

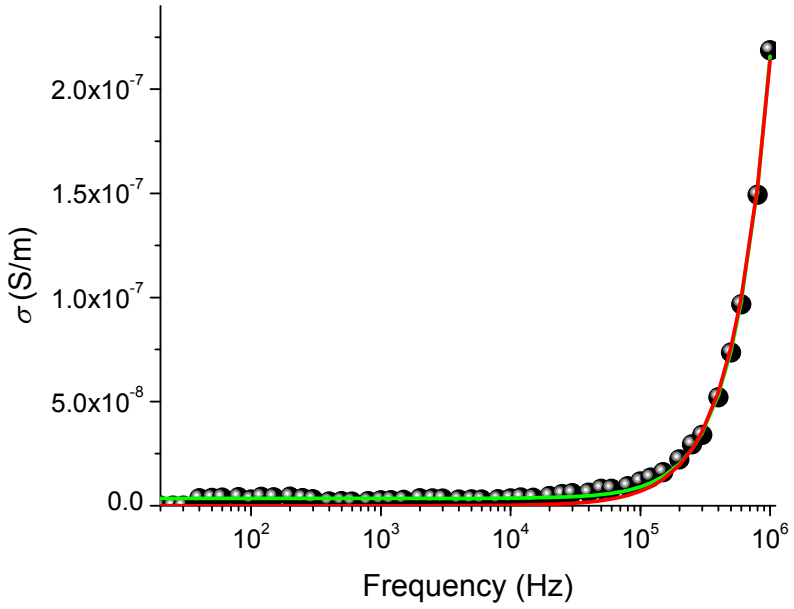

Figure 4.2 AC conductance of the HBCuPc-TPA-CN film.

4.3.3 Ground and Excited State Dynamics

Figure 4.3 is the steady-state absorption and emission of the HBCuPc-TPA-CN polymer. Similarly to the HBCuPc polymer, it showed characteristic B and Q bands absorption of CuPc.[32] The absorption at UV range may be assigned to C (270nm, d-π^*), N (347nm, d-π) and B (363nm, π-π^*) bands of the CuPc ring, respectively. And the strong peak at 302nm corresponds to the absorption of the triphenylamine moiety. The maximum B band absorption peak of HBCuPc-TPA-CN polymer showed a bathochromic shift from that of the HBCuPc polymer ($\Delta\lambda_{max} = 27nm$), along with the increased intensity of B band. It suggests that the introduction of TPA moiety increases the conjugation part in HBCuPc-TPA-CN branch and reduces π-π^* transition energy. Moreover, if we compare the lower energy onset of the absorption bands of the two CuPc dendrimer systems, apparently, the HBCuPc-TPA-CN polymer may have longer

conjugation length due to the low energy onset (E_g = 1.48eV). But, it turns out that the delocalization length doesn't increase with the conjugation length and the triplet excitation delocalization may vary from that in HBCuPc polymer. Based on our previous investigations on hyper-branched materials for high dielectric applications, one advantage was that the dielectric response will be enhanced through the increased delocalization length, that's why we didn't observe enhanced dielectric response in HBCuPc-TPA-CN polymer compared to HBCuPc polymer. Another possibility comes from that the pyramidal shape of triphenylamine moiety interferes with the close face-to-face stacking of the CuPc rings.

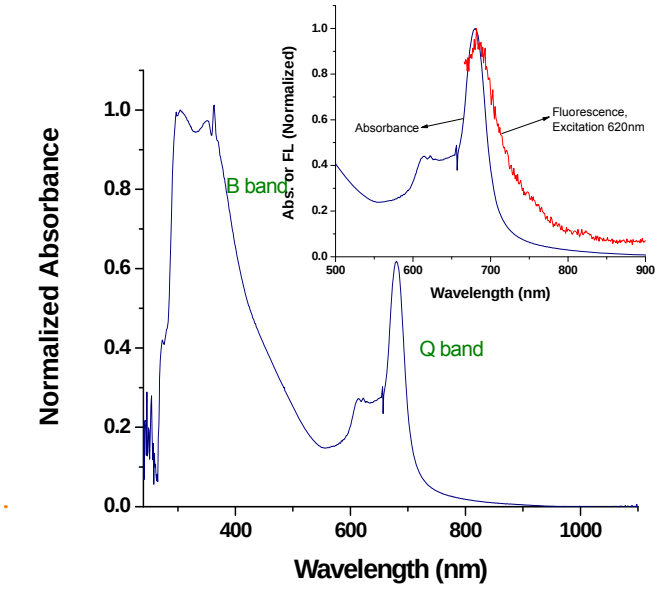

Figure 4.3 Absorption and emission (excitation at Q_y band) spectra of HBCuPc-TPA-CN Polymer

In addition, the absorption peaks shown at 622nm and 680nm were both assigned to Q band (π-π^*) transitions. A weak emission was observed when excited at Q_y band of 622nm (Figure 3 inset). However, a stronger emission was observed at an excitation of

~400nm, in contrary to the zero emission observed for the HBCuPc polymer. It indicates that this emission is mainly from TPA unit and the internal conversion from S_2 to S_1 is slower in the HBCuPc-TPA-CN polymer, thus the fluorescence is detected from both B and Q band excitation. In addition, the fluorescence peak in the red region shifts to blue region when the excitation wavelength is changed from 622nm to 400 nm, indicating that this observed red fluorescence is mainly from the second excited singlet state (S_2) and is short-lived. Apparently, the emission spectrum was distorted from the mirror image of the absorption spectrum, possibly related to other non-radiated charge transfer process.

Up-converted ultrafast fluorescence dynamics and anisotropy decay experiments have been applied successfully to the study of many π-conjugated organic materials to reveal possible ultrafast processes such as vibrational relaxation and singlet-singlet annihilation, occurring in a time scale shorter than 20ps, and to validate the presence and type of intramolecular energy and charge transfer processes.[32,57-60] Recently, several reports have been published on the Q-state and B-state fluorescence dynamics of porphyrin derivatives by means of femtosecond fluorescence up-conversion. And Anaïs Medina et al. have confirmed an accelerated charge transfer in a triphenylamine-subphthalocyanine donor-acceptor system through femtosecond transient absorption measurement.[33]

Figure 4.4 shows the polarized fluorescence decay of HBCuPc-TPA-CN polymer measured at 480nm with an exaction at 400nm. The fluorescence intensity decays were fitted with two exponentials. A fast fluorescence decay component was found in a time scale ~205 fs, larger than the instrument response function (IRF=114 fs). And the slow fluorescence decay component was in a time scale of ~1.5ps, the same magnitude with

that of the HBCuPc polymer (3 ps), and common to polaron hopping systems. In some cases, the incorporation of TPA unit to the core will induce fluorescence quenching and a fast decay is expected. However, there is a very long tail after initial decay in this system, which is possibly due to the strong π conjugation of TPA moiety, causing the trapping of excitons. A slow depolarization process in a time scale of ~3ps was occurred in this system. The slow component may be related to the transfer of excitations from the mostly delocalized TPA to the CuPc core via a typical Föster hopping mechanism or salvation induced intramolecular vibrational energy redistribution.

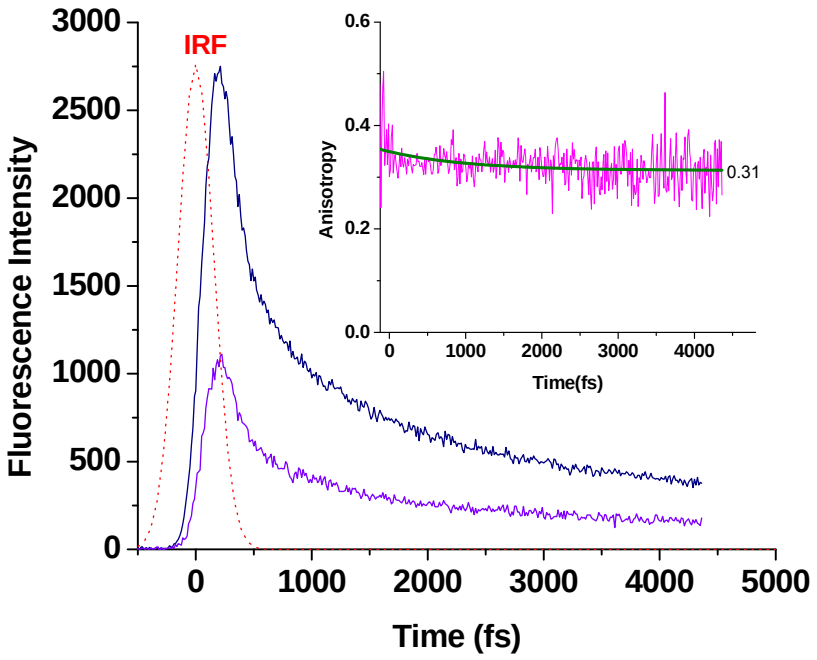

Figure 4.4 Up-converted fluorescence dynamics of HBCuPc-TPA-CN dendrimer

Moreover, previously investigated HBCuPc dendrimer only showed a very weak fluorescence emission at 480nm, but the emission of HBCuPc-TPA-CN polymer was stronger at the same wavelength and should be attributed to the triphenylamine fluorophores, which also has been found in several triphenylamine based systems. [61,62]

The inset in Figure 4.4 depicts the anisotropy decay of HBCuPc-TPA-CN polymer. The residue value of ~0.31 is possibly due to the exciton trapping during the excited-state relaxation from TPA unit. A similar exciton trapping phenomenon has been found in a novel triarylamine dendrimer system.[63]

In order to probe the nature of the excited-state interactions between the TPA moiety and CuPc core, as well to confirm the bathochromic shift due to the incorporation of TPA units, we also applied femtosecond transient absorption pump-probe spectroscopy. Figure 4.5 shows 2D transient absorption spectrum of both HBCuPc-TPA-CN and HBCuPc polymer. From the comparison of both spectra, there is an occurrence of additional charge transfer states in the HBCuPc-TPA-CN polymer, possibly due to the formation of $CuPc^{\bullet-}$-$TPA^{\bullet+}$ charge transfer complex via an intramolecular charge transfer reaction .

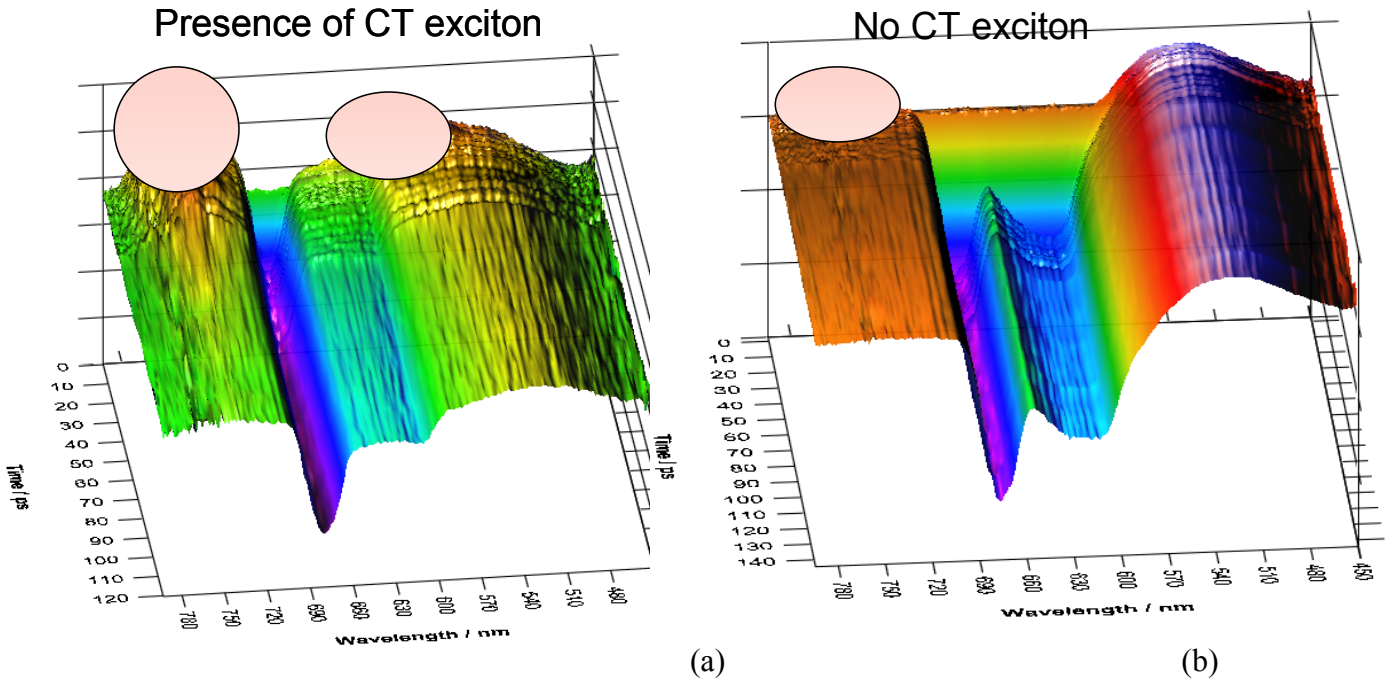

Figure 4.5 Transient absorption spectra of (a) HBCuPc-TPA-CN polymer; (b) HBCuPc polymer.

Figure 4.6 shows the transient absorption changes ΔA as a function of wavelength for a few delay times between the pump and probe pulses with an excitation at 365nm.It exhibits typical T_1-T_n triplet-triplet absorption spectra of phthalocyanine compounds.[64-66] The negative ΔA signals at 585-705 nm corresponds to the photobleaching of the S_0-S_1 transition (Q-band) and correlates to the Q_y absorption band. As the time decay is increased from 200 fs to 10.2 ps, excited state absorption (ESA) with a maximum at 742nm is slightly shifted to short wavelengths to a maximum around 739nm. The excited state absorption was assigned to photo induced absorption of mainly $TPA^{\bullet+}$ cations. The maximum peak absorption is obtained at 2 ps, corresponding to the charge pair formation. Moreover, the broad induced absorption band between 450-600nm shows blue shift as the evolution of decay time, and it could be due to excitonic polaron state formation, that is to say, the formation of charge pair complexes. Both absorption band and photobleaching band has been observed in other phthalocyanine based materials films and solutions.[67,68] The weak absorption bleaching with a maximum at ~610nm at 150ps decay time could be explained by assuming a cancelation of ground state bleaching by excited state absorption or very fast localization of excitations on the molecular species with lowest excited state energy.[67]

As evidenced from the global fitting of transient absorption kinetics, a decay component of 1.7 ps is observed, comparable to the slow component of fluorescence decay (~1.5 ps), polaron hopping charge transfer mechanism is operative in this dendrimer system. After 10.2 ps, the photo induced absorption changes decreases and finally turns to a featureless peak, in accordance to the long-lived singlet state decay. The details will be itinerated elsewhere.

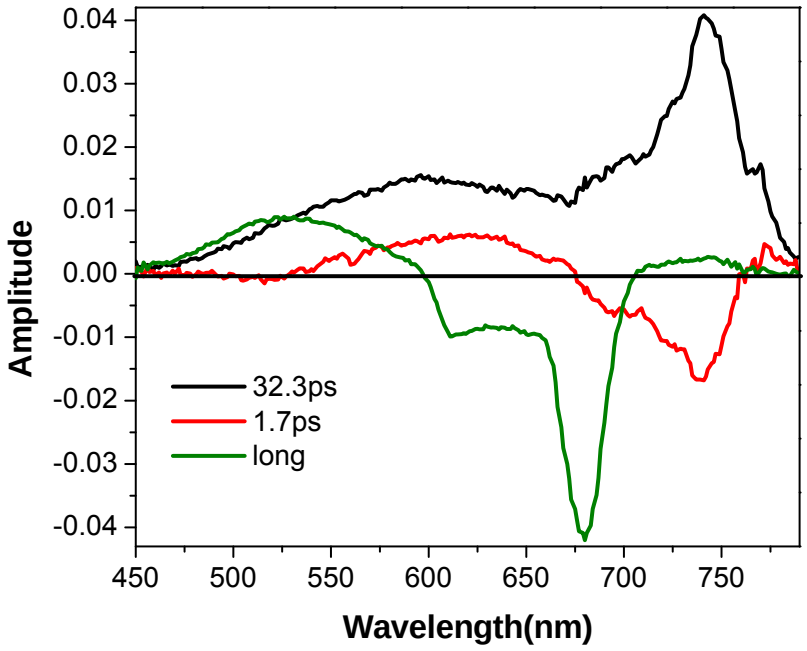

Figure 4.6 Transient absorption spectra at different time delays for HBCuPc-TPA-CN polymer in DMAc after excitation at 365nm.

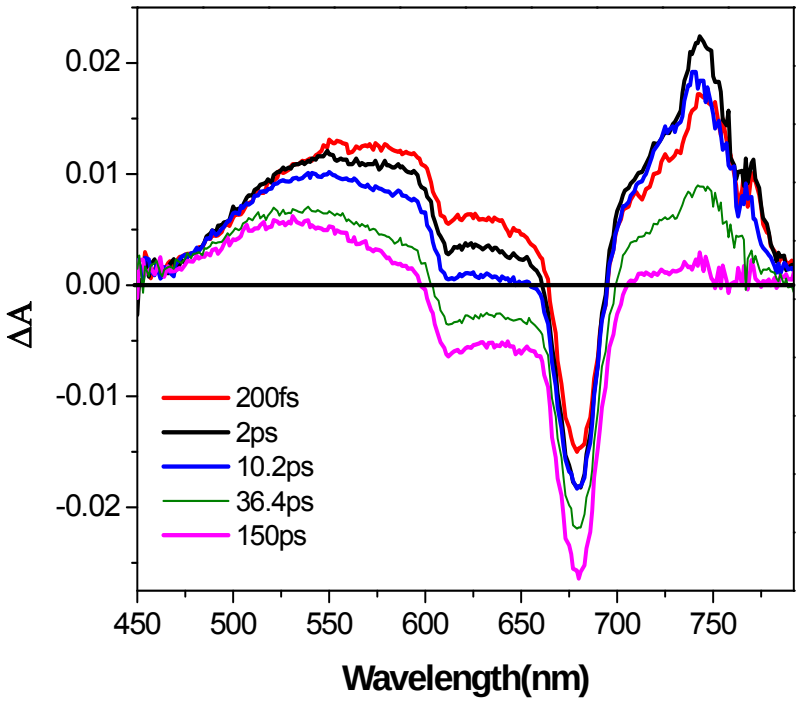

Figure 4.7 Transient spectra of principle coefficients at different time constants obtained from single value decomposition and consequent global fit analysis.

Transient spectra of principle coefficients for different time constants obtained from global fit analysis are shown in Figure 4.7, which concludes the complete excited state dynamics of HBCuPc-TPA-CN dendrimer. The faster time constant of 1.7 ps is contributed to ultrafast energy transfer from the S_2 state to S_1 state. Howe et al has found a fast decay component of ~4 ps in a PcS_4 aqueous solution.[68] The time constant of 32.3 ps is ascribed from nonradiative decay from S_1 state to the ground state in combination with intersystem crossing from S_1 to the triplet state. The excited –state decaying with a long time constant (> 1ns) is ascribed to radiative decay from S_1 state to the ground state, as the radiative decay lifetime is expected to be within nanoseconds range. [68]

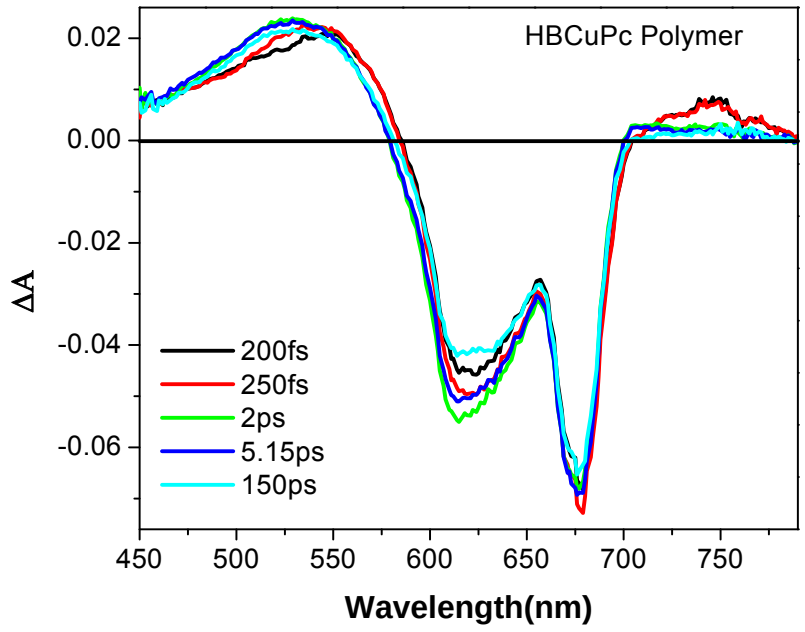

Figure 4.8 Transient absorption spectra at different time delays for HBCuPc dendrimer in DMAc after excitation at 365nm.

For a better comparison, we presented the transient absorption spectra for HBCuPc polymer at an excitation of 365nm (Figure 4.8). They show both induced absorption band and photobleaching band too. The bleaching peaks with a maximum

around 610 nm are much stronger compared that in HBCuPc-TPA-CN polymer. It can be explained by the singlet-singlet annihilation. The long wavelength absorption peaks are less pronounced in this polymer too, which suggests that stimulated absorption is less probably to occur in this system. Also, when we look at components of HBCuPc dendrimer from global fitting, as shown in Figure 9, no short time constant exists in HBCuPc dendrimer and long lifetimes are similar to that of HBCuPc. The S_2 state is short lived in this system. The conversion of S_2 state to S_1 state is so fast and we cannot detect within pulse duration (130 fs). It's not possible to exclude the intersystem crossing from S_1 to triplet state in this case.

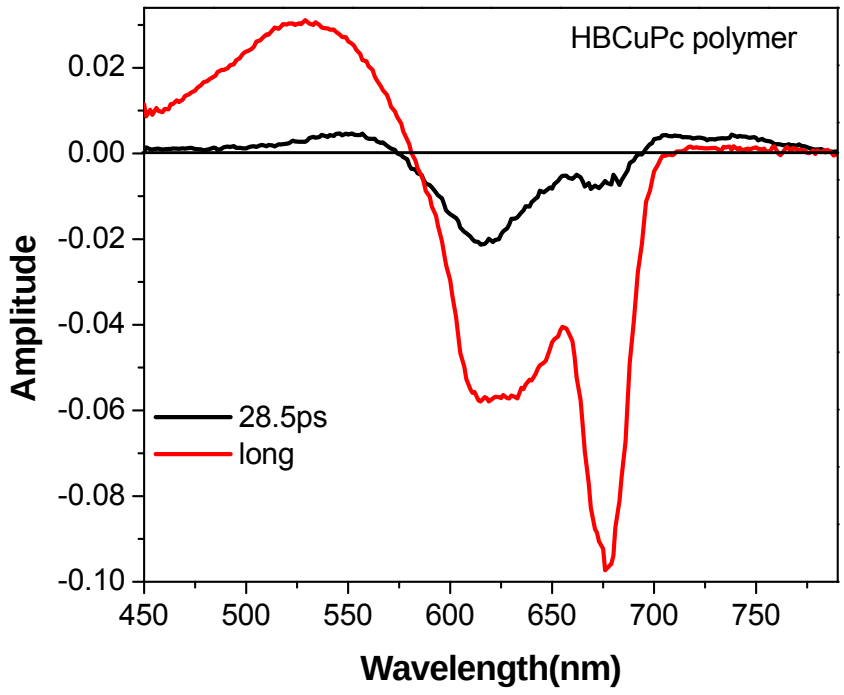

Figure 4.9 Transient spectra of principle coefficients at different time constants obtained from single value decomposition and consequent global fit analysis.

4.3.3 The effect of the substrate on the dielectric performance of the hyperbranched polymer

We also looked into the dependence of HBCuPc-TPA-CN dielectric response on the film substrate. As a comparison, we drop-casted the HBCuPc-TPA-CN polymer on a common substrate (ITO glass) using the same procedure. The thickness effect has been eliminated by keeping the films at the same thickness (~10μm). The dielectric response of HBCuPc-TPA-CN film on ITO glass (Figure 4. 10) varies from that of HBCuPc-TPA-CN film on the Al foil. There is a sharp decrease of the dielectric constant at 10KHz, and the dielectric constant at 1MHz is very low (~2), much smaller even compared to CuPc monomer (~5 at 1MHz). The large dielectric dispersion suggests that the ion polarization is the major charge transfer mechanism. When we looked at its dielectric loss, it increases at lower frequencies and demonstrates a loss peak at 100 KHz, followed by a sharp decrease towards high frequencies. In comparison to the dielectric loss of HBCuPc-TPA-CN film on Al foil, the polymer film casted on ITO glass showed a much higher dielectric loss (~0.2 at 1MHz). Our previous investigation on RSP-PAN/PEMA-co-PMMA has shown a similar dielectric dispersion behavior and suggested the primary contributions were from ion polarization and dipole orientation polarization of carriers in the system. [2] In this case, the possible source of ionic polarization is from the doping of indium oxide. The interaction between the hyper-branched polymer and indium oxide has deteriorated the dielectric performance of the polymer system, possibly due to the increased porosity in the film interface between the HBCuPc-TPA-CN polymer/ITO or the destroying of close head-to-head packing with the enclosure of indium tin oxides defects.

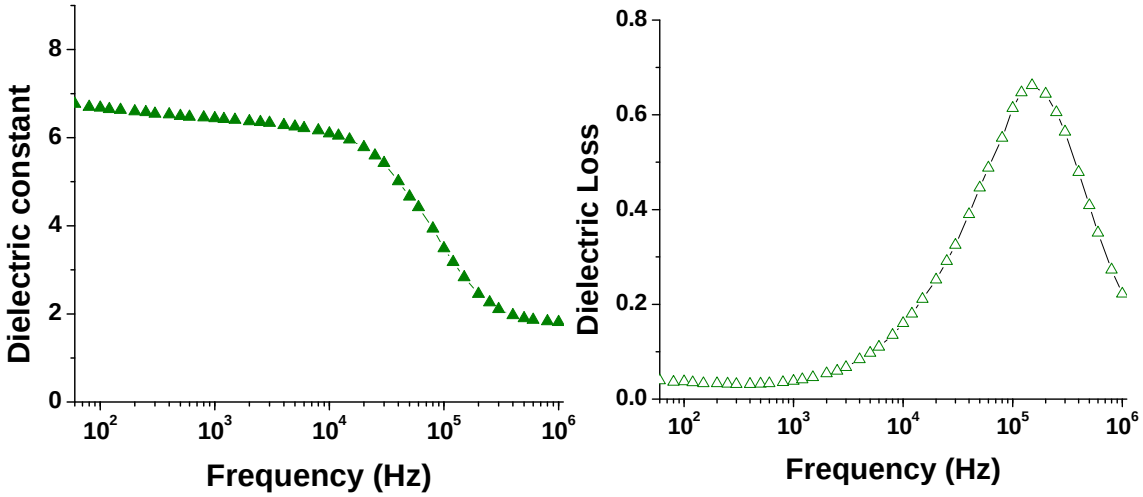

(a) (b)

Figure 4.10 a) Dielectric response and b) dielectric loss curves of HBCuPc-TPA-CN polymer pristine film on ITO glass with a thickness of 10µm.

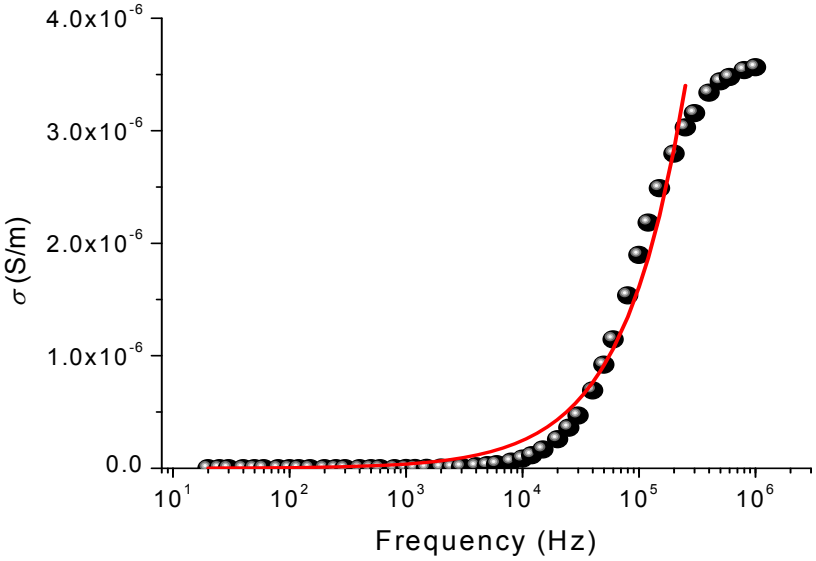

Figure 4.11 Ac conductance of HBCuPc-TPA-CN polymer pristine film on ITO glass with a thickness of 10µm.

Furthermore, the AC conductance of this dendrimer film shows a linear power-law dependence on the frequency ($\sigma = 1.3627 \times 10^{-10} \omega^{0.81464}$), which suggests that there is

only the occurrence of polaron hopping in this film. The comparably high conductance also indicates more metallic state than insulating state in this film, which is detrimental to the dielectric performance of the HBCuPc-TPA-CN polymer film especially at higher frequencies. More work on finding a good subtract is still ongoing. In order to further confirm the interaction between HBCuPc-TPA-CN dendrimer and indium tin oxide, we also looked at its interface by SEM cross section imaging (Figure 4.12). The dark holes along the interface may be filled with indium tin oxide particles, and the resulting interruption of polymer ring packing offset the enhanced dielectric response from interfacial polarization.

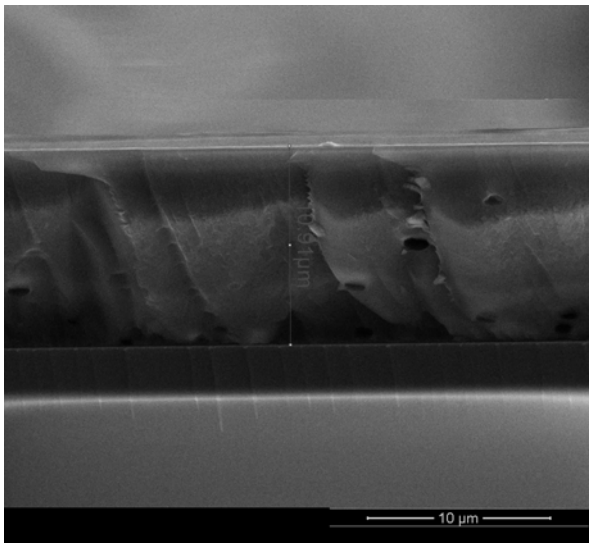

Figure 4.12 Scanning electron spectroscopy (SEM) cross section image of the HBCuPc-TPA-CN film on ITO glass.

We also found that the interface morphology of polymer casting films on different substrate varies, which may be related to the difference in their dielectric response too. Figure 4.13 demonstrates an example of interface morphology on two different substrate s respectively. The dendrimer film on Al foil is brittle, with honeycomb surface;

however, the dendrimer film on ITO glass is very homogeneous with 3D pie distributed surface. Therefore, there is a trade-off between the film homegeneity and the dielectric response. Also, if we can block the directly contact between indium tin oxide particle with the HBCuPc-TPA-CN dendrimer, a better dielectric response with reduced dielectric dispersion will be obtainable.

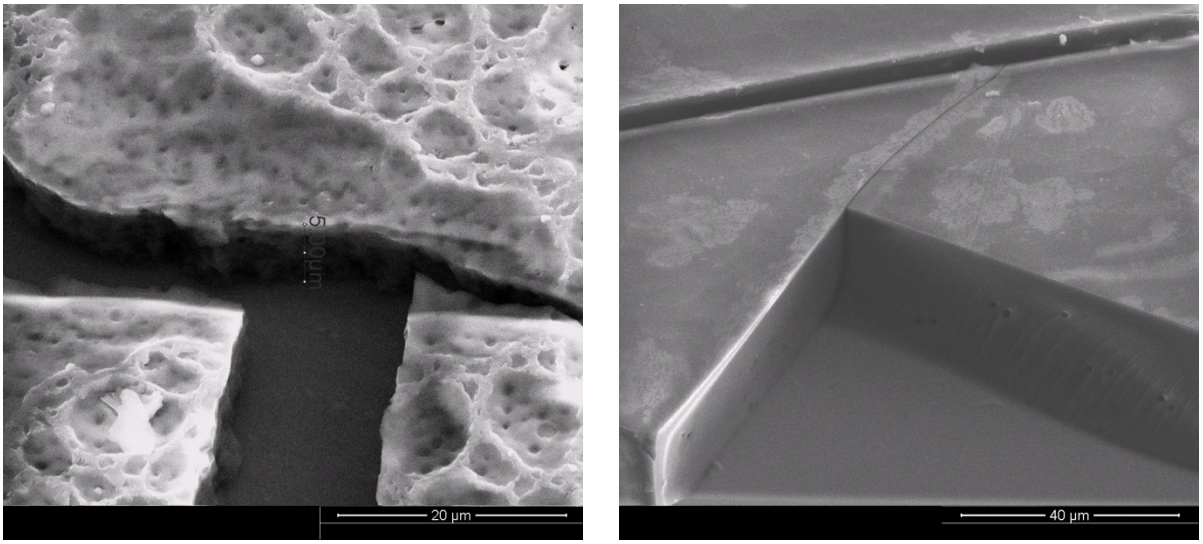

(a) **(b)**

Figure 4.13 Scanning electron spectroscopy (SEM) cross section image of the HBCuPc-TPA-CN film on (a) Al foil; (b) ITO glass.

4.4 Conclusions

In summary, a novel donor-acceptor material based on hyper-branched copper phthalocyanine systems end-capped by cyano group involving a TPA moiety has been designed and investigated. A high dielectric constant (~11) and low dielectric loss (0.002) at 1MHz have been observed due to the planar hyper-branched structure and the long delocalization length. The polaron hopping and polaron tunneling mechanisms are suggested to be the main dominating mechanisms based on the study of Ac conductance

and fluorescence dynamics. In addition, the increased conjugation length of the hyper-branched dendrimer doesn't increase the dielectric response in HBCuPc-TPA-CN dendrimer due to the interruption of close packing from the pyramidal shape of TPA moiety. The formation of charge pairs in such a hyper-branched system will play an important role in affecting the material's dielectric properties.

Reference

(1) Guo, M.; Yan, X. Z.; Kwon, Y.; Hayakawa, T.; Kakimoto, M. A.; Goodson, T. *Journal of the American Chemical Society* **2006**, *128*, 14820-14821.

(2) Yan, X. Z.; Goodson, T. *Journal of Physical Chemistry B* **2006**, *110*, 14667-14672.

(3) Amaral, F.; Rubinger, C. P. L.; Valente, M. A.; Costa, L. C.; Moreira, R. L. *Journal of Applied Physics* **2009**, *105*.

(4) Wong, C. K.; Shin, F. G. *Journal of Applied Physics* **2005**, *97*.

(5) Zhu, J. L.; Jin, C. Q.; Cao, W. W.; Wang, X. H. *Applied Physics Letters* **2008**, *92*.

(6) Jayanthi, S.; Kutty, T. R. N. *Journal of Materials Science-Materials in Electronics* **2008**, *19*, 615-626.

(7) Liu, D.; Tse, K.; Robertson, J. *Applied Physics Letters* **2007**, *90*.

(8) *Handbook of Low and High Dielectric Constant Materials and Their Applications*; Nalwa, H. S., Ed.; Academic Press: London, UK, 1999; Vol. 1.

(9) Bai, Y.; Cheng, Z. Y.; Bharti, V.; Xu, H. S.; Zhang, Q. M. *Applied Physics Letters* **2000**, *76*, 3804-3806.

(10) Bobnar, V.; Levstik, A.; Huang, C.; Zhang, Q. M. *Phys Rev Lett* **2004**, *92*, 047604.

(11) Clayton, L. M.; Sikder, A. K.; Kumar, A.; Cinke, M.; Meyyappan, M.; Gerasimov, T. G.; Harmon, J. P. *Advanced Functional Materials* **2005**, *15*, 101-106.

(12) Dang, Z. M.; Fan, L. Z.; Shen, Y.; Nan, C. W. *Chemical Physics Letters* **2003**, *369*, 95-100.

(13) Dang, Z. M.; Lin, Y. H.; Nan, C. W. *Advanced Materials* **2003**, *15*, 1625.

(14) Dang, Z. M.; Wang, L.; Yin, Y.; Zhang, Q.; Lei, Q. Q. *Advanced Materials* **2007**, *19*, 852.

(15) Dang, Z. M.; Zhou, T.; Yao, S. H.; Yuan, J. K.; Zha, J. W.; Song, H. T.; Li, J. Y.; Chen, Q.; Yang, W. T.; Bai, J. *Advanced Materials* **2009**, *21*, 2077.

(16) Li, Q.; Xue, Q. Z.; Zheng, Q. B.; Hao, L. Z.; Gao, X. L. *Materials Letters* **2008**, *62*, 4229-4231.

(17) Lu, J.; Moon, K. S.; Wong, C. P. *Journal of Materials Chemistry* **2008**, *18*, 4821-4826.

(18) Lu, J. X.; Moon, K. S.; Xu, J. W.; Wong, C. P. *Journal of Materials Chemistry* **2006**, *16*, 1543-1548.

(19) Mdarhri, A.; Khissi, M.; Achour, M. E.; Carmona, F. *European Physical Journal-Applied Physics* **2008**, *41*, 215-220.

(20) Qi, L.; Lee, B. I.; Chen, S. H.; Samuels, W. D.; Exarhos, G. J. *Advanced Materials* **2005**, *17*, 1777.

(21) Xie, Y. C.; Yu, D. M.; Min, C.; Guo, X. S.; Wan, W. T.; Zhang, J.; Liang, H. L. *Journal of Applied Polymer Science* **2009**, *112*, 3613-3619.

(22) Yao, S. H.; Dang, Z. M.; Jiang, M. J.; Bai, J. B. *Applied Physics Letters* **2008**, *93*.

(23) Yao, S. H.; Dang, Z. M.; Xu, H. P.; Jiang, M. J.; Bai, J. *Applied Physics Letters* **2008**, *92*.

(24) Rao, Y.; Wong, C. P. *Journal of Applied Polymer Science* **2004**, *92*, 2228-2231.

(25) Lu, J. X.; Wong, C. P. *Ieee Transactions on Dielectrics and Electrical Insulation* **2008**, *15*, 1322-1328.

(26) Chu, B. J.; Zhou, X.; Ren, K. L.; Neese, B.; Lin, M. R.; Wang, Q.; Bauer, F.; Zhang, Q. M. *Science* **2006**, *313*, 334-336.

(27) Lu, J. X.; Moon, K. S.; Kim, B. K.; Wong, C. P. *Polymer* **2007**, *48*, 1510-1516.

(28) Wang, J. W.; Wang, Y.; Wang, F.; Li, S. Q.; Xiao, J.; Shen, Q. D. *Polymer* **2009**, *50*, 679-684.

(29) Zhang, Q. M.; Li, H. F.; Poh, M.; Xia, F.; Cheng, Z. Y.; Xu, H. S.; Huang, C. *Nature* **2002**, *419*, 284-287.

(30) Hartman, R. D.; Pohl, H. A. *Journal of Polymer Science Part a-1-Polymer Chemistry* **1968**, *6*, 1135.

(31) Bayer, I. S.; Biswas, A.; Szczech, J. B.; Suhir, E.; Norton, M. G. *Applied Physics Letters* **2008**, *92*.

(32) Guo, M.; Yan, X. Z.; Goodson, T. *Advanced Materials* **2008**, *20*, 4167.

(33) Medina, A. S.; Claessens, C. G.; Rahman, G. M. A.; Lamsabhi, A. M.; Mo, O.; Yanez, M.; Guldi, D. M.; Torres, T. *Chemical Communications* **2008**, 1759-1761.

(34) Liaw, D. J.; Hsu, P. N.; Chen, W. H.; Lin, S. L. *Macromolecules* **2002**, *35*, 4669-4676.

(35) Ge, Z. Y.; Hayakawa, T.; Ando, S.; Ueda, M.; Akiike, T.; Miyamoto, H.; Kajita, T.; Kakimoto, M. A. *Advanced Functional Materials* **2008**, *18*, 584-590.

(36) Cravino, A.; Roquet, S.; Leriche, P.; Aleveque, O.; Frere, P.; Roncali, J. *Chemical Communications* **2006**, 1416-1418.

(37) Roquet, S.; Cravino, A.; Leriche, P.; Aleveque, O.; Frere, P.; Roncali, J. *Journal of the American Chemical Society* **2006**, *128*, 3459-3466.

(38) Tanaka, H.; Tokito, S.; Taga, Y.; Okada, A. *Chemical Communications* **1996**, 2175-2176.

(39) Yan, X. Z.; Pawlas, J.; Goodson, T.; Hartwig, J. F. *Journal of the American Chemical Society* **2005**, *127*, 9105-9116.

(40) Ranasinghe, M. I.; Varnavski, O. P.; Pawlas, J.; Hauck, S. I.; Louie, J.; Hartwig, J. F.; Goodson, T. *Journal of the American Chemical Society* **2002**, *124*, 6520-6521.

(41) Cao, G. H.; Qin, D. S.; Cao, J. S.; Guan, M.; Zeng, Y. P.; Li, J. M. *Journal of Applied Physics* **2007**, *101*.

(42) Chen, L. L.; Li, W. L.; Wei, H. Z.; Chu, B.; Li, B. *Solar Energy Materials and Solar Cells* **2006**, *90*, 1788-1796.

(43) Chu, C. W.; Shrotriya, V.; Li, G.; Yang, Y. *Applied Physics Letters* **2006**, *88*.

(44) Hagberg, D. P.; Yum, J. H.; Lee, H.; De Angelis, F.; Marinado, T.; Karlsson, K. M.; Humphry-Baker, R.; Sun, L. C.; Hagfeldt, A.; Gratzel, M.; Nazeeruddin, M. K. *Journal of the American Chemical Society* **2008**, *130*, 6259-6266.

(45) Ohta, K.; Chiba, Y.; Ogawa, T.; Endo, Y. *Bioorganic & Medicinal Chemistry Letters* **2008**, *18*, 5050-5053.

(46) Kwon, Y.; Hayakawa, T.; Kakimoto, M. A. *Chemistry Letters* **2006**, *35*, 1306-1307.

(47) Lee, T. K., Y.; Park, J.J.; Pu, L.; Hayakawa, T.; Kakimoto, M.A. *Macromolecular Rapid Communications* **2007**, 1657-1662.

(48) Ramakrishna, G.; Goodson, T. *Journal of Physical Chemistry A* **2007**, *111*, 993-1000.

(49) Bobnar, V.; Levstik, A.; Huang, C.; Zhang, Q. M. *Journal of Non-Crystalline Solids* **2007**, *353*, 205-209.

(50) Gould, R. D. *Coordination Chemistry Reviews* **1996**, *156*, 237-274.

(51) Sakai, Y.; Sadaoka, Y.; Yokouchi, H. *Bulletin of the Chemical Society of Japan* **1974**, *47*, 1886-1888.

(52) Vidadi, Y. A. R., L.D.; Chistyakov, E.A. *Sov. Phys. Solid State* **1969**, 173.

(53) Kiess, H.; Rehwald, W. *Colloid and Polymer Science* **1980**, *258*, 241-251.

(54) Pelster, R.; Nimtz, G.; Wessling, B. *Physical Review B* **1994**, *49*, 12718-12723.

(55) Wang, Z. H.; Scherr, E. M.; Macdiarmid, A. G.; Epstein, A. J. *Physical Review B* **1992**, *45*, 4190-4202.

(56) Martens, H. C. F.; Brom, H. B. *Physical Review B* **2004**, *70*.

(57) Guo, M.; Varnavski, O.; Narayanan, A.; Mongin, O.; Majoral, J. P.; Blanchard-Desce, M.; Goodson, T. *Journal of Physical Chemistry A* **2009**, *113*, 4763-4771.

(58) Varnavski, O.; Bauerle, P.; Goodson, T. *Optics Letters* **2007**, *32*, 3083-3085.

(59) Cannizzo, A.; Blanco-Rodriguez, A. M.; El Nahhas, A.; Sebera, J.; Zalis, S.; Vlcek, A.; Chergui, M. *Journal of the American Chemical Society* **2008**, *130*, 8967-8974.

(60) Muller, J. G.; Atas, E.; Tan, C.; Schanze, K. S.; Kleiman, V. D. *Journal of the American Chemical Society* **2006**, *128*, 4007-4016.

(61) D'Souza, F.; Gadde, S.; Islam, D. M. S.; Wijesinghe, C. A.; Schumacher, A. L.; Zandler, M. E.; Araki, Y.; Ito, O. *Journal of Physical Chemistry A* **2007**, *111*, 8552-8560.

(62) Huang, C. W.; Chiu, K. Y.; Cheng, S. H. *Dalton Transactions* **2005**, 2417-2422.

(63) Hagedorn, K. V.; Varnavski, O.; Hartwig, J.; Goodson, T. *Journal of Physical Chemistry C* **2008**, *112*, 2235-2238.

(64) Zhang, X. F.; Di, Y. Q.; Zhang, F. S. *Journal of Photochemistry and Photobiology a-Chemistry* **2009**, *203*, 216-221.

(65) Ohkubo, K.; Fukuzumi, S. *Journal of Porphyrins and Phthalocyanines* **2008**, *12*, 993-1004.

(66) Martin-Gomis, L.; Ohkubo, K.; Fernandez-Lazaro, F.; Fukuzumi, S.; Sastre-Santos, A. *Journal of Physical Chemistry C* **2008**, *112*, 17694-17701.

(67) Gulbinas, V.; Chachisvilis, M.; Valkunas, L.; Sundstrom, V. *Journal of Physical Chemistry* **1996**, *100*, 2213-2219.

(68) Howe, L.; Zhang, J. Z. *Journal of Physical Chemistry A* **1997**, *101*, 3207-3213.

Chapter 5

Photophysics of hyperbranched CuPc polymers: the correlation between the structure and the dielectric properties

5.1 Introduction

The perspective of the applications of organic materials in the electronic and optical devices has attracted an enormous interest from the scientific community due to the unique properties as a result of the delocalization of π orbitals. [1-7]Examples of these unique properties are: the mutual transition between the insulator and the conductor, which depends on the highest occupied molecular orbital (HOMO)-lowest occupied molecular orbital (LUMO) band gap; [1] the excellent thermal stability and mechanical strength. [4] Among various applications of organic materials, one important research area is focused on the potential of creating organic high dielectric constant materials by utilizing different polarization mechanisms, such as the interface polarization, electronic polarization and hyperelectronic polarization. [8-12]The particularly attractive features of organic high dielectric constant materials are the possibility to yield low dielectric loss, high breakdown strength as well as relatively low cost. [10,12]

Some organic materials have been reported with intrinsic high dielectric constant properties. For example, Zhang et al. observed a dielectric constant ~1,200,000 at 100 Hz in a polyacene quinine radical polymer (PAQR) synthesized by solid-state polymerization. [13]And the high dielectric constant was contributed to the hyperelectronic

polarization due to the long range delocalization along the polymer backbone. However, the dielectric loss was huge (tanδ ~30) and no frequency dependence was reported. [13] Another example is that Nalwa et al. observed a dielectric constant as high as 10^5 in a KOH treated CuPc oligomers and Maxwell-Wagner interface polarization mechanism was in practice. [14] Based on the investigations so far, it has been found that the structure and function group of the polymer materials are closely related to their dielectric properties. For instance, the work conducted by Zhang and his co-workers in HO-PAQR and RO-PAQR polymers found that the dielectric constant would be lowered by adding hydroxyl and alkoxyl function groups, which suggests that the planar conjugation of the associated π orbital plays an important role in achieving high dielectric constant in such PAQR systems. [13] Another group from Penn State has conducted an intensive research on the connection between different phases of PVDF and their dielectric properties. [15-17]The crystalline phase of PVDF will affect the packing of the material as well as its photophysics, which determines the dielectric responses of the material. In this chapter, I am going to discuss the relationship between the structure of the hyperbranched copper phthalocyanine polymers and the corresponding dielectric properties, and trying to understand the physics underlying the relationship via a series of electronic and optical characterization measurements. Also, a modified hyperbranched CuPc structure (HBCuPc-CN) was synthesized and characterized.

5.2 Experimental Section

5.2.1 Materials.

The synthesis of the HBCuPc and HBCuPc-TPA-CN polymers has been described in previous chapters. In this chapter, another modified hyperbranched CuPc polymer (HBCuPc-CN) will be synthesized and investigated. A similar synthesis route as previously reported was followed to prepare the HBCuPc-CN polymer. [12,18,19] In brief, four equivalent 4,4'(1,3-phenoxybis(oxy))diphthalonitrile monomer was mixed with one equivalent CuCl in 40 mL dimethylacetamide (DMAc) solution first, followed by the stirring of the mixture at 200 °C for 6 hrs. Consecutive filtration, washing and dying steps were repeated to purify and separate the reaction products. And finally HBCuPc-CN powder was obtained. ^{1}H-NMR, ^{13}C-NMR, IR, UV-Vis, TGA and GPC measurements were carried out to characterize and determine the structure of the HBCuPc-CN polymer. Based on the relative ratio as compared to the absorbance of the pure CuPc, the content of CuPc unit in HBCuPc-CN was calculated as 85%. Dimethylacetamide (DMAc) was purchased from Aldrich Co., dried with CaH_2 and distilled in vacuum prior to the use.

5.2.2 Preparation of HBCuPc-CN films.

The HBCuPc-CN polymer films were prepared by solution cast method. A certain amount of the polymer powder was dissolved in 1mL DMAc solutions first, and then the solution was stirred for 5.5 hrs at 40°C, with another 10 hrs of the mechanic stirring at room temperature, followed by the sonication for extra 10 mins. After that, the solution was dropped onto an Al foil by pipette and dried in air overnight. Then, the film was moved into the oven and annealed at different temperature intervals for 10 hrs, followed

by a final drying process in vacuum at 125°C for 10hrs. Finally, the film was slowly cooled down to room temperature. The typical thickness of the HBCuPc-CN dendrimer is 15 μm, measured using the Veeco surface profiler.

5.2.3 Dielectric Measurement

Measurements of the capacitance and dielectric loss were made by a 4284A HP LCR meter over the frequency range of 20 Hz to 1 MHz. Prior to the measurement, a thin layer (500 Å) of Au particle was sputtered on both sides of the sample. The dielectric constant values were inferred from the equation $\varepsilon_r = \frac{C_p \cdot t}{\varepsilon_0 \cdot \pi(\frac{d}{2})^2}$, where ε_0 is the dielectric permittivity of the vacuum (8.85 x 10^{-12} F/m); d is effective contact diameter of the sample and t is the thickness of the sample.

5.2.4 UV-Vis Absorption and Steady-State Fluorescence.

Ultraviolet (UV)-visible absorption spectra were recorded with an Agilent Technologies 8453 spectrophotometer. Steady-state fluorescence measurements were performed on a sensitive Fluomax-2 fluorimeter. For both measurements, the sample solution was prepared from the stock solution by diluting as required. The stock solution was made by dissolving 1 milligram of HBCuPc-CN powder in 3 mL DMAc solution and sonicating the mixture for 20 mins.

5.2.5 Pump-Probe Transient Absorption Measurements.

The pump beams used in the present investigation were obtained from the fourth harmonic of the idler beams and were focused onto the sample cuvette. The probe beam was delayed with a computer controlled motion controller and then focused into a 2 mm

sapphire plate to generate white light continuum. The white light was then overlapped with the pump beam in a 2 mm quartz cuvette containing the sample and the change in absorbance for the signal was collected by a CCD detector (Ocean optics). Data acquisition was controlled by the software from Ultrafast Systems Inc. A typical power of probe beam was less than 30 nJ, and the pump beam was around 50-400 nJ per pulse. For the present transient absorption measurements of hyperbranched CuPc polymers, we have used the pump power of 250 nJ per pulse and the kinetics was found to be independent of pump-power for all the investigated hyperbranched CuPc systems. Magic angle polarization was maintained between the pump and probe using a wave plate. The pulse duration was obtained by fitting the solvent response, which was 130 fs. The sample was stirred with a rotating magnetic stirrer and no photodegradation of the sample has been observed.

5.3 Results and Discussion

5.3.1 Structure of the HBCuPc-CN Dendrimer

As shown in Figure 5.1 was the synthesis and the structure of the modified HBCuPc-CN polymer system. CN- end group was attached to the polymer in order to increase the polarity of the material. Two ether bridges connecting the neighboring CuPc rings were attached to the meso position instead of ortho position of the benzene ring in previous investigated HBCuPc polymer. The separation distance between CuPc rings increased and the coupling between them weakened thereafter.

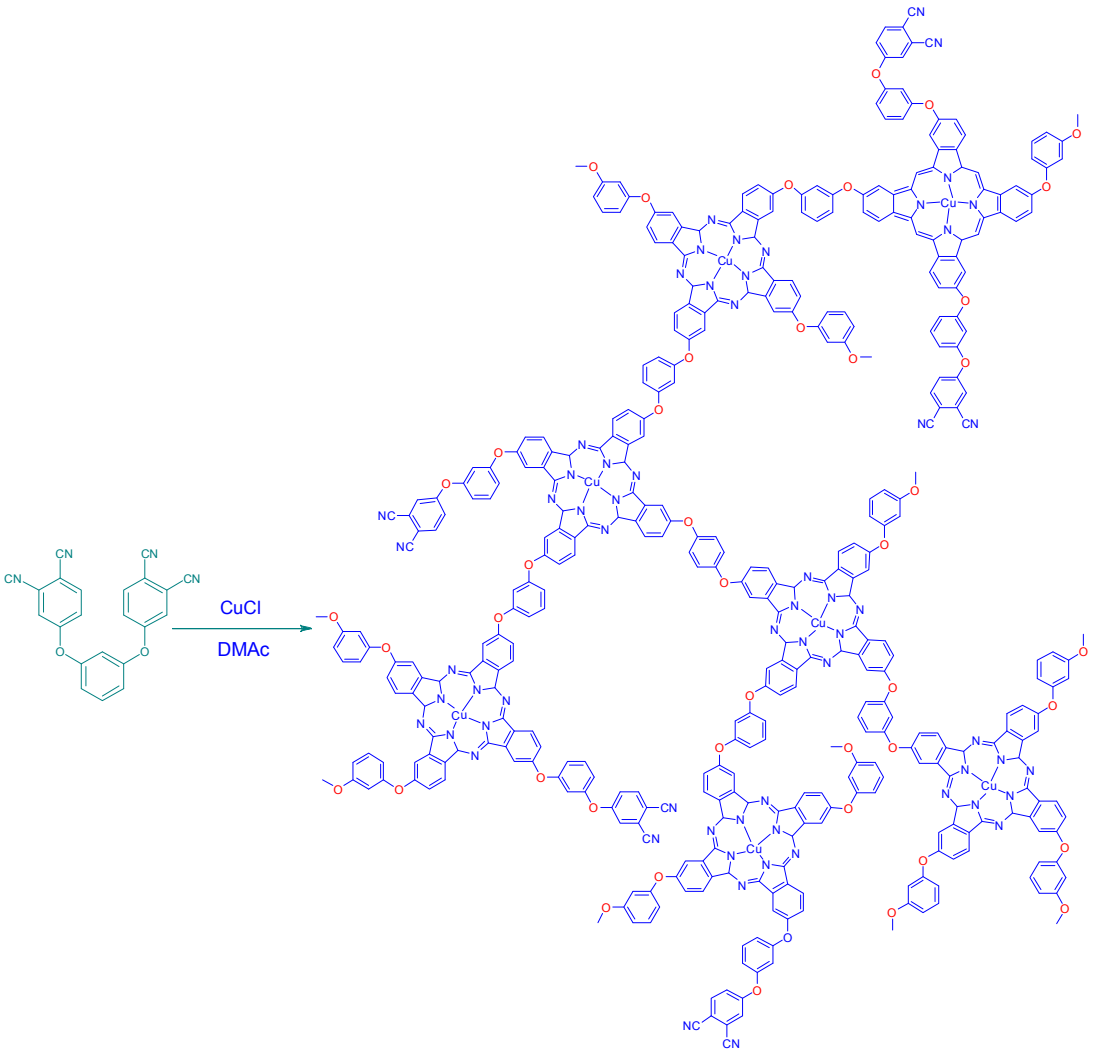

Figure 5.1 The structure of the HBCuPc-CN polymer

5.3.2 Dielectric Constant of the HBCuPc-CN polymers and their dependence on the properties of surfactants and solvents.

Conjugated polymers typically possess a frequency (ω) dependent complex dielectric constant ($\varepsilon^*(\omega)=\varepsilon_r(\omega)-i\varepsilon_i(\omega)$). The dielectric constant ($k=\varepsilon_r/\varepsilon_0$) denotes the ability of the dielectric material to store the charge under electromagnetic field and transit the energy and the dielectric loss ($\tan\delta=\varepsilon_r/\varepsilon_i$) denotes the angle between the voltage and the charging current. To investigate the dielectric behavior of this modified HBCuPc-CN

polymer, the capacitance measurement was conducted at room temperature in the frequency range (20Hz-1MHz). Figure 5.2 showed the variation of the dielectric constant and dielectric loss of a 15 μm dielectric film as a function of the frequency. The dielectric constant was ~9.8 at 1MHz, higher than that of the CuPc monomer and is appropriate for high energy density capacitor applications. [8] In addition, it exhibited weak frequency dependence. In this case, the hyperelectronic polarization follows the change of the electric field and it contributes to the dielectric constant. However, due to the weak coupling between neighboring CuPc rings, they have flexible rotation and the face-to-face packing is interfered, therefore less enhancement is observed compared to the HBCuPc polymer which was connected at ortho position. The dielectric loss decreased upon the increase of the frequency and ended up at ~0.0025 at 1MHz. This is because the induced charge gradually fails to follow the reversing field causing a reduction in the electric oscillations as the frequency is increased. For the purpose of the illustration, the dielectric constant and dielectric loss of three series of hyperbranched CuPc polymers at 1MHz were presented in Table 5.1. Even though the dielectric constant of the HBCuPc-CN is not the highest, the low dielectric loss as well as improved solubility makes this material very attractive for capacitor applications too. The comparison also suggested the importance of the structure and the function group on the dielectric constant of these hyperbranched CuPc materials. All three materials possess low dielectric loss and low dielectric dispersion, which suggests that these are intrinsic properties of the hyperbranched CuPc materials and possibly due to the disorder in the amorphous state of the material. [12]

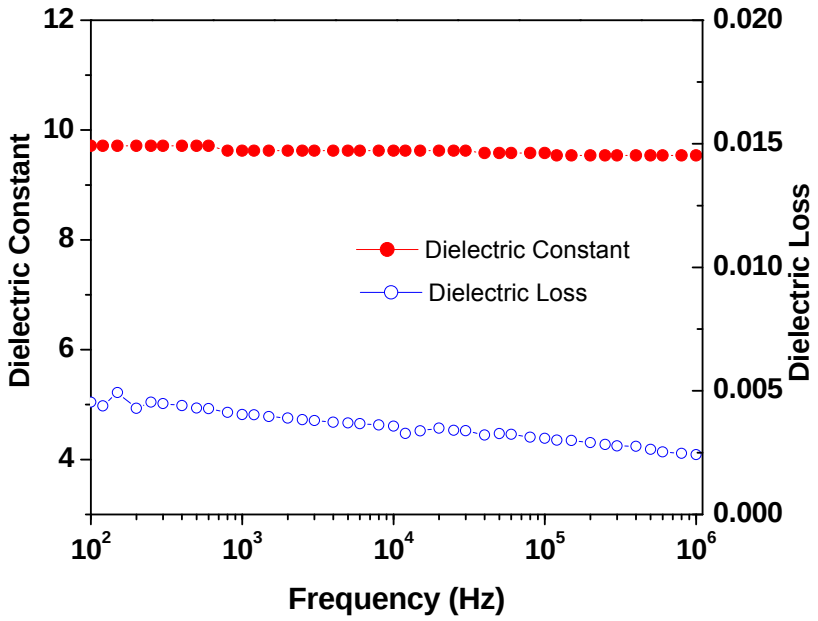

Figure 5.2 the dielectric response of the HBCuPc-CN polymer with a thickness of 15μm.

Table 5.1 The dielectric constant and dielectric loss of three hyperbranched CuPc polymers at 1MHz.

Material	Dielectric Constant	Dielectric Loss
HBCuPc polymer [12]	15	0.002
HBCuPc-TPA-CN polymer	11	0.004
HBCuPc-CN polymer	9.8	0.0025

The experimental values of the conductivity were fitted in the following equation and a log-log plot of the power law was generated, as seen in Figure 5.3.

$$\sigma_{AC} = A + B\varpi^{s} \tag{5.1}$$

Where A, B are constants and s is a fitting parameter.

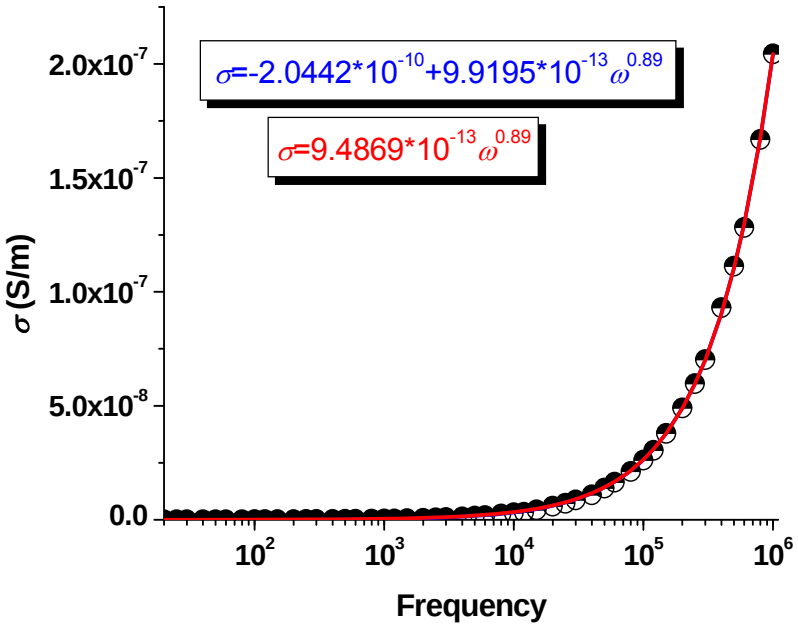

Figure 5.3 the AC conductance of HBCuPc-CN polymer with a thickness of 15μm.

The best fit of the conductivity data to the log-log plots of the power law gives an s value of 0.89, very close to that of the HBCuPc dendrimer film. [12] Therefore, both polaron hopping and polaron tunneling mechanisms are possibly operative in this system. As the separation distance between two CuPc rings are larger in the HBCuPc-CN polymer, the probability of hopping may be higher. Furthermore, the rotation flexibility inhibits the intermolecular electron transfer, which is supported by the observed higher AC conductivity too.

To optimize the film performance, different solvents and surfactants were used. For example, the film casted from dimethylfluoride (DMF) solvent exhibited a more homogeneous surface morphology with improved solubility; however, there is a trade-off between the film solubility and the dielectric response (~3). This indicated that the interaction between the solvent and the HBCuPc-CN polymer played an important role.

The surfactant was able to improve the film forming ability of the hyperbranched polymer dielectric film due to their viscous nature. A very small portion of poly(ethylene glycol) (PEG), poly(vinyl alcohol) (PVA) and polyvinyl sulfonate (PES) have been added into the HBCuPc-CN/DMAc solution, the dielectric response of the composite was improved compared to that of the surfactant in terms of the enhanced dielectric constant, lower dielectric loss as well as low dielectric dispersion. But the problems came up with the phase separation and polymer recrystallization. More details could be referred to the Appendix A. A lot of work needs to be done in the future to understand the role played by the surfactant and to optimize the composition ratio between the surfactant and the polymer.

5.3.3 Optical properties of the HBCuPc-CN polymer.

The excited state dynamics of Pc solution and film have been widely studied by techniques such as transient absorption and electron paramagnetic resonance (EPR). [20-25]For example, Ito et al. have utilized the transient absorption spectroscopy to study the excited state relaxation process of free-base (H_2Nc) and oxovanadium naphthalocyanine (VONc). They found a decay component in a time scale of ps and suggested that the relaxation is governed by the IC and ISC. [20] In order to monitor the evolution of charge transfer states over the time and understand the electrical conduction mechanisms of the HBCuPc-CN polymer, pump-probe transient absorption measurement was performed. As shown in Figure 5.4 is the transient absorption spectra of HBCuPc-CN at different time delays after an excitation at 365nm. The positive ΔA signals were observed at two regions, either below 550 nm or above 700 nm. And the negative ΔA signal was observed between 550 and 700 nm. The transient absorption spectrum of the HBCuPc-CN polymer

was similar to that of other reported Pc materials. [22,23,26-28] The bleaching peaks at longer wavelength with a maximum at 680nm appeared at the same position of the Q band absorption band, which corresponds to the singlet-singlet annihilation. The bleaching peaks with a maximum around 610 nm are weaker compared to that in the HBCuPc polymer, which suggests that the singlet-singlet annihilation is less probably to occur in the HBCuPc-CN polymer. Also, when we looked at decay components of the HBCuPc-CN polymer from the global fitting, as shown in Figure 5.5, two components were found in similar to that of the HBCuPc polymer. The S_2 state is short lived in this system too. The intermediate component was in a time scale of 49.3 ps, almost doubles that in HBCuPc polymer, hence the decay process from Q band excitation to the ground state is much slower in the HBCuPc-CN. This may be able to explain the smaller dielectric constant found in the HBCuPc-CN polymer.

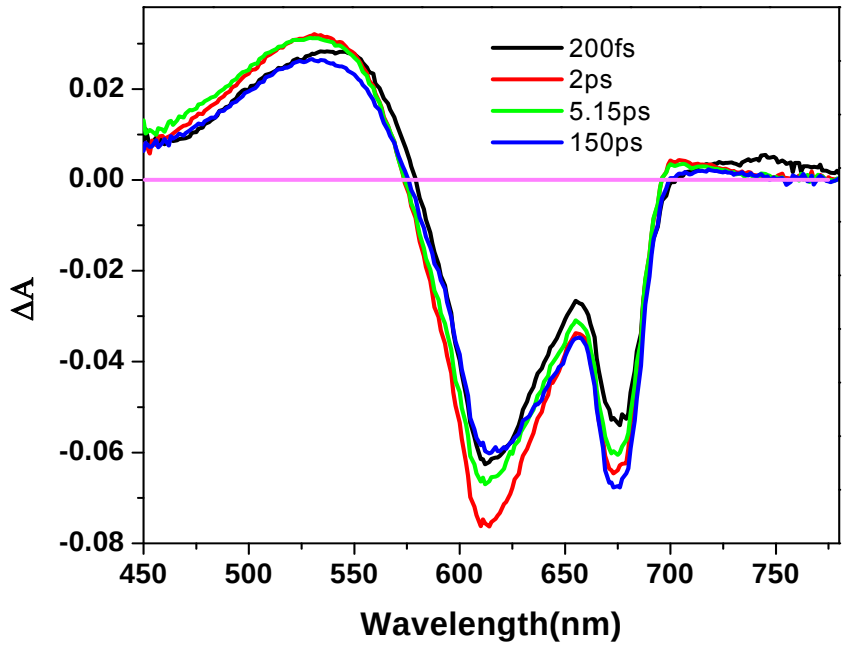

Figure 5.4 Transient absorption spectra at different time delays for HBCuPc-CN polymer in DMAc after excitation at 365nm

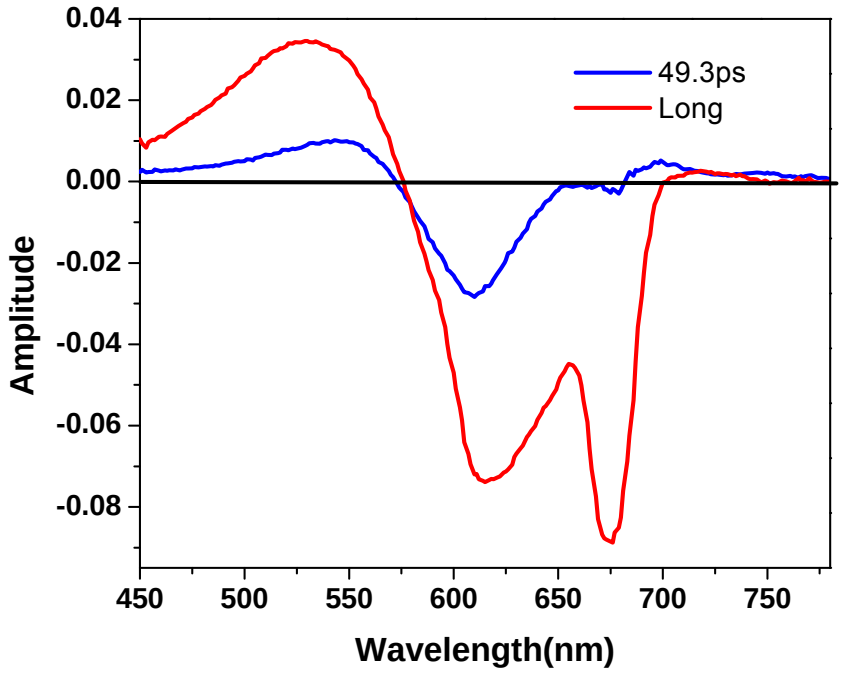

Figure 5.5 Transient spectra of principle coefficients at different time constants obtained from single value decomposition and consequent global fit analysis.

The different ground and excited state dynamics of three hyperbranched CuPc systems can be better described by the steady-state absorption and transient absorption spectra as shown in Figure 5.6 and Figure 5.7 respectively. All three polymers showed the typical major absorption bands (B or Soret band) and the Q bands of CuPc. However, the ratio between the two bands is different, which suggests the interaction of the neighboring CuPc rings and the population of the conversion from S_2 state to S_1 state varied with the structure. And HBCuPc-CN polymer has the strongest interaction between the neighboring CuPc.

The excited state dynamics of three hyperbranched CuPc polymers were different too. The detailed comparison between the HBCuPc and HBCuPc-TPA-CN polymer has been described in chapter 4. The peaks of positive ΔA signals of three hyperbranched

CuPc polymers at higher energy band were in a close proximity. And the HBCuPc polymer showed the weakest photobleaching.

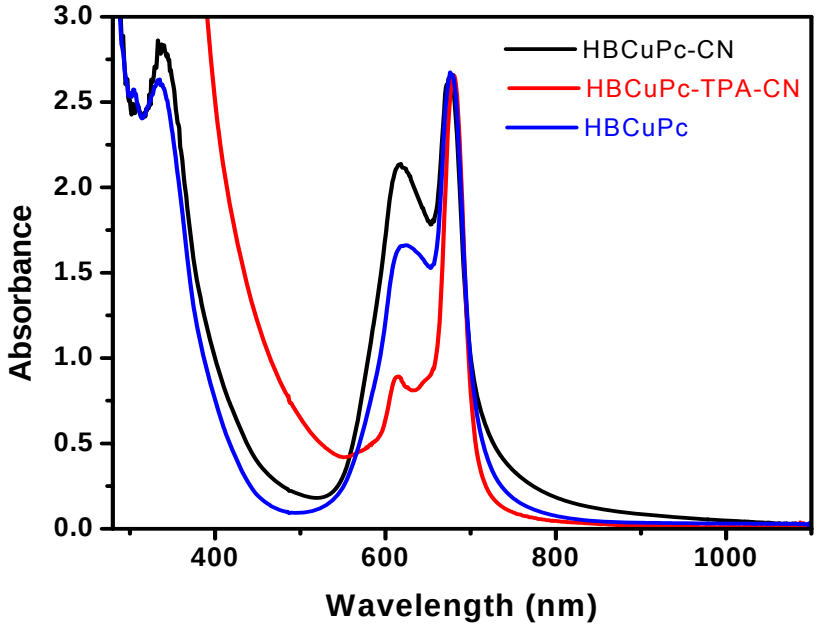

Figure 5.6 The UV-Vis spectra of three hyperbranched CuPc polymers.

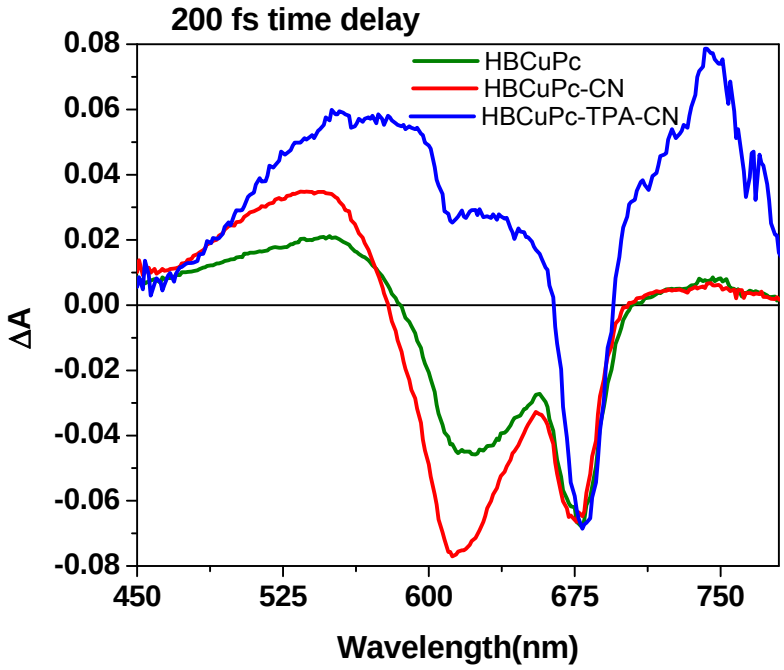

Figure 5.7 the transient absorption dynamics of three hyperbranched CuPc polymers at 200 fs with an excitation at 365nm.

5.4 Conclusion

The low dielectric loss and small dielectric dispersion of the investigated hyperbranched CuPc polymers are beneficial for high energy density capacitor applications at high frequency (KHz-MHz). Through the comparison in both the electrical conduction and the ground as well as excited state dynamics, the charge carrier transport in this type of dendrimer system is better understood and the design criteria is derived thereafter. More analysis of the photophysics of three different hyperbranched CuPc polymers is still needed.

Reference

(1) Heeger, A. J. *Journal of Physical Chemistry B* **2001**, *105*, 8475-8491.

(2) Edman, L.; Summers, M. A.; Buratto, S. K.; Heeger, A. J. *Physical Review B* **2004**, *70*.

(3) Braga, D.; Horowitz, G. *Advanced Materials* **2009**, *21*, 1473-1486.

(4) Shirota, Y. *Journal of Materials Chemistry* **2000**, *10*, 1-25.

(5) Dimitrakopoulos, C. D.; Malenfant, P. R. L. *Advanced Materials* **2002**, *14*, 99.

(6) *Organic Electronic Materials: Conjugated polymers and low molecular weight organic solids*; Farchioni, R.; Grosso, G., Eds.; Springer: New York, 2001; Vol. 41.

(7) Perry, J. W.; Mansour, K.; Lee, I. Y. S.; Wu, X. L.; Bedworth, P. V.; Chen, C. T.; Ng, D.; Marder, S. R.; Miles, P.; Wada, T.; Tian, M.; Sasabe, H. *Science* **1996**, *273*, 1533-1536.

(8) *Handbook of Low and High Dielectric Constant Materials and Their Applications*; Nalwa, H. S., Ed.; Academic Press: London, UK, 1999; Vol. 1.

(9) *Dielectric Phenomena in Solids: With Emphasis on Physical Concepts of Electronic Processes* Kao, K. C., Ed.; Academic Press: London, UK, 2004.

(10) Zhang, Q. M.; Li, H. F.; Poh, M.; Xia, F.; Cheng, Z. Y.; Xu, H. S.; Huang, C. *Nature* **2002**, *419*, 284-287.

(11) Xu, J. W.; Bhattacharya, S.; Pramanik, P.; Wong, C. P. *Journal of Electronic Materials* **2006**, *35*, 2009-2015.

(12) Guo, M.; Yan, X. Z.; Kwon, Y.; Hayakawa, T.; Kakimoto, M. A.; Goodson, T. *Journal of the American Chemical Society* **2006**, *128*, 14820-14821.

(13) Zhang, J.; Zhu, D.; Matsuo, M. *Polymer* **2008**, *49*, 5424-5430.

(14) Nalwa, H. S.; Dalton, L. R.; Vasudevan, P. *European Polymer Journal* **1985**, *21*, 943-947.

(15) Wang, J. W.; Shen, Q. D.; Bao, H. M.; Yang, C. Z.; Zhang, Q. M. *Macromolecules* **2005**, *38*, 2247-2252.

(16) Bauer, F.; Fousson, E.; Zhang, Q. M. In *12th International Symposium on Electrets (ISE 12)* Salvador, BRAZIL, 2005, p 1149-1154.

(17) Bao, H. M.; Song, J. F.; Zhang, J.; Shen, Q. D.; Yang, C. Z.; Zhang, Q. M. *Macromolecules* **2007**, *40*, 2371-2379.

(18) Kwon, Y.; Hayakawa, T.; Kakimoto, M. A. *Chemistry Letters* **2006**, *35*, 1306-1307.

(19) Lee, T. K., Y.; Park, J.J.; Pu, L.; Hayakawa, T.; Kakimoto, M.A. *Macromolecular Rapid Communications* **2007**, 1657-1662.

(20) Ito, F.; Inoue, T.; Tomita, D.; Nagamura, T. *Journal of Physical Chemistry B* **2009**, *113*, 5458-5463.

(21) Mi, J.; Guo, L. J.; Liu, Y.; Liu, W. M.; You, G. J.; Qian, S. X. *Physics Letters A* **2003**, *310*, 486-492.

(22) Brozek-Pluska, B.; Jarota, A.; Kurczewski, K.; Abramczyk, H. In *29th European Congress on Molecular Spectroscopy* Opatija, CROATIA, 2008, p 338-346.

(23) Rodriguez-Morgade, M. S.; Plonska-Brzezinska, M. E.; Athans, A. J.; Carbonell, E.; de Miguel, G.; Guldi, D. M.; Echegoyen, L.; Torres, T. *Journal of the American Chemical Society* **2009**, *131*, 10484-10496.

(24) Ishii, K.; Kobayashi, N. In *48th International Conference on Coordination Chemistry* Kochi, Japan, **1998**, p 231-250.

(25) Takeuchi, S.; Ishii, K.; Kobayashi, N. *Journal of Physical Chemistry A* **2004**, *108*, 3276-3280.

(26) Zhang, X. F.; Di, Y. Q.; Zhang, F. S. *Journal of Photochemistry and Photobiology a-Chemistry* **2009**, *203*, 216-221.

(27) Ohkubo, K.; Fukuzumi, S. *Journal of Porphyrins and Phthalocyanines* **2008**, *12*, 993-1004.

(28) Martin-Gomis, L.; Ohkubo, K.; Fernandez-Lazaro, F.; Fukuzumi, S.; Sastre-Santos, A. *Journal of Physical Chemistry C* **2008**, *112*, 17694-17701.

Chapter 6

Investigations of energy migration in an organic dendrimer macromolecule for sensory signal amplification

6.1. Introduction

The need for rapid and safe detection of ultra-trace analytes from highly explosive substances, such as trinitrotoluene (TNT) and its derivatives is vital for various applications because of their toxicity. [1-4] A number of analytical techniques have been developed to detect explosives, such as liquid chromatography, gas chromatography (GC) with chemiluminescence, Raman, infrared and ion mobility spectroscopies. [3-7] A recent progress has been achieved in Goodson's group by using the nonlinear two-photon absorption method. [8] This technique allows the detection of particular explosives which has a linear absorption spectrum in the visible or ultra-violet spectral regions. The sensitivity will be enhanced due to the amplified quenching mechanisms. From the material side, molecule specific antibodies are commonly used to target specific explosives. [9,10]And organic macromolecules have been proven to be an effective approach of creating a very sensitive sensor material.[8,11,12] For example, a poly(ethylene-co-glycidyl methacrylate) (PEGM) polymer/ peptide composite has shown an effective detection of TNT. [11] And in our group, we have found a varying generations of phosphorous dendrimer systems (G1-G4), which contains 12, 24, 48 and 96 chromophores respectively, were good sensor materials for TNT detection. [8] The key

findings we have gained from the two-photon excited fluorescence measurements as well as fluorescence quenching measurements on these dendrimers are: [8] (1) the two photo absorption cross section (δ_{TPA}) increased with the generation number. G4 dendrimer exhibited a large δ_{TPA} of ~ 56000 GM (1GM = 10^{-50} cm^4 s/photon), higher than that of previous investigated polymeric sensor materials; (2) the fluorescence of G4 dendrimer was very sensitive to the concentration of TNT regardless of the excitation route (one or two photon). The sensitivity increases with the generation number; (3) a large quenching constant was obtained for G4 dendrimer, which was ~ 1400 M^{-1}, higher than other polymer systems used for TNT detection under the same condition; (4) the fluorescence quenching mechanism was dominated by dynamic quenching process. As the understanding of exciton migration is crucial to the development of this novel sensing technology, we carried out the investigations on this aspect.

Actually, energy migration in organic macromolecules is an important area of research as it relates to many applications involving optical and electronic effects. [13] For example, in the chemosensory applications, the issue of energy migration has been suggested to be a dominant mechanism in the amplified sensing response of certain energetic materials. [14] And in organic conjugated polymers, the increased conjugation length may lead to more sensitive response to energetic materials. [14] Indeed, the issue of localization in organic systems has been considered for many all organic macromolecular systems. Mukamel et al. [15] has conducted theoretical investigation on the process of coupled chromophore systems in organic dendrimer systems based on phenyl acetylene chromophores unit, and found that excitons could be localized on a particular branching point. [15] Later, experiments with ultra-fast laser pulses (in either fluorescence up-

conversion or transient absorption) demonstrated that electronic coupling between chromophores within a macromolecular geometry such as a dendrimer could be strong. [16-22] Chernyak and Tretiak later showed theoretically how one could extend the calculation of the Hamiltonian for the strongly interacting systems beyond the Frenkel exciton limit. [23] All above are critical points in terms of the discussion on the energy migration and exciton diffusion in multi-chromophore or conjugated polymer sensory systems.

It has been reported to use the steady-state measurements to probe the mechanism of energy transport in certain organic macromolecules. Here, the dependence (or independence) of the oscillator strength is used as a method to isolate the processes governed by a purely columbic (Förster) or a short range (wave function) overlap Dexter mechanism. [24] Also, the steady-state anisotropy may be used to probe the long-lived residual anisotropy of particular systems. [25,26] This method may provide qualitative information regarding the energy-migration at long times mostly by use of the residual long-lived anisotropy value. However, many of the intra-molecular interactions that are important in enhancing the exciton migration rate (and subsequently the fluorescence quenching ability) are governed by fast electronic processes which can only be probed by ultra-fast spectroscopic techniques. These processes affect the overall energy migration pathway in macromolecules and in chemosensory applications where they are responsible for the sensitivity and Stern-Volmer results. In our previous reports of ultra-fast energy migration we have found that the specific geometry of organic dendrimers may allow for strong electronic coupling leading to an ultra-fast (~50fs) energy transfer time. [16-22]

There have been reports of the use of exciton migration to explain the enhanced sensitivity of amplified fluorescence quenching measurements with steady-state techniques, the detailed analysis with a specific model and with both nonlinear and time-resolved techniques in systems with defined geometry has not been reported. The quenching factor (F_0/F_q) found in Stern-Volmer plots for sensing TNT can be both modeled and related to real ultra-fast and long-lived lifetimes. It can be shown that for the case of organic macromolecule of *m* chromophores the enhanced quenching can be related to the degree of exciton migration *p* (number of participating chromophores in the exciton migration) as [27]

$$\frac{F_0}{F_q} = (1 + K_m n_a)\left(\frac{1}{1 - \left(\frac{p}{m} - 1 \right) K_m n_a} \right), \tag{6.1}$$

Where F_0, F_q denote fluorescence intensities for non-quenched and quenched samples respectively, K_M is the association constant for macromolecule and analyte, and n_a is the number density of the analyte. Since $K_M n_a p/m \ll 1$ for trace detection with very low analyte concentration this can be approximated as: [27]

$$\frac{F_0}{F_q} \approx 1 + \frac{p}{m} K_M n_a , \tag{6.2}$$

Where higher terms on n_a have been neglected. It can be seen here that as *p* approaches unity, the system then behaves as if it was comprised of isolated units in a macromolecule and there is no enhanced sensitivity to the quenching. As *p* approaches *m*, the system behaves as having an exciton delocalized over the major part of the macromolecule and the increased sensitivity scales with the value of *m* due to enhanced

association constant K_m. This can also relate to the results of ultra-fast anisotropy decay. For the case of anisotropy decay between coupled, randomly oriented chromophores in a macromolecule, one finds the residual value is given as [28,29]

$$r_\infty = 0.4/p, \tag{6.3}$$

This or similar value was often measured in steady states measurements and used in estimation of the exciton migration domain. [25,26] Measurements of the time-resolved anisotropy decay are very powerful in probing the ultrafast kinetics observed in the organic macromolecular systems when coupling is relatively strong. [16] This anisotropy decay measurement also allows one to develop a good comparison between the results and conclusions obtained from steady-state measurements with those of more detailed analysis. In our previous investigations we have shown that with steady-state estimates alone one cannot accurately describe either the exciton migration length or time-scale, and this may cause overestimates of the exciton diffusion length. With these ultrafast techniques and with the model above we are looking for a clearer description for the scale of exciton diffusion length in organic macromolecules which are useful for amplified sensing applications.

In this chapter, the use of a specific model and nonlinear and time-resolved measurements to investigate the energy migration process in amplified fluorescence quenching effects of TNT in dendrimer G1 to G4 is described. With these techniques, we may be able to describe more closely the limits of exciton migration (and its mechanism) in fluorescence quenching applications in TNT sensors.

6.2 Experimental Section

Synthesis of organic dendrimers. Organic dendrimers with large two-photon cross section (e.g. 55,900 GM for dendrimer generation 4) were synthesized by grafting a large number of TP-active chromophores to phosphorus dendrimers generation 1 to 4 which were terminated by $P(S)Cl_2$ end group. More detailed descriptions of the synthesis and characterization of these dendrimers were given in the literature. [30] Dendrimer generations 1 to 4 bear 12, 24, 48 and 96 chromophores respectively. All dendrimer generations absorb in the 380nm region and emit in the 430-500nm region. In addition, they possess high quantum yields up to 0.75, and even the highest generation G4 has a quantum yield of 0.48. [30] Figure 6.1 shows the chemical structure of dendrimer generation 1 to 4 as well as TNT.

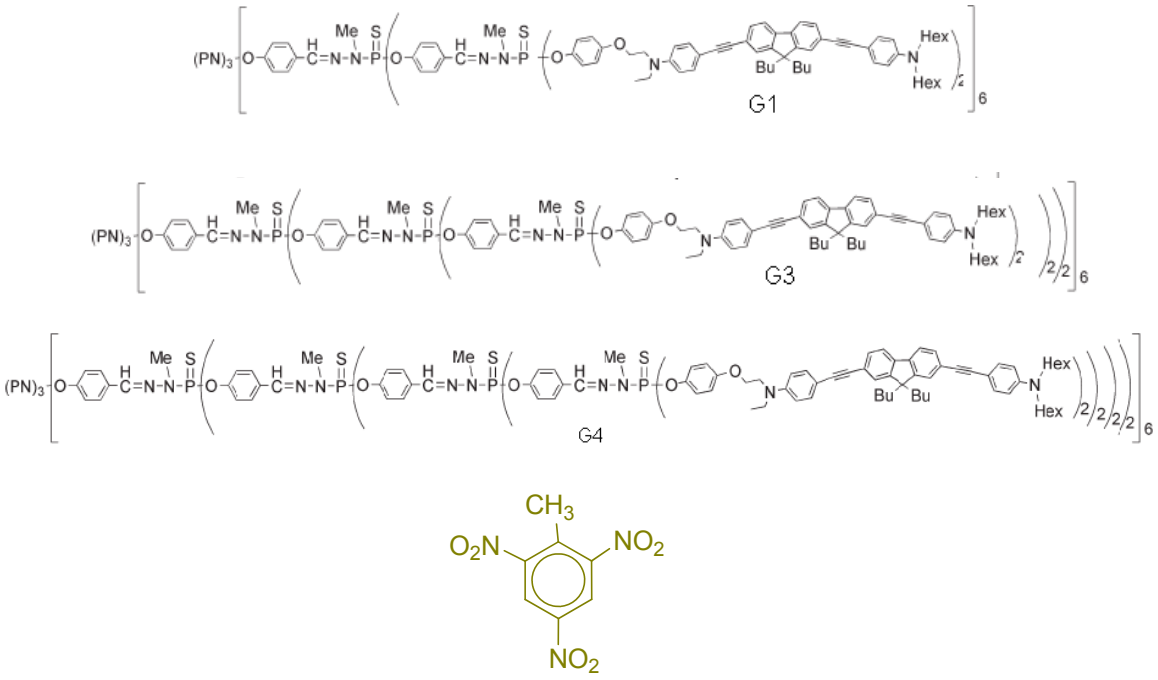

Figure 6.1 Chemical structure of four generation dendrimers (G1-G4) and quencher of TNT used in fluorescence quenching experiments. [8,27,30]

Steady-State Absorption and Emission. Ultraviolet (UV)-visible absorption spectra were recorded with an Agilent Technologies 8453 spectrophotometer. Steady-state fluorescence measurements were performed on a Fluomax-2 fluorimeter. Both toluene and tetrahydrofuran (THF) were used as solvents for all spectroscopic measurement.

Time-Resolved Fluorescence Spectroscopy. Time-resolved polarized fluorescence measurements were carried out on a femtosecond fluorescence upconversion set-up. [27] The detailed description of the set-up has been itinerated elsewhere. [21,31] In brief, the solution was excited with frequency-doubled light from a mode-locked Ti-sapphire laser (Tsunami, Spectra Physics) with a pulse width of ~ 100fs in a wavelength range of 385-430nm. A Berek compensator was utilized to control the polarization of the excitation beam for fluorescence anisotropy measurement. The sample cell was 1mm thick and was held in a rotating holder to avoid possible photodegradation and other accumulative effects. The horizontally polarized fluorescence emitted from the sample was up-converted in a nonlinear crystal of β-barium borate. This system acts as an optical gate and enables the fluorescence to be resolved temporally with a time resolution of about 200fs (FWHM). [21,31] Spectral resolution was achieved by dispersing the up-converted light in a monochromator and detecting it by using a photo-multiplier tube (Hamamatsu R1527P).

The fluorescence anisotropy decay was calculated according to the expression:

$$r(t) = \frac{I_{par} - GI_{per}}{I_{par} + 2GI_{per}} \quad , \tag{6.4}$$

Here, I_{par} and I_{per} are the intensities of fluorescence polarized vertically and horizontally to the polarization of excited light respectively. The *G* factor accounts for the

varying sensitivities for the detection of emission at vertically and horizontal polarization configurations. The *G* factor was corrected using standard dye in this experiment.

Fluorescence quenching experiment. Fluorescence quenching experiments were carried out by micro-titration in solution. The titration procedure involved the placement of a 1.5ml sample solution in a 0.5cm Quartz cell. Initially, the fluorescence spectrum was recorded in the absence of a quencher at room temperature using the Fluoromax-2 (SPEX) spectrophotometer. To the initial solution, micro-liter additions of a solution that contained the sample at the same concentration and the quencher at a known concentration were performed, and fluorescence spectra were acquired after each micro-liter addition. Stern-Volmer plots were made with the acquired data. [27]

6.3 Results and Discussion

Two solvents with different polarities (THF and toluene) were used to dissolve dendrimers G1 to G4. Steady state absorption and fluorescence spectra of the dendrimers in toluene were reported in the reference. [30] Shown in Figure 6.2 are the normalized absorption and fluorescence spectra of the dendrimer generations from G1 through G4 in THF.

The absorption spectrum is nearly independent of the generation number, which indicates the existence of a weak interchomophore coupling in the ground state configuration. [24] [32]At the same time the fluorescence spectra of the dendrimers show dependence on the generation number, which indicates stronger interchromophore interactions in the excited state. This dependence can also be associated with slightly different relaxation configurations for different generations resulting from more densely packed periphery groups for larger dendrimers. [33] Even if the absorption spectra are

essentially the same in THF and toluene, the fluorescence spectra in THF slightly deviate from those in toluene and demonstrate increased Stokes shift. [30]This fluorescence dependence on solvent can be rationalized by higher polarity of THF with respect to toluene and the dipolar character of the chromophores. [34]

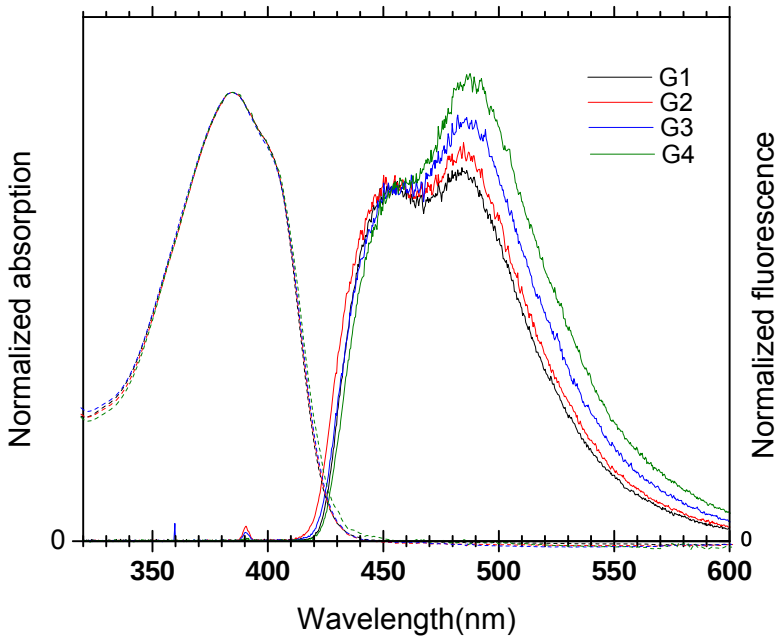

Figure 6.2 Normalized absorption and steady-state emission spectra (excited at 380nm) in THF of the dendrimer generations G1-G4 bearing 12, 24, 48, and 96 chromophores respectively. [27]

In our previous work we found that the fluorescence of the dendrimers is sensitive to the presence of TNT. [8] Due to the strong two-photon absorption properties of these dendrimers, the sensors based on the fluorescence quenching can be efficiently activated by the near-infrared light using two photon absorption route for the excitation. [8] The quenching efficiency can be quantified with the Stern-Volmer relation:

$$F_0 / F_q = 1 + K_{SV} [M], \qquad (6.5)$$

In this equation, F_0 is the initial fluorescence intensity without quencher, F_q is the fluorescence intensity in the presence of the quencher (TNT) with a concentration [M], and K_{sv} is the Stern-Volmer constant. We have measured the fluorescence quenching efficiency as a function of the dendrimer generation number. The Stern-Volmer (S-V) plots for the lowest and highest generation numbers (G1, G4) are shown in Figure 6.3.

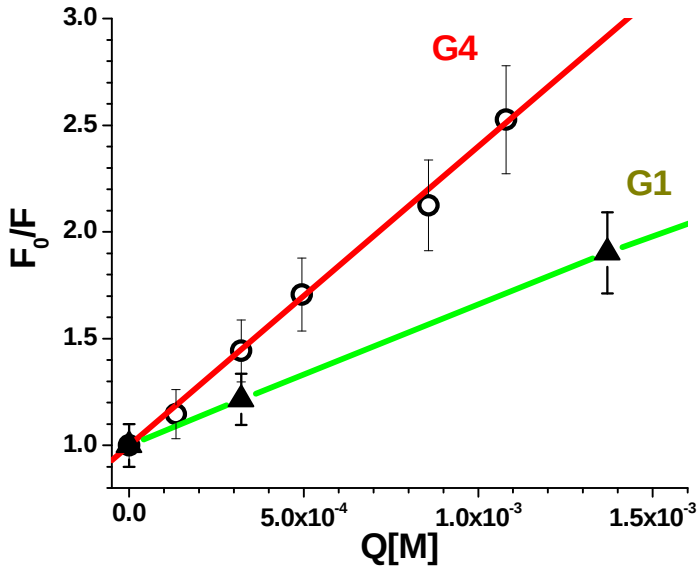

Figure 6.3 Stern-Volmer plot for the fluorescence quenching of dendrimers with TNT. The comparison of two-photon excited fluorescence quenching (excitation at 800nm) of dendrimers G1 and G4 by TNT respectively is shown. The scattering of the data points characterizing the signal-to-noise ratio of two-photon approach with relatively small average laser intensity of a few milliwatts remains quite small and the dependence obtained using one-photon excitation is analogous. [27]

The Stern-Volmer quenching constant K_{SV} for the G4 dendrimer was found to be ~1400 M^{-1}, [8] which is systematically higher as compared to S-V factors obtained under similar conditions for various amplifying polymers used for TNT detection. [25,35] It is also seen from Figure 6.3 that the S-V factor as well as quenching efficiency rises with the

increase of the generation number. In order to better understand this encouraging trend in the enhancement of the sensing performance with higher generation dendrimers and the quenching mechanism behind this trend, we have performed detailed investigations on the exciton migration in these dendrimers by means of femtosecond time-resolved spectroscopy. In polymers studies [14,36-39] as well as in investigations in Langmuir-Blodgett films [25,40] and nanofibrils, [40] an exciton migration was proposed to explain the high quenching efficiency in these systems. In addition, from previous charge and energy transport studies on dendrimers by our group, it was observed that dendrimers can possess excellent exciton transport properties, [18,21,22,31] implying the possibility of amplified quenching in these systems. In the dendrimer systems G1-G4 studied here, chromophores are distributed over near spherical surface of the dendrimer. [30]

It is seen in the Table 6.1 that the average area per chromophore decreases with generation number, which leads to a more dense packing of the chromophores in higher generations. It can be also seen in a way that the distance between chromophores becomes shorter with increasing generation. It is well known that for the Förster energy transfer mechanism associated with Coulombic interchomophore interaction, the transfer rate is inversely proportional to the six power of the distance d between chromophores. [41]To illustrate the scaling of possible Förster–type interchomophore energy transfer rate with the size of the dendrimer, the parameter d^6 is shown in the Table 6.1. Also shown in the table is the two-photon absorption cross-section (σ_2), which is impressive for all and in particular for the dendrimer generation G4. It was mentioned above that the steady state one-photon absorption spectra (Figure 6.2) showed no dependence on generation number, which indicates weak interaction between chromophores in the absorption

configuration. Two-photon cross-section increases near linearly with the number of chromophores further supporting the idea of a relatively weak interchromophore coupling regime in these systems. Time-resolved spectroscopy methods such as time-resolved fluorescence anisotropy allow one to follow exciton migration over the surface and directly connect it to the quenching dynamics and nonlinear properties. [16]

Table 6.1 Geometrical parameters and two-photon responses of the dendrimers G1-G4. [27]

Dendrimer Generation	Diameter (nm)	Surface area (nm^2)	# of chromophores	Surface Area per chromophore (nm^2)	Average distance d between chromophores (nm)	d^{6a} (nm^6)	σ_2 at λ_{TPA} (max)/GM[b22]
G1	4.79	72.04	12	6.00	2.45	216.00	8880
G2	6.74	142.64	24	5.94	2.44	209.58	17700
G3	8.66	235.48	48	4.90	2.21	116.65	29800
G4	10.60	352.8	96	3.675	1.92	9.63	55900

[a] d^6 is inversely proportional to the Föster energy transfer time (hopping time) between chromophores. [b] σ_2 – two-photon absorption cross-section, $1GM=10^{-50}cm^4$ s photon $^{-1}$

6.3.1 Time-Resolved Fluorescence.

The time-resolved fluorescence intensity decay taken at the magic angle of the polarizer is shown in Figure6.4. Fluorescence decay has been detected at 470nm.

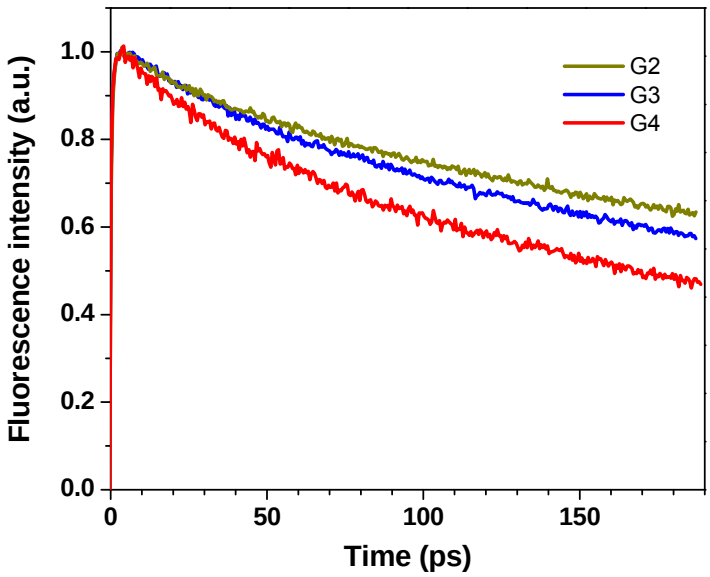

Figure 6.4 Normalized time dependent fluorescence decay of the dendrimer generations from 2 to 4 (G2 to G4) in THF solution. Excitation wavelength - 400nm, detection wavelength - 470nm. [27]

With fitting these decay curves it was found that a decay component in a time scale of ~ 70ps is present for all three different generations along with the long component of 700ps. No substantial contribution of the dynamics faster than 70ps has been measured except small detection-wavelength-dependent solvation components (~1ps). The long time component of the fluorescence decay (~700ps) was previously accurately measured using time-correlated single photon counting and found to be near independent of the dendrimer size. [30] We have fitted the isotopic fluorescence profile to a two-exponential decay function keeping the long decay time fixed at 700ps. The results are listed in Table 6.2.

It is seen from the table that the contribution of ~70ps component increases with the increase of the dendrimer size. This finding may help to rationalize the decrease of quantum yield at higher generation dendrimers reported earlier (0.48 for G4 vs 0.71 for

G2). [30] As the contribution of the fast decaying fluorescence to the time-integrated fluorescence is very small, the quantum yield should be proportional to the relative contribution of the long 700ps-component. The ratio of amplitudes for G2 and G4 $(A_2)_{G2}/(A_2)_{G4}$ = 1.40 while the ratio of quantum yields $(QY_{G2})/(QY_{G4})$ = 1.46. [30] These numbers are in a good agreement taking into account the simplified model used for the interpretation. Furthermore, the ~70ps-time component can be correlated to the average time for the exciton to reach the intrinsic quenching site (defect) in the system. The relatively long time lag of 70ps between the excitation and quenching by intrinsic defects allows the exciton with a short hopping time ~1 ps (see below) to perform multiple hops between chromophores, thus covering substantial area on the surface of the dendrimer. However, the intrinsic quenching originated from defects remains small in G4 dendrimer, as its quantum yield is still relatively high ~48%.

Table 6.2 Time Components and Their Amplitudes for the Fluorescence Up-Conversion Results at the Excitation of 400 nm for the Dendrimer THF Solutions [27]

	t_1/ps	A_1	t_2/ps	A_2
G1	66	0.079	700	0.921
G2	65	0.198	700	0.802
G3	80	0.287	700	0.713
G4	77	0.426	700	0.574

6.3.2 Time-resolved fluorescence anisotropy

The anisotropy decay is utilized to monitor the exciton migration over the dendrimer spherical surface. For different orientations of the chromophores, each interchromophore exciton migration step leads to the reorientation of the emitting dipole and results in fluorescence depolarization. [13,29] The fluorescence depolarization dynamics can be followed by means of the time-resolved spectroscopy and connected in this case to the exciton migration parameters. [22,28,29] While this approach is more or less straightforward for randomly oriented chromophores or for the morphologies possessed well defined angular distributions, it is difficult to apply this approach to near linear systems similar to polymers. In an ideal polymer the transition moment is not supposed to change orientation in course of the exciton migration along the linear chain, leaving the fluorescence being polarized and not sensitive to exciton migration. In organic polymers due to imperfections in the chain (kinks, other defects) and interchain energy transfer, emission dipole does change orientation and fluorescence anisotropy decays to some residual value. [42,43] However, the particular geometry and the mutual chains arrangements are not well known, making it very difficult to connect the fluorescence anisotropy to the exciton path and exciton migration length. Dendrimers are known to possess much more ordered organization of building blocks with defined geometry and different orientations. [44,45] This constitutes a fundamental advantage of the dendrimers in terms of our ability to follow important exciton migration parameters, such as delocalization length, interchromophore coupling strength, and hopping range by means of fluorescence anisotropy. [16-22]

Anisotropy decay results for the dendrimer system G3 on different time scales are shown in Figure 6.5 and 6.6. Fluorescence was excited at 400nm. The experimental fluorescence anisotropy *R(t)* was calculated from the decay curves for the intensities of fluorescence polarized parallel $I_{par}(t)$ and perpendicularly $I_{per}(t)$ to the polarization of the excitation light according to the equation 6.4. The factor *G* accounts for the difference in sensitivities for the detection of emission in the perpendicular and parallel polarized configurations. Starting from anisotropy close to ~ 0.4, the anisotropy decays to near zero value on a time scale ~100ps. Taking into account a very large size of G3 and viscosity of toluene (~0.56 cP at 25^0), the longest time decay component in G3 anisotropy is not associated with the overall molecular rotation (rotational diffusion) of G3 in toluene. Interdendrimer energy transfer can be also ruled out because at the concentration used in this experiment ($c \sim 10^{-5}$ -10^{-4}M), the average intermolecular distance is about 50nm while the Förster radius for the energy transfer can be estimated to be a few nanometers. This combination of parameters (including G3 fluorescence lifetime ~700ps[30]) leads to intermolecular energy transfer time on a sub-millisecond time scale. Therefore we should assign the transition dipole reorientation to the intramolecular (intra-dendrimer) process and it is due to the exciton migration over the surface.

As seen from Figure 6.5 fluorescence anisotropy decays to near zero after 200ps. Taking into account the experimental error, the anisotropy value in this area (>200ps) should not exceed 0.02. For randomly oriented chromophores it implies migration (equilibration) over ~20 chromophores (Eq. 6.3).

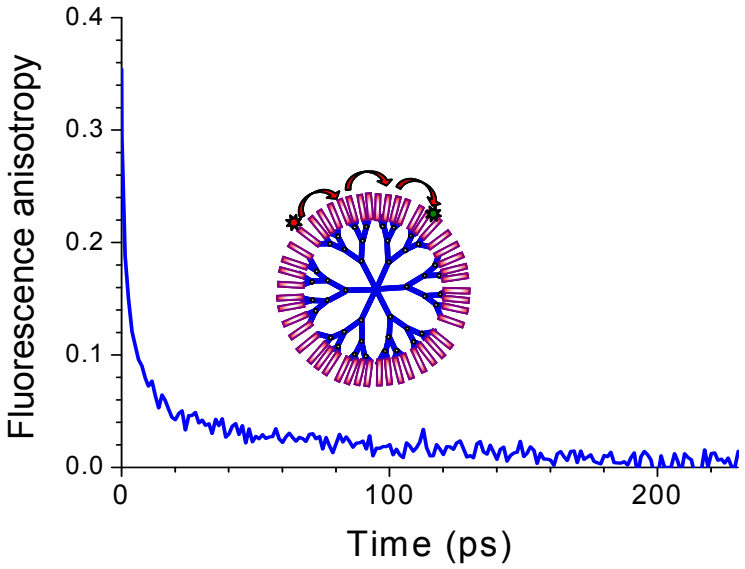

Figure 6.5 A schematic description of the time dependent fluorescence anisotropy decay of dendrimer G3 in toluene due to exciton migration along the dendrimer surface. [27]

In the case of regular organization of chromophores at a fixed angle with respect to the surface, the change of the emission dipole can be roughly correlated to the position on the surface. Using simple equation for the fluorescence anisotropy in case of hindered rotation (in our case it means averaging over the angles within the cone of accessible dipole orientations): [41]

$$r = 0.4\left[\frac{1}{2}(\cos\theta_C)(1+\cos\theta_c)\right]^2 \qquad (6.6)$$

Where θ_C is the cone angle and the range of θ_C can be estimated in course of the exciton migration from the anisotropy r. This simple estimation gives the angle $\theta_C = 69^0$ which corresponds to 32% of sphere's surface to be covered by exciton. The number of

chromophores on this spherical segment is ≅16 for G3. This gives us an estimation of the number of chromophores covered by exciton migration in the limiting case of regular organization of the chromophores at a fixed angle with respect to the dendrimer surface.

Fluorescence anisotropy decay on a short time scale is shown in Figure 6.6. The raw fluorescence anisotropy decays from an initial value ~0.34 at time zero to the anisotropy of ~0.14 at time of 3ps. In case of fast dynamics, the measured profiles $I_{par}(t)$, $I_{per}(t)$ are the results of a convolution of the instrument response function with true fluorescence intensity profiles. In this case the raw anisotropy looks different from the true anisotropy profile at short times and its peak appears at negative times. Parameters of true anisotropy decay can be estimated by best fit procedures assuming the convolution of the instrument response function (IRF) with model parallel and perpendicular fluorescence intensity profiles. [46,47] The best fit to a two-exponential anisotropy decay model is shown in Figure 6.6 by the solid line. The best fit anisotropy was found to decay from initial value of 0.40±0.03 within the time constant of 575±20fs.

This time constant is relatively long as compared to some other strongly interacting dendrimer systems, [16,18,31] which may indicate the incoherent hopping exciton transport in this system. [22]The fast decay component is generation dependent and fluorescence anisotropy decays much faster in a higher generation dendrimer, as the dendrimer becomes more densely packed and the distance between chromophore shortens (see discussion below). The fluorescence anisotropy decay curves of different dendrimer generations (G2 to G4) on long time scale are plotted in Figure 6.6.

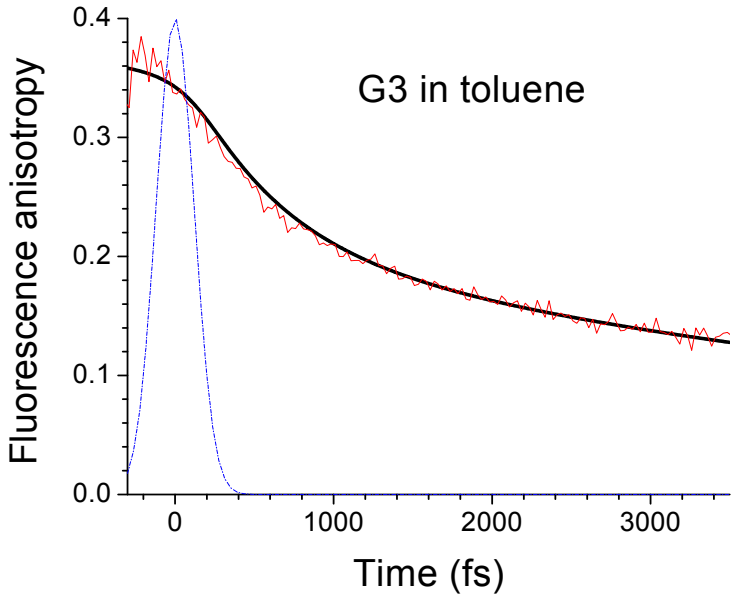

Figure 6.6 Short time scale of time-resolved fluorescence anisotropy of dendrimer G3 in toluene with instrument response function IRF (blue dotted line). Excitation wavelength – 400nm, detection wavelength – 480nm. The dark solid line is the result from best fit modeling. [27]

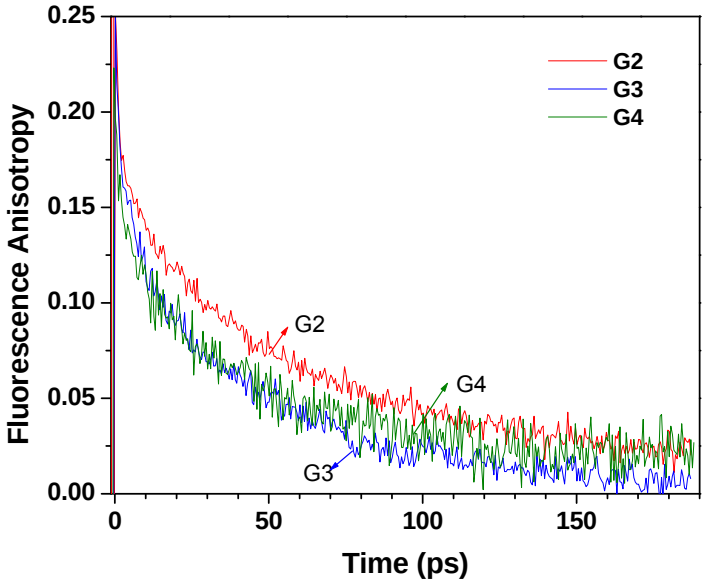

Figure 6.7 Comparison of intermediate time scale of time-resolved fluorescence anisotropy of different dendrimer generations G2 (red), G3 (blue) and G4 (cyan) in THF solution. Excitation wavelength – 400nm. [27]

It is seen that the anisotropy decay on this time scale weakly depends on dendrimer generation. While the decay profiles for G3 and G4 are the same within the experimental error, the anisotropy for G2 decays slightly slower. This slower decay can be associated with less densely packed chromophores for smaller generation dendrimers. The shorter time components in anisotropy decay showed the same decreasing trend with the increase of the generation number (see Figure 6.11a and discussion below).

To gain an insight into the molecule architectural effect, we investigate the behavior of fluorescence anisotropy decay in different polarity solvents (THF and toluene) for dendrimer generation from G1 to G4. The anisotropy decay in varying solvents can provide information on the details of the arrangement and interaction between the chromophores in different solvents.

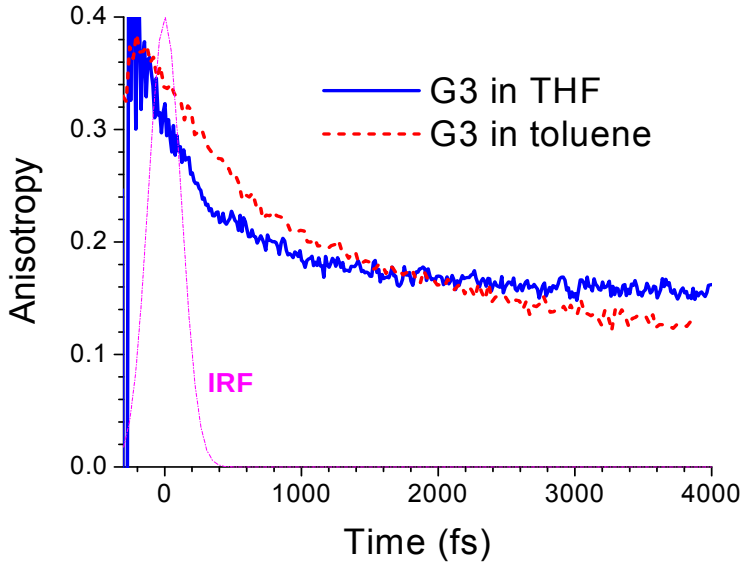

Figure 6.8 The solvent effect (THF and toluene) on the time-resolved fluorescence anisotropy of the dendrimer G3 on a short time scale. Instrument response function (IRF) is also shown (dash-dot line). [27]

Based on our investigation, the different generation of dendrimers G1, G2, G3 and G4 display the same trend regarding to the anisotropy decay behavior in these two solvents. Figure 6.8 shows an example of the fluorescence anisotropy profiles for dendrimer G3 in THF and in toluene. In general the G3 anisotropy decay in both solvents (THF and toluene) can be approximated by a two-exponential decay function on this time scale. A fast initial decay on the time scale of hundreds of fs gives way to a slower decay in ps time scale. It is seen from Figure 6.8 that in a more polar solvent of THF (polarity index of 4), the first decay component($\tau_s \cong 180$fs) is shorter than that in toluene (polarity index of 2.4) with the fast decay component of $\tau_s \cong 575$fs (derived from more accurate fitting with IRF convolution compared to the value published [8]). As opposite to the trend in short components the second decay component in THF is longer compared to that in toluene (Figure 6.8). More polar solvent THF can facilitate the chromophore aggregation on the dendrimer's surface, especially at higher generations where the increasing packing density and strong interchromophore interactions can favor the self-organization process. [48] The deviation of the decay behavior in two different solvents may be rationalized in terms of degree of clusterization (surface aggregate formation) , that is to say, in a more polar solvent (THF in this case), the inhomogeneous distribution of chromophores on the dendrimer surface will result in multi-exponential anisotropy decay profile. The first decay component in this case may be related to the intracluster relaxation; it becomes faster due to the increased aggregation and the decreased distance between chromophores inside surface chromophore aggregates in THF. The longer decay component reflects the intercluster hopping rate, which is reasonable to be slower for higher generations due to the formation of more isolated surface aggregates. Two-component anisotropy decay due

to clusterization within the photosynthetic antenna has been reported by Prof. Fleming and co- authors. [49]Our anisotropy data also indicate the distribution of chromophore on the dendrimer surface to be more uniform in a less polar solvent (toluene). If we go back to the anisotropy decay in toluene, the absence of the ultrafast dynamics (<500fs) points to an incoherent hopping regime for exciton migration over the dendrimer surface. Weak clusterization and inhomogeneous distribution of the chromophores on the surface can lead to some distribution of the hopping times in toluene solution too. The shortest time components in anisotropy decay may reflect the fastest hopping rates in the systems. The average hopping rate can be estimated from the e-times drop in fluorescence anisotropy decay which occurs at ~3ps. This time scale can be compared to the decay process responsible for fluorescence quenching on intrinsic defects (~70ps) described above. The comparison suggests that exciton is able to perform ~23 hops before being quenched by intrinsic defect. This estimation based on the comparison of the fluorescence and fluorescence anisotropy decay times is in good agreement with this made above on the base of the residual anisotropy analysis. These results undoubtedly demonstrate the multistep exciton migration process which produces a long exciton diffusion domain over the dendrimer surface beneficial for the efficient amplified quenching of the explosives, such as TNT.

6.3.3 Quenching dynamics and its connection to the exciton transport

Figure 6.9 schematically displays the difference between fluorescence dynamics for dendrimer sample with TNT (concentration: 5 X 10^{-3}M) $F_q\ (t)$ and that for pure dendrimer solution $F_0\ (t)$.

It is seen that the fluorescence from the sample with quencher (TNT) decays faster than that without quencher, which reflects the substantial rise of the number of quenched excitons on the picosecond time scale. It is worth noting that the difference in the decay profiles saturates roughly at the same time scale as that at which fluorescence anisotropy completely decays (see Figs. 6.5, 6.7). The quenching ratio $Q(t) = F_q(t)/F_0(t)$ represents the fraction of quenched excitations at a given delay time t. The time-resolved quenching ratio $Q(t)$ on short time scale is shown in Figure 6.10. It is seen from this figure that ~10% of fluorescence is quenched within the time resolution of the upconversion setup. Taking into account the absence of any measurable fast dynamics for $Q(t)$ in the vicinity of instrument response function, this fraction of quenching can be considered as instantaneous or true static, and related to the excitation photons being absorbed on non-emissive sites. This is different from the quenching dynamics in conjugated polyelectrolyte where the fast time component has been detected for $Q(t)$ in time-resolved experiments. [39] In our experiments the fastest time component in the quenching ratio decay is ~ 1.5ps. This is close to the ~0.58ps fast time component found in anisotropy experiments (Figure 6.6). Both time constants represent the hopping time between adjacent chromophores by order of magnitude while exact expressions for the anisotropy and for the exciton trapping time can be different. [28,29,50] The major part of the fluorescence quenching by TNT occurs on the time scale ~150ps (Figure 6.9) and should be considered as a dynamic quenching. The fluorescence anisotropy which reflects the exciton migration over the chromophores on the dendrimer surface also decays to zero around 150ps. This directly connects the exciton migration over the surface of the

dendrimer to the dynamic quenching proving the crucial role of exciton migration in the enhanced fluorescence quenching in dendrimer macromolecules.

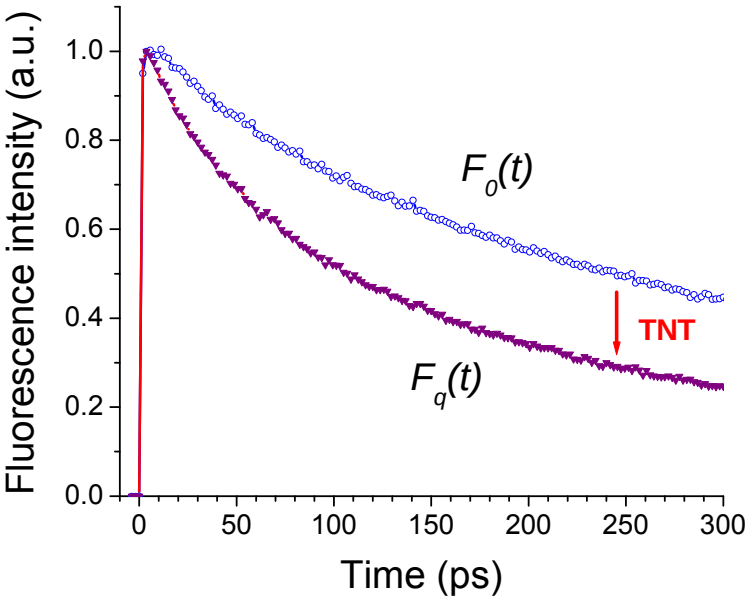

Figure 6.9 Difference in fluorescence dynamics between the pure dendrimer G3 solution (open circles) and the solution after exposure to TNT (filled triangles).Excitation wavelength -400nm, detection wavelength – 480nm. [27]

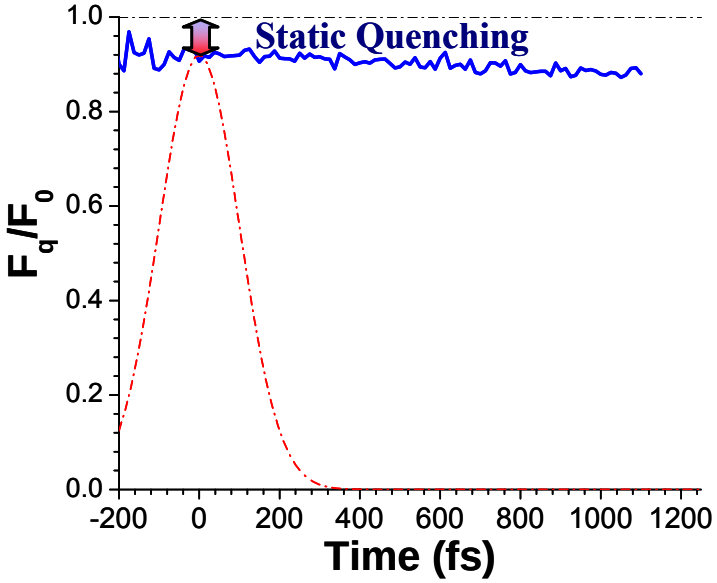

Figure 6.10 Quenching ratio F_q/F_0 as a function of time on a short time scale. It shows a fractional static contribution to the fluorescence quenching.

It is also seen from Figure 6.9,6.10 that both static and dynamic quenching components take account together for the fluorescence quenching by ~ 50% at long delays, which is in excellent agreement with steady state measurements which showed the same total amount of quenching at this TNT concentration.

Simple estimation of the TNT diffusion controlled quenching at the quencher concentration at 10^{-3}M gives the maximum value of collision time about 100ns, [41]whereas the experimental time scale of the dynamic quenching is in the picosecond range from time-resolved measurement studies. Comparison of time integrated fluorescence quenching with the dynamic drop in fluorescence (Figure 6.9) proves that in our case the contribution from the dynamic quenching associated with the diffusion of TNT in solution is negligible. For this case the fluorescence quenching is in major part a fast dynamic process on a picosecond time scale, which results from the fast exciton migration on the dendrimer surface from the initially excited site to the site associated with TNT-chromophore complex.

In order to get further insight into the quenching mechanism, we compared the quenching dynamics for different generations of the dendrimers. As we mentioned above (Figure 6.3) the quenching performance is better for higher generation dendrimers. Figure 6.11a, b show time-resolved fluorescence anisotropies for the dendrimers G1 and G3 respectively. It is seen from Figure 6.11a that the initial anisotropy decay rate is faster for G3 as compared to G1. Best fit analysis which included convolution with instrument response function revealed fast components 0.992 ps and 0.575 ps for G1 and G3, respectively. The initial anisotropy decay rate is directed by the hopping rate between the chromophores on the dendrimer surface indicating that the hopping rate is higher for G3.

Overall anisotropy decay for G3 remains faster for G3 on the longer time scale (Figure 6.11b) as well.

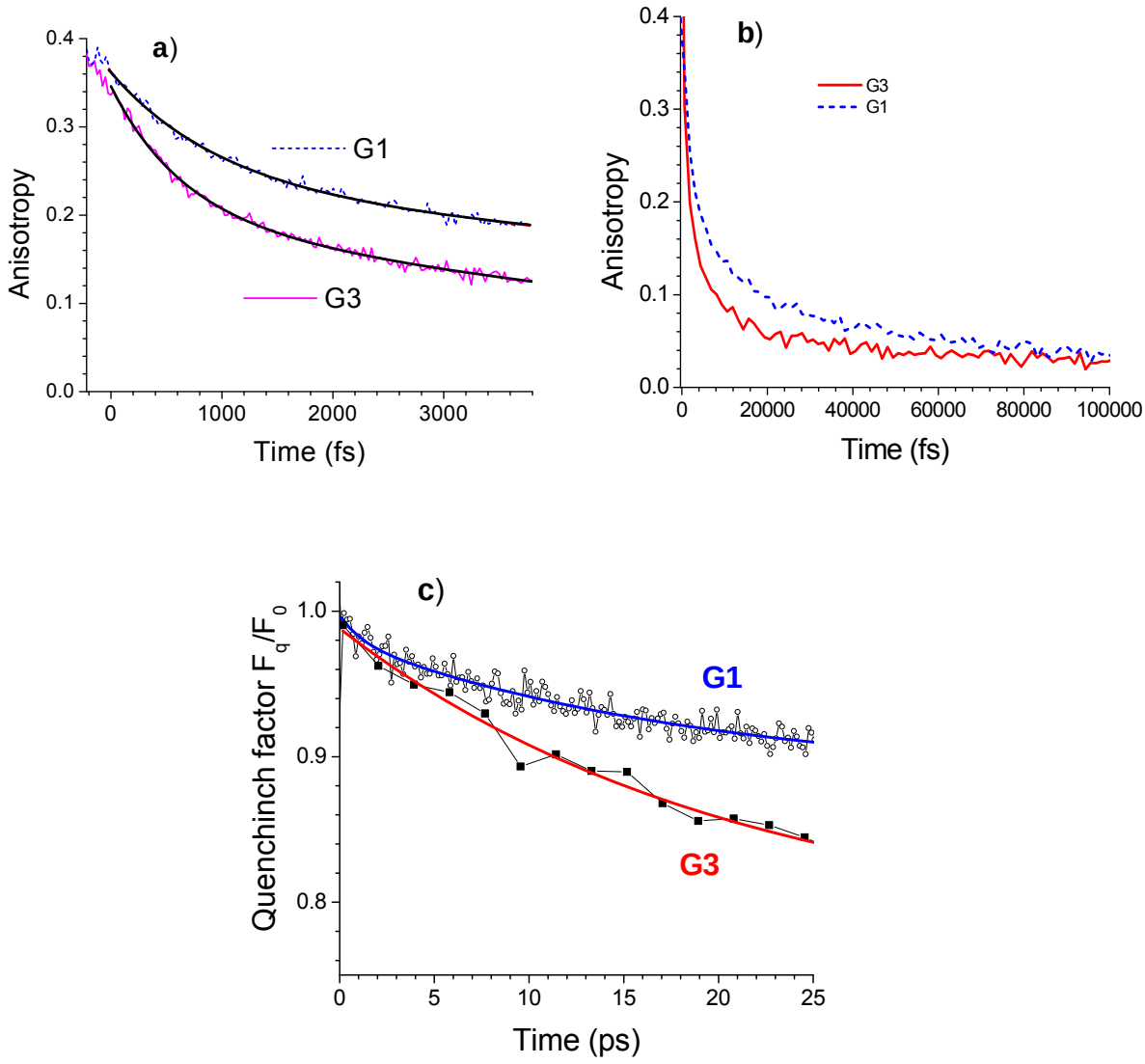

Figure 6.11 Fluorescence anisotropy decay of dendrimers in short time scale (a), long time scale (b) and the quenching dynamics (c) for dendrimers G1 and G3 respectively. [27]

The ratio of hopping rates in G3 and G1 (0.992/0.575=1.73) is in a good agreement with the ratio of Förster transfer rates estimated from geometrical parameters listed in the Table 1 $r_{G3}^6 / r_{G1}^6 = 216.0/117.7 = 1.83$. This clearly indicates that the faster

exciton migration rate in G3 results from more dense packing and smaller interchromophore separation on the surface of higher generation dendrimers. The quenching ratio F_q/F_0 dynamics of G1 and G3 for the same TNT quencher concentration is shown in Figure 6.11c. It is clearly seen from this figure that the fraction of quenched chromophores increases faster for higher generation dendrimer G3. This is the direct consequence of higher interchromophore hopping rate in G3 detected by fluorescence anisotropy measurements. Higher hopping rate in G3 as compared to G1 facilitates larger exciton migration domain in G3. Larger number of chromophores covered by the exciton migration results in the better sensing performance for larger dendrimers found in simple model calculations (Eq. 6.2) and in our experiments (Figure 6.3). Comparing the Stern-Volmer factor obtained for the G4-dendrimer in solution (~1400M^{-1}) [8] with those obtained under similar conditions for the various amplifying polymers used for TNT detection, [35] one can see that the dendrimer's S-V- factor K_{SV} is systematically higher. This can be associated with system's architecture. In polymers the exciton transport is supposed to be mostly one dimensional ("molecular wire" approach), [37]while in large dendrimers the exciton transports over the near spherical surface i.e. quasi-two-dimensional. It was shown by E.W. Montroll[41] that the number of steps <n> required by the exciton to reach a trapping center scales differently on the relative concentration of trapping centers. In particular <n> ~N^2 in one dimensional case, while <n> ~N logN in two dimensional system (N is the number of chromophores per one trapping (quenching) center).[41] It is seen that for the same low quencher concentration (large N), the number of steps required for exciton to reach quencher in two-dimensional system is smaller than that for one dimensional system. This means that the number of hopping steps required

for exciton to reach the quenching site is smaller for quasi-two-dimensional dendrimer surface as compared to linear polymer. This may contribute to the enhanced sensing response of the dendrimers relative to polymers.

6.4 Conclusions

We have investigated the exciton dynamics in new dendritic materials which are promising two photon sensors for TNT detection. These materials possess the exceptional combination of large δ_{TPA} with efficient amplified fluorescence quenching by TNT. We have directly connected fluorescence time-resolved anisotropy measurements with that of the excitation migrating over the dendrimer surface to the quenching site. Our investigation showed that this exciton migration over many units to the TNT-dendrimer complex sites plays a dominant role in the fluorescence quenching process. The time components describing the exciton migration over the dendrimer surface are in the same range as those observed for the dynamic quenching, thus proving that the exciton migration over the dendrimer surface is the main contributor to the observed dynamic fluorescence quenching. This validates the efficient amplified quenching mechanism associated with exciton migration over dendrimer surface as a main quenching mechanism. Our results also indicate that the migration over quasi-two-dimensional dendrimer surface results in more efficient amplified quenching than that along the one-dimensional polymer chains ("molecular wires").

Reference

(1) Devolpi, A.; Rhodes, E. A. *Science* **1992**, *258*, 14-15.

(2) Hannink, N.; Rosser, S. J.; French, C. E.; Basran, A.; Murray, J. A. H.; Nicklin, S.; Bruce, N. C. *Nature Biotechnology* **2001**, *19*, 1168-1172.

(3) Moore, D. S. *Review of Scientific Instruments* **2004**, *75*, 2499-2512.

(4) Steinfeld, J. I.; Wormhoudt, J. *Annual Review of Physical Chemistry* **1998**, *49*, 203-232.

(5) Ray, M. D.; Sedlacek, A. J.; Wu, M. *Review of Scientific Instruments* **2000**, *71*, 3485-3489.

(6) Wu, M.; Ray, M.; Fung, K. H.; Ruckman, M. W.; Harder, D.; Sedlacek, A. J. *Applied Spectroscopy* **2000**, *54*, 800-806.

(7) Lewis, M. L.; Lewis, I. R.; Griffiths, P. R. *Applied Spectroscopy* **2004**, *58*, 420-427.

(8) Narayanan, A.; Varnavski, O.; Mongin, O.; Majoral, J. P.; Blanchard-Desce, M.; Goodson, T. *Nanotechnology* **2008**, *19*.

(9) Anderson, G. P.; Moreira, S. C.; Charles, P. T.; Medintz, I. L.; Goldman, E. R.; Zeinali, M.; Taitt, C. R. *Analytical Chemistry* 2006, *78*, 2279-2285.

(10) Hagleitner, C.; Hierlemann, A.; Lange, D.; Kummer, A.; Kerness, N.; Brand, O.; Baltes, H. *Nature* **2001**, *414*, 293-296.

(11) Cerruti, M.; Jaworski, J.; Raorane, D.; Zueger, C.; Varadarajan, J.; Carraro, C.; Lee, S. W.; Maboudian, R.; Majumdar, A. *Analytical Chemistry* **2009**, *81*, 4192-4199.

(12) Jaworski, J. W.; Raorane, D.; Huh, J. H.; Majumdar, A.; Lee, S. W. *Langmuir* **2008**, *24*, 4938-4943.

(13) Scholes, G. D.; Rumbles, G. *Nature Materials* **2006**, *5*, 683-696.

(14) Yang, J. S.; Swager, T. M. *Journal of the American Chemical Society* **1998**, *120*, 11864-11873.

(15) Chernyak, V.; Poliakov, E. Y.; Tretiak, S.; Mukamel, S. *Journal of Chemical Physics* **1999**, *111*, 4158-4168.

(16) Goodson, T. G. *Accounts of Chemical Research* **2005**, *38*, 99-107.

(17) Ramakrishna, G.; Varnavski, O.; Kim, J.; Lee, D.; Goodson, T. *Journal of the American Chemical Society* **2008**, *130*, 5032.

(18) Ranasinghe, M. I.; Varnavski, O. P.; Pawlas, J.; Hauck, S. I.; Louie, J.; Hartwig, J. F.; Goodson, T. *Journal of the American Chemical Society* **2002**, *124*, 6520-6521.

(19) Varnavski, O.; Bauerle, P.; Goodson, T. *Optics Letters* **2007**, *32*, 3083-3085.

(20) Varnavski, O.; Menkir, G.; Goodson, T.; Burn, P. L. *Applied Physics Letters* **2000**, *77*, 1120-1122.

(21) Varnavski, O.; Samuel, I. D. W.; Palsson, L. O.; Beavington, R.; Burn, P. L.; Goodson, T. *Journal of Chemical Physics* **2002**, *116*, 8893-8903.

(22) Varnavski, O. P.; Ostrowski, J. C.; Sukhomlinova, L.; Twieg, R. J.; Bazan, G. C.; Goodson, T. *Journal of the American Chemical Society* **2002**, *124*, 1736-1743.

(23) Wu, C.; Malinin, S. V.; Tretiak, S.; Chernyak, V. Y. *Nature Physics* **2006**, *2*, 631-635.

(24) Thompson, A. L.; Gaab, K. M.; Xu, J. J.; Bardeen, C. J.; Martinez, T. J. *Journal of Physical Chemistry A* **2004**, *108*, 671-682.

(25) Kim, Y.; Zhu, Z. G.; Swager, T. M. *Journal of the American Chemical Society* **2004**, *126*, 452-453.

(26) Rose, A.; Tovar, J. D.; Yamaguchi, S.; Nesterov, E. E.; Zhu, Z. G.; Swager, T. M. *Philosophical Transactions of the Royal Society a-Mathematical Physical and Engineering Sciences* **2007**, *365*, 1589-1606.

(27) Guo, M.; Varnavski, O.; Narayanan, A.; Mongin, O.; Majoral, J. P.; Blanchard-Desce, M.; Goodson, T. *Journal of Physical Chemistry A* **2009**, *113*, 4763-4771.

(28) Yeow, E. K. L.; Ziolek, M.; Karolczak, J.; Shevyakov, S. V.; Asato, A. E.; Maciejewski, A.; Steer, R. P. *Journal of Physical Chemistry A* **2004**, *108*, 10980-10988.

(29) Finger, K. U.; Marcus, A. H.; Fayer, M. D. *Journal of Chemical Physics* **1994**, *100*, 271-286.

(30) Mongin, O.; Krishna, T. R.; Werts, M. H. V.; Caminade, A. M.; Majoral, J. P.; Blanchard-Desce, M. *Chemical Communications* **2006**, 915-917.

(31) Varnavski, O.; Yan, X. Z.; Mongin, O.; Blanchard-Desce, M.; Goodson, T. *Journal of Physical Chemistry C* **2007**, *111*, 149-162.

(32) Kopelman, R.; Shortreed, M.; Shi, Z. Y.; Tan, W. H.; Xu, Z. F.; Moore, J. S.; BarHaim, A.; Klafter, J. *Physical Review Letters* **1997**, *78*, 1239-1242.

(33) Bosman, A. W.; Janssen, H. M.; Meijer, E. W. *Chemical Reviews* **1999**, *99*, 1665-1688.

(34) Mongin, O.; Porres, L.; Moreaux, L.; Mertz, J.; Blanchard-Desce, M. *Organic Letters* **2002**, *4*, 719-722.

(35) Zhao, D.; Swager, T. M. *Macromolecules* **2005**, *38*, 9377-9384.

(36) Thomas, S. W.; Joly, G. D.; Swager, T. M. *Chemical Reviews* **2007**, *107*, 1339-1386.

(37) Swager, T. M. *Accounts of Chemical Research* **1998**, *31*, 201-207.

(38) Yang, J. S.; Swager, T. M. *Journal of the American Chemical Society* **1998**, *120*, 5321-5322.

(39) Muller, J. G.; Atas, E.; Tan, C.; Schanze, K. S.; Kleiman, V. D. *Journal of the American Chemical Society* **2006**, *128*, 4007-4016.

(40) Naddo, T.; Che, Y. K.; Zhang, W.; Balakrishnan, K.; Yang, X. M.; Yen, M.; Zhao, J. C.; Moore, J. S.; Zang, L. *Journal of the American Chemical Society* **2007**, *129*, 6978.

(41) J.R.Lakowicz; 2 ed.; Kluwer Academic/Plenum Publishers: New York, **1999**.

(42) Kim, Y. R.; Lee, M.; Thorne, J. R. G.; Hochstrasser, R. M.; Zeigler, J. M. *Chemical Physics Letters* **1988**, *145*, 75-80.

(43) Grage, M. M. L.; Wood, P. W.; Ruseckas, A.; Pullerits, T.; Mitchell, W.; Burn, P. L.; Samuel, I. D. W.; Sundstrom, V. *Journal of Chemical Physics* **2003**, *118*, 7644-7650.

(44) Fréchet, J. M. J. T., D. *Dendrimers and Other Dendritic Polymers*; Wiley: Chichester, UK, **2001**.

(45) *Dendritic Molecules: Concepts, Synthesis, Perspectives*; Newkome, G. R. M., C.N.; Vögtle, F., Ed.; Wiley-VCH: Weinheim, Germany, **2001**.

(46) Soutar, I.; Swanson, L.; Christensen, R. L.; Drake, R. C.; Phillips, D. *Macromolecules* **1996**, *29*, 4931-4936.

(47) Cross, A. J.; Fleming, G. R. *Biophysical Journal* **1984**, *46*, 45-56.

(48) Wang, B. B.; Zhang, X.; Jia, X. R.; Luo, Y. F.; Sun, Z.; Yang, L.; Ji, Y.; Wei, Y. *Polymer* **2004**, *45*, 8395-8402.

(49) Bradforth, S. E.; Jimenez, R.; Vanmourik, F.; Vangrondelle, R.; Fleming, G. R. *Journal of Physical Chemistry* **1995**, *99*, 16179-16191.

(50) Montroll, E. W. *Journal of Mathematical Physics* **1969**, *10*, 753.

Chapter 7

Conclusions and Future Outlook

7.1 Conclusions

Hyperbranched and dendritic systems targeted at high dielectric constant applications because of the long range polaron delocalization are investigated and proposed to be a novel approach which differs from traditional percolation systems. Aside from the electronic polarization and interface polarization mechanisms, the hyperelectronic polarization operative in such systems makes the biggest contribution to the high dielectric response observed at high operational frequencies. The advantages of this approach will include (1) the polaron delocalization in certain branched or dendritic molecules which can extend to several molecule units leading to a longer delocalization length; (2) the drift distance of charge carriers which can be elongated and result in a hyperelectronic polarization; (3) the planar structure which may facilitate the head to head packing through the self-assembly.

Three series of hyperbranched CuPc based polymers were first synthesized by our collaborators using copper fusion methods which resulted in high yield (67%) and good solubility. All hyperbranched CuPc systems possess cyano end-group in order to enhance the polarity. But the weight percentage of the CuPc and the bridging group and the position of CuPc rings varied. The electronic properties, in particular the dielectric properties of these hyperbranched polymers were tested and the underlying charge transfer mechanisms were probed by means of several ultrafast spectroscopy techniques,

such as femtosecond fluorescence up-conversion spectroscopy and pump-probe transient absorption spectroscopy. We are the first group to conduct a systematic investigation on both ground and excited state charge transfer mechanisms of hyperbranched CuPc dendrimers, and work to bridge the gap between the knowledge on the dielectric properties and optical properties of hyperbranched CuPc dendrimers.

Chapter 3 discussed the electronic and optical properties of the first sets of hyper-branched CuPc (HBCuPc) polymers. They have shown an excellent dielectric response over the test frequency range (20Hz to 1MHz). The dielectric constant of the HBCuPc pellet with a thickness of 76 μm reached 46 at 1MHz and showed an extremely low dielectric dispersion (a change of ~1% from 20Hz to 1MHz). This value is significant as compared to that of CuPc monomers (~5).And in terms of the practical application requirements at high frequencies, this material showed the most satisfactory performance compared to other CuPc based materials. The dielectric loss was greatly reduced too. It went below 0.004 at 1MHz in a cast film of HBCuPc dendrimer with a thickness of 10 μm, in addition to a very weak dependence on the frequency. In general, high dielectric constant will be accompanied with large dielectric loss and both will show strong frequency dependence, which is typical for some hyperbranched systems with hyperelectronic polarization. For instance, the hyperbranched polyaniline exhibited a dielectric constant ~200 as well as a dielectric loss ~1 at 1MHz. However, this HBCuPc polymer shows an exception, as even a HBCuPc polymer pressed pellet possessed a low dielectric loss (<0.01) at 1MHz. From the analysis of the AC conductance, both polaron hopping and polaron tunneling charge transfer mechanisms were found to be operative in this HBCuPc system because the power law dependence of the AC conductance on the

frequency was derived. Additionally, the steady-state emission and femtosecond fluorescence anisotropy decay provided evidence to support the polaron hopping mechanisms found in the HBCuPc from AC conductance analysis. For example, a slow component in a time scale of 3 ps was derived from the best fit of the fluorescence anisotropy decay curve, the time scale is in a good agreement with the polaron hopping process found in other disordered organic systems.

To get a closer look at the charge transfer mechanisms operative in the HBCuPc system, time-of-flight charge carrier mobility measurement was carried out on the HBCuPc dendrimer film cast on the silicon wafer. The charge carrier mobility was unusually high (in the order of ~10^{-4} $cm^2V^{-1}s^{-1}$), closely correspondent with the exhibited fast dielectric response. In addition, the interesting findings about the non-Arrhenius temperature dependence and the Poole-Frenkel negative electric field dependence were presented. At high temperature, more thermally activated sites were available and extended-state conductivity possibly occurred. However, at low temperature, the packing of Pc rings becomes more ordered and when the distance between the neighboring phthalocyanine rings approached a critical value (< 5Å), polaron tunneling occurred and made a significant contribution to the higher mobility observed at low temperature as compared to that at high temperature. Simulations based on the Bässler's Gaussian disorder model were run to gain a deep insight into the transport mechanisms of charge carriers. Moreover, in contrary to the typical positive electric field dependence found in phthalocyanine monomer films, the HBCuPc polymer showed the negative field dependence and the positional disorder was considered as the main contributor.

The direct inspiration for the immediate follow-up works on the design and characterization of HBCuPc-TPA-CN polymer came from the striking results from the investigation of the HBCuPc dendrimer. The work was discussed in detail in chapter 4. In this modified design, the effective conjugation between the triphenylamine moiety and the CuPc ring was targeted at increasing the conjugation length as well as changing the charge transfer properties of the CuPc dendrimer system. From the device fabrication standpoint, this design will enable the enhancement of the dielectric film formation ability. The cast dielectric film of HBCuPc-TPA-CN dendrimer exhibited a reproducible and good dielectric response. The dielectric constant is around 11 and the loss tangent is about 0.002 at 1MHz. AC conductance analysis suggested that the charge carriers in HBCuPc-TPA-CN polymer were mainly transferred through "hops" between CuPc rings and even the tunneling. In addition to the electronic and hyperelectronic polarization, ionic polarization was presented in the system too, which was represented by the appearance of peak in the dielectric loss vs. frequency curve. The increased conductivity was natural because of the formation of charge transfer complex in the HBCuPc-TPA-CN polymer and was influenced by the interaction strength between the donor and the acceptor. In addition, the existence of electron traps induced by triphenylamine has the effect of immobilizing a large proportion of the injected carriers, which may offset the rise in dielectric constant due to the increase of the conjugation length. Other factors such as the hindrance to the molecular packing due to the pyramidal shape of triphenylamine moiety have been taken account for the inferior dielectric response of the HBCuPc-TPA-CN polymer as compared to that of the HBCuPc polymer. In order to optimize the fabrication of the dielectric film and understand the influence of the interaction between

the dielectric material and the conducting substrate at the interface on the dielectric response, we also prepared samples by adding an extra sonication process before the casting of the film, or substitute the alumina substrate by the indium tin oxide (ITO) glass and the coating glass from silicon nitrate. In latter cases, a thin layer of Au was evaporated on both sides of the sample to act as conductive electrodes. The ITO and silicon nitrate functioned as dopants to the polymer film and a strong dielectric dispersion because of the interface polarization was produced. Scanning electron spectroscopy (SEM) cross section measurement showed a clear comparison on the interface of the HBCuPc-TPA-CN polymer/alumina and the HBCuPc-TPA-CN polymer/ITO glass. Our goal is to design a high dielectric constant and low dielectric loss material for high frequency applications; therefore, alumina seems to be a better substrate material at this point.

Donor –acceptor interaction has been extensively studied for various usages such as organic photovoltaic cells and this is the first time being explored for the contribution to the dielectric response in hyper-branched polymer systems. A similarly accelerated charge transfer via Förster hopping was found in the HBCuPc-TPA-CN polymer, as evidenced from the femtosecond fluorescence spectroscopy measurement. Excited state dynamics probed by ultrafast pump-probe transient absorption measurement indicated the formation of charge transfer excitations in the HBCuPc-TPA-CN polymer as compared to the HBCuPc polymer. Both polymers showed typical triplet-triplet absorption spectra of phthalocyanine compounds with induced absorption and photobleaching band. However, the excited state dynamics differed in two systems. For example, the S_2 state is short lived in the HBCuPc polymer. As a consequence, a fast decay time (1.7ps) in the global

fitting results of HBCuPc-TPA-CN polymer was absent from that of the HBCuPc polymer. The findings in the HBCuPc-TPA-CN polymer proved that the concept of using long-range polaron delocalization in hyper-branched or dendritic systems to enhance the dielectric response is valid. However, the dielectric response is critically dependent on the interplay between the conjugation length and the donor-acceptor interaction.

One critical factor in the design of high dielectric all-organic materials is the structure of the material. Hence, in chapter 5, the HBCuPc polymer structure was modified by connecting CuPc at meta position instead of ortho position of the benzene ring. Under this situation, the separation distance between CuPc rings increased. This modified structure will enable larger polarization and result in larger conductivity, as shown from AC conductance measurement. The dielectric constant was ~9.8 with a low dielectric loss of ~0.0025 at 1MHz. Because the long separation distance between neighboring CuPc rings, the coupling is weak and the self-assembly ability of the molecule is poor. This may be a plausible reason to explain the obtained dielectric constant as compared to previously investigated hyperbranched CuPc polymer systems. To optimize the dielectric film performance, different solvents and surfactants were used. For example, the film casted from dimethylfluoride (DMF) solvent exhibited a more homogeneous surface morphology with improved solubility; however, there is a trade-off between the film solubility and the dielectric response (~3). This indicated that solvent played an important role by affecting the morphology of the polymer particle in the solution. The addition of surfactants, such as polyvinyl sulfonate (PES), poly (ethylene glycol) (PEG) and poly(vinyl alcohol) (PVA), were able to improve the formation ability of the dielectric film. This portion of work can be referred to the appendix A in the

dissertation. But a lot of future work needs to do to have a clearer understanding the role being played by the surfactant and to optimize the composition ratio between the surfactant and the hyperbranched polymer as well as solving problems such as the phase separation and the precipitation. The optimized parameters are not clear yet and a remarkable ongoing work is carried out in this aspect.

We have conducted a profound understanding of different types of hyperbranched CuPc polymers. A big portion of the contribution is made on the comparison between the ground and excited state dynamics of different dendrimers to help the understanding of the corresponding difference in the dielectric response. This piece of understanding is really useful for establishing the structure-function relationship and sketching a map for optimized designs for high dielectric applications.

We also carried out the investigation on how the packing structure will affect the dielectric response in such hyper-branched polymer systems. The electron magnetic resonance (EPR) experiment was able to provide useful information about the disorder at various temperatures and it can be correlated with the non-Arrhenius temperature dependence found by TOF measurement.

A supplementary work was carried out to study the dielectric properties of a series of hybrid polyaniline/ $BaTiO_3$ composites with a core-shell structure. The hybrid material exhibited a higher dielectric constant ($\varepsilon_r \sim 29$) as compared to the pure polyaniline ($\varepsilon_r \sim 7$) at 1MHz. The dielectric loss could be reduced in comparison to that of $BaTiO_3$ nanoparticles. A good example is that a threefold reduction of the dielectric loss of the hybrid system was observed. This enhancement was due to the interface polarization and could be explained by Maxwell-Wagner percolation theory. The key parameters are the

crystalline size and morphology of the $BaTiO_3$, the concentration ratio between the polyaniline (polymer matrix) and $BaTiO_3$ (fillers) and the efficiency of the coating by the polymer matrix. However, the details of this work were skipped in this dissertation.

Other work included the optimization of the dielectric film fabrication process, trying to overcome the difficulties arising from the phase separation, polymer aggregation and the recrystallization as well as the solubility. We also collaborated with companies such as General Electric Company (GE) to test the fabricated dielectric films and targeted at the fabrication of capacitor prototypes.

7.2 Future Outlook

Some progress has been made in the development of organic materials for high dielectric constant applications, such as high energy density capacitors. However, organic high dielectric constant materials still face some significant technical challenges. Generally speaking, the dielectric constant in an organic material is typically low (~3). The increase in the dielectric constant will be normally compensated for by high dielectric loss and large dielectric dispersion. In addition, most organic materials are thermally stable only up to the glass transition temperature, which is lower than the decomposition temperature of most ceramics. Therefore, the stability in a harsh or high temperature environment is an issue too.

Our exploratory work in the hyperbranched copper phthalocyanine has shown that the utilization of the long range delocalization in conjugated molecules provides a novel avenue to achieve high dielectric constant as well as low dielectric loss. In our investigation, copper phthalocyanine was selected as the building unit of the hyperbranched polymer and a great enhancement was obtained as compared to that in a

CuPc monomer. Other studies in phthalocyanine materials have suggested that the metal ion inside a phthalocyanine ring plays an important role in the optical and electronic properties as well as the processibility of the phthalocyanine materials. For example, the iron phthalocyanine monomer has a dielectric constant ~19 and dielectric loss ~0.31 at 1 KHz with relatively low dielectric dispersion. Hence, if we can substitute the central copper ion in hyperbranched copper phthalocyanine polymer with other metal ions and conduct a systematic study on the influence of the metal ion on the dielectric response of the hyperbranched phthalocyanine materials, a hyperbranched phthalocyanine high dielectric constant material with optimum performance is able to obtain.

Hyperbranched copper phthalocyanine materials have shown a great potential in the application as a high dielectric constant material and hyperelectronic polarization is suggested as the main contributing polarization mechanism to the enhanced dielectric response. Pohl et al. also found a hyperelectronic polarization in polyacene quinone radical (PAQR) polymers, which resulted in a very large dielectric response (>10,000 at 100Hz). [1,2] All these findings indicate that hyperelectronic polarization is an effective polarization mechanism contributing to the improved dielectric response in certain organic materials. In order to explore other organic materials which possibly possess the same operative polarization mechanism, the profound understanding of the hyperelectronic polarization mechanism as well as other polarization mechanisms is critical. This understanding will be helpful not only on how to design a new high dielectric constant material, but also on how to tune the dielectric properties of the existing high dielectric constant materials. For this purpose, a theoretical model needs to be constructed and possibly be able to account for the parameters such as the

delocalization length, the coupling strength and the separation distance between neighboring molecules.

From the engineering side, the breakdown voltage is an important characteristic of a high performance dielectric material. A high breakdown voltage is necessary as the square of the breakdown voltage is proportional to the maximum energy density. Our research has found a high dielectric constant in the hyperbranched copper phthalocyanine polymeric materials and the ongoing work is focused on the evaluation of the breakdown voltage of these materials. Even though the technique of the breakdown voltage measurement is available, the size and the shape of the test specimen need to be configured in specifics.

For the purpose of the commercialization, special attention needs to be paid to the following areas: (1) the development of synthesis methods for the mass production of the high dielectric constant material with an affordable cost; (2) the development of an effective electronic packaging technology to maximize the energy density in an electronic device.

Reference

(1) Hartman, R. D.; Pohl, H. A. *Journal of Polymer Science Part a-1-Polymer Chemistry* **1968**, *6*, 1135.

(2) Wyhof, J. R.; Pohl, H. A. *Journal of Polymer Science Part a-2-Polymer Physics* **1970**, *8*, 1741.

APPENDIX A

The Effect of Surfactants on the Dielectric Response of hyperbranched CuPc Polymer

A.1 Introduction

The film fabrication process is essential to the dielectric properties of the hyperbranched polymer dielectric films. Different types of surfactants were added to the hyperbranched CuPc polymer/DMAc solution in order to improve the film forming ability. Polyvinyl Sulfonate (PES), poly(ethylene glycol) (PEG) and poly(vinyl alcohol) (PVA) were the surfactants under investigation.

A.2 Results and Discussion

A.2.1 Polyvinyl Sulfonate (PES) surfactant

The advantages of PES as a surfactant in this study lie in its excellent solubility in the DMAc, good film forming ability as well as high glass transition temperature (225°C). The solubility in DMAc for the PES will help to alleviate the phase separation problem and avoid the miscibility issue between the solvents for both the PES and the HBCuPc polymer. As shown in scheme A.1 is the structure of the PES.

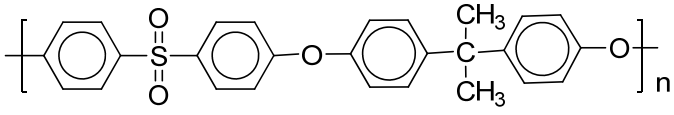

Scheme A.1 The structure of the PES polymer

To a vial, 37.18 mg of PES was dissolved into 3 mL DMAc solution and stir for two hrs. Then ten drops of the PES/DMAc solution was added into the HBCuPc-CN/DMAc solution (3.5mg HBCuPc polymer/0.5mL DMAc) and the mixture was stirred for another 5 hrs. After the casting of the composite film on the Al foil, the film was heat treated under vacuum to evaporate all the solvents. The dielectric response of the PES cast film with a thickness of ~12 μm is illustrated in Figure A.1. The dielectric constant was about 2.4 and not dependent on the frequency. The dielectric loss was ~ 0.0018 up to 10 KHz and then increased with the frequency at high frequency range, similar to the dispersion of PES. However, the dielectric constant of pure PES was ~3.8 and the dielectric loss was ~0.14 at 1MHz.

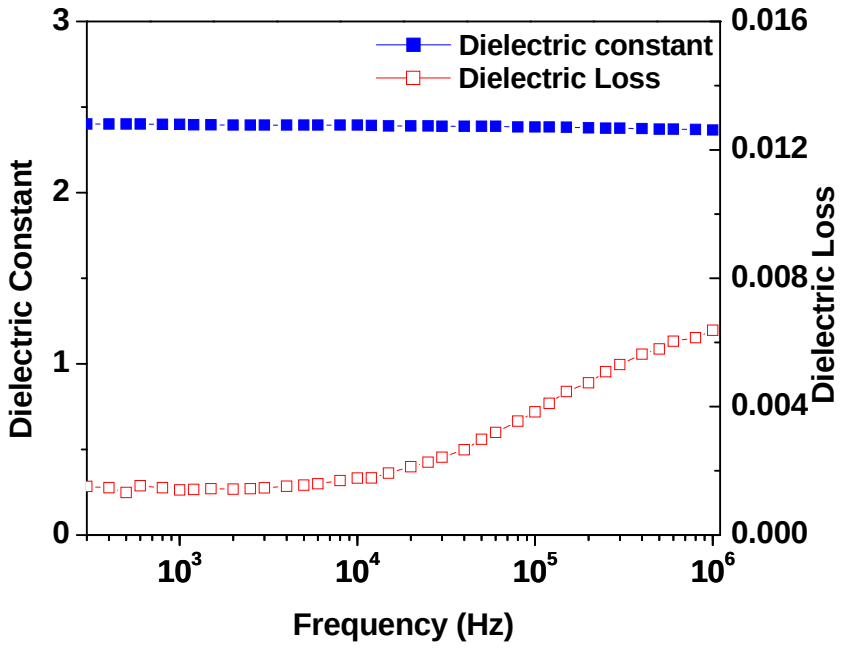

Figure A.1 The dielectric constant and dielectric loss of the HBCuPc-CN/PES composite film.

When we looked at the morphology of the film surface, there were actually two layers of the film (the top clear layer consisted of PES and the bottom green layer

consisted of HBCuPc-CN polymer). I even tried different volume ratio between the PES and HBCuPc-CN polymer solution and observed the same phenomena of the film and the dielectric responses were similar to the one shown in Figure A.1.

A.2.2 Poly(ethylene glycol) (PEG) surfactant

The PEG polymer has several advantages: relatively high dielectric constant (~5), good solubility in DMAc as well as good film forming ability. As shown in scheme A.2 is the structure of the PEG

Scheme A.2 The structure of the PEG polymer

First, 5.3 mg HBCuPc polymer was dissolved in 0.4 mL DMAc solution and stirred for 6 hrs. At the same time, 2.2 mg PEG powder was dissolved in 0.4 mL DMAc solution and stirred for 6 hrs too. Then, mixed both 0.2 mL HBCuPc/DMAc solution with 0.2 mL PEG/DMAc solution and stirred for 6 hrs. After the casting of the composite film on Al foil, the film was dried in air, followed by a continuous heat-treatment under vacuum for 8 hrs. The film surface became more homogeneous and the phase separation was alleviated in some point. As seen in Figure A.2, both the dielectric constant and dielectric loss of 5 μm thick composite film showed strong frequency dependence. The dielectric constant of the composite film was ~3 and the dielectric loss was ~ 0.011 at 1MHz.

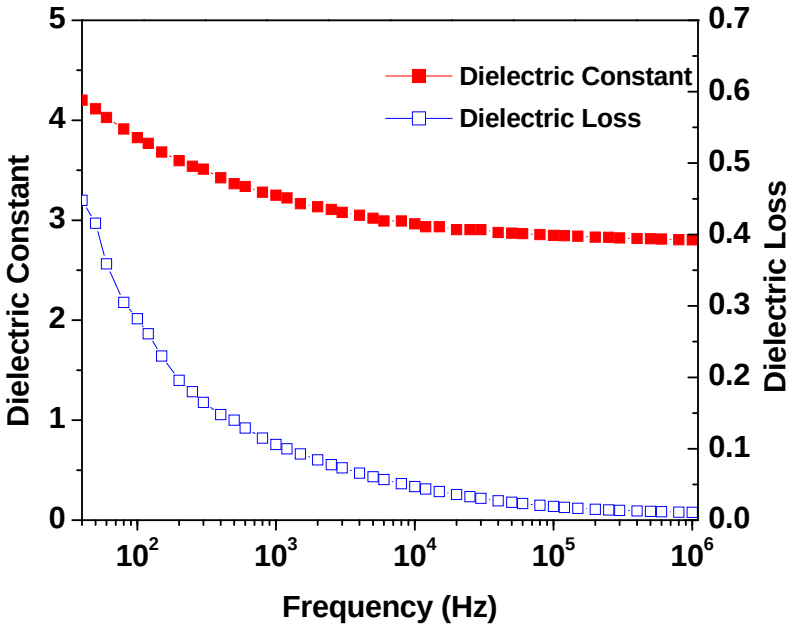

Figure A.2 The dielectric constant and dielectric loss of the HBCuPc/PEG composite film.

A.2.3 Poly(vinyl alcohol) (PVA) surfactant

The PVA has very good film forming ability as well as relative low dielectric dispersion. In addition, it is fully degradable and will decompose quickly at a temperature > 200 °C. However, the dielectric constant of PVA itself was really low (k=1.9~2.0) and it is only soluble in water. The structure of PVA is shown in Scheme A.3.

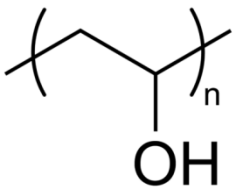

Scheme A.3 The structure of the PVA polymer

2.4 mg HBCuPc powder was dissolved in 0.2 mL DMAc and stirred for 6 hrs, while 1.1 mg PVA was dissolved in 1 mL water and stirred for 6 hrs with the heating at 60 °C. The PVA/H_2O solution was very viscous. After mixing both solutions, the mixture was heated at 40°C and stirred for 6 hrs, followed by a sonication procedure of 15 mins. No phase separation was observed at the solution level. The film preparation procedure was the same as the HBCuPc/ PEG composite film and the final film has a thickness of ~13 μm. The dielectric properties of the HBCuPc/PVA film are shown in Figure A.3.

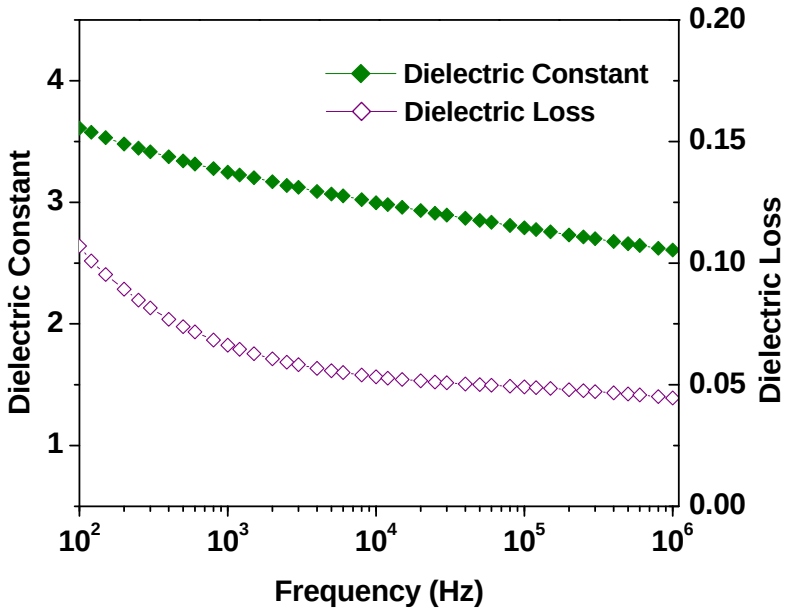

Figure A.3 The dielectric constant and dielectric loss of the HBCuPc/PVA composite film.

The frequency dependence of the dielectric constant and the dielectric loss of the HBCuPc/PVA composite film was weaker compared to the HBCuPc/PEG composite film. And the dielectric constant is higher than that of the pure PVA film.

In summary, the dielectric performances of all composite films with three different types of surfactants were not as good as what we expected. Actually, the dielectric performances of pure hyperbranched CuPc polymers were better than the

composite films. A systematic study on the factors such as the optimum ratio between the hyperbranched polymer and the surfactants and the molecular weight of the surfactants are still going on.